Fakultät für Medizin

Institut für Klinische Chemie und Pathobiochemie

Klinikum rechts der Isar

Determining the Requirement of Caspase-1 Catalytic Activity for Inflammasome-Induced Unconventional Secretion of IL-1 and Cell Death

Katharina Sophie Schneider

Vollständiger Abdruck der von der Fakultät für Medizin der Technischen Universität München zur Erlangung des akademischen Grades eines

Doctor of Philosophy (Ph.D.)

genehmigten Dissertation.

Vorsitzender: Univ.-Prof. Dr. Arthur Konnerth

Betreuer: Priv.-Doz. Dr. Olaf Groß

Prüfer der Dissertation:

1. Univ.-Prof. Dr. Jürgen Ruland

2. Univ.-Prof. Dr. Thorsten Buch

Die Dissertation wurde am 11.11.2015 bei der Fakultät für Medizin der Technischen Universität München eingereicht und durch die Fakultät für Medizin am 15.01.2016 angenommen.

Contents

Acknowledgments

First and foremost, I would like to thank Dr. Olaf Groß for supervising my PhD studies. He has always been available for inspiring discussions and supported me with constructive advices. I was again and again impressed by his immense knowledge and profited enormously from his experience and ideas. His enthusiasm for research made working in his lab a rewarding experience.

Also, I would like to thank Prof. Thorsten Buch and Dr. Philipp Jost for being my thesis committee reviewers. Due to their valuable scientific input, we had productive meetings, which allowed me to critically evaluate my progress. They thereby contributed substantially to the success of this project.

Ronald Naumann and his group at the Max-Planck-Institute in Dresden provided me with embryonic stem cells and performed blastocyst injection of stem cell clones for this project. Their work thus played a fundamental role and I am very thankful for our fruitful collaboration.

Dr. Guillaume Médard from the group of Prof. Bernhard Küster helped with designing and performing mass spectrometry analysis. I would like to thank them for this valuable contribution.

I thank the current and former members of my group for their friendship and support. The bright and cooperative atmosphere has motivated me innumerous times and made it a very enjoyable working environment.

For the non-scientific part, I thank my parents, my sister, and my grandmother, who have support me throughout my life. Their care and confidence in me let me overcome difficulties and achieve my goals.
The most extensive help I received from Martin Brandenburg, who fought with me for the success of this project. I thank him for his infinite patience and understanding and how reliably I could count on him.

Table of figures

Abstract

Inflammasomes are cytoplasmic multiprotein complexes with central roles in the initiation of innate immune responses in myeloid cells. They consist of a pattern recognition receptor, which recruits Caspase-1 following activation. This process is mediated by homotypic domain interactions, usually via the adaptor protein ASC. The various inflammasome receptors respond to different stimuli, together covering a broad range of exogenous and endogenous danger signals. A major outcome of inflammasome activation is the secretion of proinflammatory IL-1 family cytokines like IL-1α, IL-1β, and IL-18. In addition, Caspase-1 is able to induce a special from of programmed cell death called pyroptosis. While it has been clearly demonstrated that cytokine secretion and cell death depend on Caspase-1, the role of Caspase-1 catalytic activity during these events is controversial.

To conclusively investigate the protease activity-dependent functions of Caspase-1 while circumventing the limitations immanent to competitive inhibition by peptide-based inhibitors, I generated a *Caspase-1* transgenic mouse line carrying an inactivating mutation of the active site cysteine (*C284A*). The animals presented with a normal general health and immune system as compared to wild-type littermates. I analyzed myeloid cells of the transgenic mice in inflammasome activation by different receptors. My results revealed that chemical inhibition of Caspase-1 is incomplete, preventing maturation of proIL-1β but still allowing for cell death and cytokine secretion. In contrast, genetic ablation of catalytic activity abolished all Caspase-1-dependent events.

In combination with overexpression analyses of Caspase-1 cleavage-site mutants, this study provided new insights into the function of Caspase-1 as the executioner enzyme of inflammasome activation. It thereby unraveled so far undescribed modes-of-action, which built a promising basis for elucidating the whole pathway downstream of Caspase-1 activation more comprehensively. In addition, this work revealed the shortcomings of the available chemical inhibitors for Caspase-1. Thus, the findings presented herein might help developing alternative strategies for the design of novel Caspase-1 inhibitors with superior clinical efficacy as compared to existing therapies.

Abbreviations

A	alanine
3´	3-prime
5´	5-prime
aa	amino acid
AIM2	absent in melanoma 2
Ala	alanine
alum	aluminium hydroxide
AP1	activator protein 1
APC	antigen-presenting cells
APC	Allophycocyanin
APS	ammonium persulfate
ASC	apoptosis-associated speck-like protein containing a CARD
Asn	asparagine
Asp	aspartic acid
ATP	adenosintriphosphate
BDCA-2	blood DC antigen 2
BIR	baculoviral inhibition of apoptosis protein repeat
BMDCs	bone marrow-derived dendritic cells
BMDM	bone marrow-derived macrophages
bp	base pair
BSA	bovine serum albumin
C	cysteine
CARD	caspase-recruitment domain
CLR	C-type lectin receptors
cfu	colony-forming unit
cmk	chloromethylketone
Co-IP	co-immunoprecipitation
CpG	cytosine triphosphate deoxynucleotide-guanine triphosphate deoxynucleotide
Cys	cysteine
D	aspartic acid
DAMP	damage-associated molecular pattern
DC	dendritic cell
DC-SIGN	DC-specific ICAM3-grabbing non-integrin
DCIR	DC-inhibitory receptor
DMEM	Dulbecco's Modified Eagle Medium
DMSO	dimethyl sulfoxide
DNA	deoxyribonucleic acid
DPBS	Dulbecco's phosphate-buffered saline
DSP	dithiobis(succinimidyl propionate)
dsRNA	double-stranded RNA

DSS	disuccinimidyl suberate
DTT	Dithiothreitol
E	glutamic acid
E. coli	Escherichia coli
EDTA	Ethylenediaminetetraacetic acid
ELISA	enzyme-linked immunosorbent assay
ER	endoplasmatic reticulum
ESC	embryonic stem cell
F	phenylalanine
FACS	fluorescence-activated cell sorting
FBS	fetal bovine serum
FITC	Fluorescein
fmk	fluoromethylketone
Flt3	Fms-like tyrosine kinase 3
GFP	green fluorescent protein
Glu	glutamic acid
GM-CSF	Granulocyte-macrophage colony-stimulating factor
H	histidine
HA	Human influenza hemagglutinin
HIN	hematopoietic interferon-inducible nuclear antigen
His	histidine
I	isoleucine
ICAM	intracellular adhesion molecule 3
iE-DAP	g-D-glutamyl-mesodiaminopimelic acid
IFI16	interferon gamma inducible protein 16
IFIX	interferon inducible protein X
IFN	interferon
IL	interleukin
ILCs	innate lymphoid cells
IRF	interferon regulatory factors
ITAM	tyrosine-based activation motif
ITIM	tyrosine-based inhibitory motif
K	lysine
kb	kilobasepair
L	leucine
LB	Lysogeny broth
LDH	lactate dehydrogenase
LGP2	laboratory of genetics and physiology 2
LIF	leukemia inhibitory factor
LPS	lipopolysaccharide
LRR	leucine rich repeat
M-CSF	macrophage colony-stimulating factor
MDA-5	melanoma differentiation-associated gene 5

MDP	muramyl-dipeptide
MDP	mayor basic protein
MHC	mayor histocompatibility complex
MICL	myeloid inhibitor C-type lectin receptor
mlt	melted
MNDA	myeloid nuclear differentiation antigen
MS	mass spectrometry
MSU	mosodium urate crystals
MyD88	myeloid differentiation factor 88
N	asparagine
nc	non-cleavable
NET	neutrophil extracellular trap
NF-kB	nuclear factor kappa-light-chain-enhancer of activated B cells
NK	natural killer
NLR	Nod-like receptor
NLRC	NACHT, LRR, and CARD-containing protein
NLRP	NACHT, LRR, and PYD-containing protein
Nod	nucleotide-binding and oligomerization domain
Nod2	nucleotide-binding oligomerization domain-containing protein 2
PAMP	pattern-associated molecular pattern
PCR	polymerase chain reaction
PE	Phycoerythrin
PFA	Paraformaldehyde
poly(dA:dT)	poly(deoxyadenylic-deoxythymidylic)
PRR	pattern recognition receptor
PYD	pyrin N-terminal homology domain
RBC	red blood cell
R	arginine
RIG-I	retinoic acid-inducible gene I
Ripk	receptor-interacting serine/threonine-protein kinase
RLR	RIG-I-like receptors
rm	recombinant murine
RNA	ribonucleic acid
ROS	reactive oxygen species
RPMI	Roswell Park Memorial Institute
S.D.	standard deviation
SDS	sodium dodecyl sulfate
SDS-PAGE	sodium dodecyl sulfate polyacrylamide gel electrophoresis
SEM	standard error of the mean
SPF	specific pathogen-free
ssRNA	single-stranded RNA
S. typhimurium	*Salmonella enterica* subspecies I Serovar *typhimurium*
Syk	spleen tyrosine kinase

T	threonine
TEMED	N,N,N',N'-Tetramethylethylendiamine
TIR	Toll/interleukin-1 receptor
TLR	Toll-like receptor
TNFα	tumor necrosis factor alpha
TRIF	TIR-domain-containing adaptor protein inducing IFNβ
Trp	tryptophan
Tyr	tyrosine
V	valine
Val	valine
VSV	Vesicular stomatitis virus
W	tryptophan
WB	Western blot
wt	wild-type
Y	tyrosine

1 Introduction

1.1 The innate immune system

The innate immune system functions as the first line of defense to protect the organism from invading pathogens. Both humoral (e.g. complement system) and cell-based mechanisms mediate this activity. Cells involved in innate immunity are equipped with germline-encoded pattern recognition receptors (PRRs). This panel of evolutionarily conserved receptors recognizes a broad range of danger molecules that can be of exogenous (pathogen-associated molecular pattern, PAMP) or endogenous (danger-associated molecular pattern, DAMP) origin. Examples for PRRs in mammals are the membrane-bound Toll-like (TLRs) and C-type lectin receptors (CLRs). In the cells' cytoplasm, receptors of different families are present to serve this purpose, including NOD-like receptors (NLRs), RIG-I-like receptors (RLRs), and PYHIN (pyrin and HIN domain-containing) receptors.

The innate immune system lacks the adaptability of the adaptive immune system, which is mediated by receptor rearrangement, affinity maturation, or memory functions. Thus, the range of reactions is limited and inflexible in a way. However, with its ability for immediate responses and the broad panel of PRRs, the innate immune system plays a pivotal role in protecting the body from harmful influences. By the production of antimicrobial substances, it helps to keep pathogens in check. The secretion of cytokines and chemokines alarms other immune cells and shapes adaptive immune responses.

1.1.1 Cells of the innate immune system

A diverse group of leucocytes constitutes the innate immune system. Different granulocytes (mast cells, eosinophils, basophils, and neutrophils), monocytes, macrophages, dendritic cells (DCs), natural killer (NK) cells, and innate lymphoid cells (ILCs) have all been shown to fall into this category. Except for NK cells and ILCs, which are classified as lymphocytes, all innate immune cells belong to the myeloid lineage.

Mast cells derive from common myeloid progenitor cells in the bone marrow but differentiate finally only after migration into vascularized tissues (Kirshenbaum et al.). They are most prominent in the skin and mucosa of different organs, like the lung and intestine. Although they have been best characterized for their role in inducing IgE-mediated allergic responses, they are also important in wound healing and fighting parasitic infections (Urb and Sheppard, 2012). Basophils have a very similar mode of action and are associated with the induction of type 2 adaptive immune responses. Like mast cells, they possess granules containing histamine and heparin as central inflammatory molecules. However, basophil granulocytes are mainly found in the blood and not in the tissue (Voehringer, 2013). Similarly, eosinophils respond to parasites, too and are furthermore known for their tissue-damaging contributions in asthma. Unlike basophils and mast cells, the granules they release contain, among others, reactive oxygen species (ROS), cytokines, and the toxic major basic protein (MBP) (Rosenberg et al., 2012).

Neutrophils as the third and most abundant subgroup of granulocytes are phagocytes. They circulate in the blood but transmigrate into infected or damaged tissue upon sensing of activating cytokines and chemokines (Borregaard, 2010; Metchnikoff, 1892). This process is initiated by the endothelium, which upregulates adhesion molecules in response to inflammation and thus enables extravasation of the neutrophils (Ley et al., 2007). At the site of infection, neutrophils ingest microorganisms and kill them by releasing ROS and antimicrobial proteins into their phagosomes. In addition, neutrophils are able to unleash various antimicrobial compounds, which are stored in different granules, into the extracellular space to fight pathogens (Kolaczkowska and Kubes, 2013). A radical step in the antimicrobial effects that neutrophils exhibit, is the fatal expulsion of DNA nets. These so-called neutrophil extracellular traps (NETs) consist of nuclear DNA and proteins as well as granular proteins. NETs prevent spreading of microbes, facilitate their phagocytosis by other immune cells, and even have direct bactericidal properties (Brinkmann et al., 2004).

Like T and B cells, NK cells derive from a common lymphoid progenitor and are able to kill virus-infected cells and cancer cells. By coordinated release of

vesicles that contain the proteins perforin and granzymes, they cause lysis or induce apoptosis of the target cell. NK cells identify stressed cells by detection of activating and the absence of inhibitory signals simultaneously on the target cell's surface (Vivier et al., 2010).

Macrophages and DCs are phagocytes. In addition, they possess the potential of serving as antigen-presenting cells (APCs) for lymphocytes of the adaptive immune system. In the last years, novel observations have been made about the developmental origin of macrophages and DCs. These findings have led to a complete realignment of the established model.

1.1.2 Monocytes, macrophages, and dendritic cells

DCs and macrophages are tissue-resident cells (Metchnikoff, 1892; Steinman and Cohn, 1973). It was long believed that they are the progeny of monocytes that originate in the bone marrow from common monocyte-DC precursors (MDP). Subsequently, monocytes would enter the bloodstream and migrate into the tissue for final differentiation into macrophages or DCs. Recently however, it became obvious that there exist several subtypes of DCs and macrophages, and that the developmental process is not as linear as assumed.

Macrophages do not represent the descendants of circulating monocytes but derive from embryonic precursors that populate the organs prior to birth (Davies et al., 2011; Hashimoto et al., 2013; Yona et al., 2013). A steady-state is maintained by self-renewal of these cells (Davies et al., 2013). Nevertheless, in case of inflammation, monocytes can invade the tissue where they transform into monocyte-derived macrophages to assist the resident cells (Geissmann et al., 2010). A main function of macrophages is phagocytosis. They are not only responsible for the clearance of microorganisms but also of dying or dead cells and foreign substances. When their PRRs become activated, macrophages engulf the pathogen or dangerous compound into phagosomes. Within the cell, they fuse with lysosomes containing hydrolytic enzymes to degrade the ingested particles. ROS are also used by macrophages as microbicidal agents. Furthermore, they produce growth factors and cytokines, for instance TNFα, IL-

1 family members, IL-6, and IL-12 to coordinate further innate and adaptive immune responses (Murray and Wynn, 2011).

DCs are the most professional APCs and initiators of adaptive immune responses in lymph nodes. Remarkably, DCs are able to present ingested antigens in combination with MHC class I and MHC class II molecules. The special ability of these cells to show exogenous antigens in the context of MHC class I is known as “cross-presentation” and enables DCs to activate not only naïve helper T cells but also cytotoxic T cells (Bevan, 1976). DCs can be further divided into different subgroups: conventional DCs (cDCs), plasmacytoid DCs (pDCs), and monocyte-derived DCs. In the bone marrow, MDPs can differentiate into monocytes or the common DC progenitor (CDP). Both, pre-cDCs and pDCs derive from this progenitor in dependence of the cytokine Fms-like tyrosine kinase 3 (Flt3) (Satpathy et al., 2012). These cells leave the bone marrow via the blood to seed lymphatic and non-lymphatic organs. Pre-DCs mature into cDCs at the site of settlement. Based on expression patterns for certain surface molecules, cDCs can be further subgrouped and this classification is in line with functional differences (Satpathy et al., 2012). While one subset is specialized in activating cytotoxic T cells, the other is better in stimulating helper T cell and B cell responses (Dudziak et al., 2007; Pooley et al., 2001). Activation of cDCs via PRRs induces migration of the cells to the draining lymph node and the upregulation of MHC and co-stimulatory molecules. These preparations optimally equip cDCs for their interaction with T lymphocytes (Satpathy et al., 2012). During infectious challenges, monocytes can contribute to the third subset of DCs, the monocyte-derived DCs. However, their exact role and interplay with cDCs remain poorly defined to date (Ginhoux and Jung, 2014). pDCs reside primarily in the lymph nodes. They have been shown to mainly play a role in innate and adaptive immune responses to viral infections. As they exhibit a low expression of MHC class II and co-stimulatory molecules they are less suitable for activation of helper T cells as compared to cDCs (Reizis et al., 2011).

Isolation of DCs and macrophages from the mouse is difficult and yields only low amounts of cells. To circumvent this problem, protocols were established for *in vitro* differentiation of macrophages and DCs from bone marrow progenitor

cells (Groß, 2011; Lutz et al., 1999; Manzanero, 2012). These methods allow obtaining sufficient amounts of primary cells for *in vitro* experiments. These so called bone marrow-derived macrophages (BMDMs) or bone marrow-derived dendritic cells (BMDCs) are most closely related to the monocyte-derived macrophages and dendritic cells that exist *in vivo*. Although they are artificially generated cells and are therefore not identical to their physiological counterparts, BMDMs and BMDCs express cellular responses typical for macrophages and DCs *in vivo*. They therefore have been widely accepted as models to study signal transduction processes of PRRs, present also in tissue-resident DCs and macrophages.

1.1.3 Pattern recognition receptors in myeloid cells

To maximize the chance for detection of pathogens, innate immune cells have their PRRs positioned at all strategically important compartments. TLRs and most CLRs are transmembrane proteins, which sample the surroundings for exceptional events. NLRs, RLRs, and PYHIN family proteins on the other hand, scan the cytoplasm for the presence of pathological patterns.

1.1.3.1 Toll-like receptors

TLRs can be subgroup by their cellular localization. TLR1, 2, 4, 5, and 6 are found on the plasma membrane, whereas TLR3, 7, 8, and 9 are associated with the intracellular membrane of endosomes. All TLRs are type I transmembrane proteins. They consist of an ectodomain of leucine rich repeats (LRRs) for ligand interaction and an intracellular Toll/interleukin-1 receptor (TIR) domain (Akira et al., 2006). Another classification, based on the recognition of PAMPs, can be applied to TLRs. The extracellular TLRs, TLR1, 2, 4, and 6, bind lipids. In particular, TLR4 senses lipopolysaccharide (LPS) present in the cell walls of Gram-negative bacteria (Arbour et al., 2000; Hoshino et al., 1999). TLR2 forms heterodimers with TLR1 and TLR6 and detects in these combinations triacyl and diacyl lipopeptide, respectively (Ozinsky et al., 2000; Takeuchi et al., 2001). The intracellular TLRs, TLR3, 7, 8, and 9, react to nucleic acids derived from

viruses and bacteria. This distribution of the receptors is in line with the presence of pathogenic degradation products in late endosomes and lysosomes. In detail, TLR3 is activated by dsRNA (Alexopoulou et al., 2001), whereas TLR7 recognizes synthetic imidazoquinolines and single-stranded RNA (ssRNA) (Diebold et al., 2004; Hemmi et al., 2002). TLR8 shares great homology with TLR7 and was shown in humans to assist in detection of ssRNA as well as synthetic ligands (Heil et al., 2004). Bacterial and viral DNA exposing unmethylated CpG motifs are bound by TLR9 (Akira et al., 2000). TLR5 senses bacterial flagellin (Hayashi et al., 2001). Lastly, in addition to these, TLR10, 11, and 12 have been described but their roles have only been poorly defined to date.

Binding of a ligand causes dimerization of the respective TLRs and thereby direct or indirect intracellular recruitment of an adaptor protein to their TIR domains. The two main adaptor molecules are myeloid differentiation factor 88 (MyD88) and TIR-domain-containing adaptor protein inducing IFNβ (TRIF). The choice of adaptor protein decides which signaling pathway is activated. While MyD88 acts downstream of all TLRs except for TLR3, TRIF is engaged by TLR3 and TLR4 only (Kawai and Akira, 2007). Recruitment of the adaptors triggers a signaling cascade that culminates in activation of different transcription factors. MyD88 induces the production of proinflammatory cytokines, like TNFα, proIL-1β, IL-6, and IL-8, by activation of the transcription factors NF-κB (Medzhitov et al., 1998) and activator protein 1 (AP1) (Takeuchi and Akira, 2010). Similarly, TRIF causes the expression of proinflammatory cytokines via NF-κB (Yamamoto et al., 2002). However, in addition, TRIF is capable of upregulating type I interferons by activating interferon regulatory factors (IRFs) (Hoebe et al., 2003; Yamamoto et al., 2003). TLR7 and 9 represent exceptions within this system as they are able to induce type I interferon production in a MyD88-dependent manner (Negishi et al., 2006; Schmitz et al., 2007).

The activation of TLRs leads furthermore to the upregulation of costimulatory molecules on the activated cell (Cella et al., 1997; Kaisho et al., 2001). In combination with the production of proinflammatory cytokines and type I interferons, TLRs therefore play an important role in shaping innate immune responses and in initiating adaptive immune responses.

1.1.3.2 C-type lectin receptors

CLRs represent a huge family of proteins that are either found as transmembrane receptors or in a soluble form in the extracellular space. Some of the type II transmembrane CLRs function as PRRs. These receptors are characterized by one or more extracellular C-type lectin-like domains (CTLD) (Drickamer, 1989). The previously used but more restricted term C-type (Ca^{2+}-dependent) carbohydrate recognition (lectin) domain (CRD) was replaced by CTLD, after it was discovered that not all proteins carrying such domains recognize carbohydrates and/or bind calcium (Zelensky and Gready, 2005).

The most prominent CLRs that directly mediate pattern recognition are DC-associated C-type lectin 1 (Dectin-1), Dectin-2, and macrophage inducible C-type lectin (Mincle). Dectin-1 detects β-1,3-linked glucans (Brown et al., 2003; Palma et al., 2006), which are commonly found in the cell walls of fungi and some bacteria. Notably, Dectin-1 is a Ca^{2+}-independent CLR (Brown and Gordon, 2001). Dectin-2 senses high mannose structures as present in fungal cell walls in the typical Ca^{2+}-dependent manner (McGreal et al., 2006). Similarly, the CRD of Mincle binds α-mannans and was shown to thereby detect, among others, *Candida albicans*, *Malassezia* species, and *Mycobacterium tuberculosis* (Wells et al., 2008; Yamasaki et al., 2009). Furthermore, Mincle responds to dead cells via sensing of the ribonucleoprotein SAP130 (Yamasaki et al., 2009).

Either directly via their immunoreceptor tyrosine-based activation motif (ITAM) domain (Dectin-1) or indirectly via ITAM-containing adaptors (Dectin-2, Mincle), the receptors engage spleen tyrosine kinase (Syk). Syk-dependent signaling ultimately causes NF-κB activation and subsequently production of proinflammatory cytokines (Groß et al., 2006; Robinson et al., 2009). However, the role of CLRs extends beyond transcriptional activation of cytokine production. For example, Dectin-1 and Dectin-2 were shown to also induce ROS formation, thereby linking CLR signaling to inflammasome activation (Groß et al., 2009; Ritter et al., 2010; Underhill et al., 2005).

The roles of CLRs in pathogen recognition are not exclusively of activating nature. Some receptors modulate or even suppress signaling of other PRRs like for example TLRs. Into the latter group fall the DC-inhibitory receptor (DCIR), myeloid inhibitor C-type lectin receptor (MICL), blood DC antigen 2 (BDCA-2),

and DC-specific intracellular adhesion molecule 3 (ICAM3)-grabbing non-integrin (DC-SIGN). DCIR and MICL contain an immunoreceptor tyrosine-based inhibitory motif (ITIM). Their activation dampens TLR8 and TLR9 responses (Meyer-Wentrup et al., 2008; 2009) and IL-12 production in response to LPS and zymosan (Chen et al., 2006). Interestingly, BDCA-2 contains an ITAM domain but nevertheless lowers, by interaction with Syk, expression of TLR9-dependent type I interferons and TLR-mediated IL-6 and TNFα production (Cao et al., 2007; Dzionek et al., 2001; Röck et al., 2007). The physiological activators of DCIR, MICL, and BDCA-2 have not been identified and thus, studies on these receptors have been performed using antibodies for stimulation. In contrast to regulatory CLRs with inhibitory functions on TLR signaling, DC-SIGN potentiates the transcriptional activity of NF-κB following TLR stimulation, leading to an increase specifically in IL-10 expression (Gringhuis et al., 2007). DC-SIGN detects high mannose and fucose patterns on a broad range of bacteria, viruses, and fungi (Geijtenbeek et al., 2002; Gringhuis et al., 2007). The closest homolog to human DC-SIGN in mice is SIGNR3, which exhibits similar features (Powlesland et al., 2006; Tanne et al., 2009).

1.1.3.3 Nod-like receptors, RIG-I-like receptors, and PYHIN family proteins

In contrast to the above-mentioned membrane-associated receptors, proteins of the NLR, RLR, and PYHIN families are found as PRRs in the cytoplasm of myeloid cells.

Members of the RLRs are retinoic acid-inducible gene I (RIG-I), melanoma differentiation-associated gene 5 (MDA-5), and laboratory of genetics and physiology 2 (LGP2) (Yoneyama et al., 2005; 2004). MDA-5 and RIG-I are composed of two N-terminal caspase-recruitment domains (CARDs), a central DExD/H box helicase/ATPase domain, and a C-terminal regulatory domain. They both sample the cytoplasm for viral double-stranded RNA (dsRNA) but differ in the recognition of certain viruses (Takeuchi and Akira, 2010). The binding of RNA causes an activating conformational change in the receptors. Via IRF-3 and IRF-7 as well as NF-κB, this leads to type I interferon expression

and the production of proinflammatory cytokines, respectively (Paz et al., 2006). Independent of the described transcriptional effects, RIG-I was shown to trigger apoptosis-associated speck-like protein containing a CARD (ASC)-dependent inflammasome activation (Poeck et al., 2009). LGP2 lacks the N-terminal CARDs important for downstream signaling and is believed to function as a negative regulator of MDA-5 and RIG-I (Yoneyama et al., 2005).

The family of NLRs is comprised of 22 genes in humans and even more in mice. They show a tripartite structure with a central nucleotide-binding and oligomerization domain (NOD or NACHT domain). Most of the NLRs contain a C-terminal leucine-rich repeat (LRR), which is involved in ligand detection. The N-terminus exhibits the greatest variability among NLRs. Some possess a CARD, others a pyrin domain (PYD), or a baculoviral inhibition of apoptosis protein repeat (BIR) domain (Inohara et al., 2005). NLRs can be clustered into three groups by similarities in their domain structures, which overlaps with phylogenetic analysis: NODs (Nod1-2, Nod3/Nlrc3, Nod4/Nlrc5, Nod5/NLRX1, CIITA), NLRPs (Nlrp1-14), and IPAFs (Ipaf/Nlrc4, Naip) (Schroder and Tschopp, 2010). The roles of several NLRs in innate immune responses are quite well understood by now. The exact functions of others, however, still await clarification.

Nod1 and Nod2 consist of LRRs, a NACHT domain, and a CARD. Upon sensing of bacterial peptidoglycans (g-D-glutamyl-mesodiaminopimelic acid (iE-DAP) and muramyl dipeptide (MDP), respectively) they activate NF-κB involving the kinase Ripk2 (Kufer et al., 2006). Nod5 is associated with mitochondria but its functions are controversial. NAIPs are characterized by BIR domains instead of CARDs. Naip2 and 5 have been shown to assist the other member of their subfamily, Nlrc4, in ligand recognition and inflammasome activation (Zhao et al., 2011). Likewise, several proteins of the NLRP subgroup have been identified as Caspase-1-activating inflammasome receptors and their functions will be discussed in detail below. They are all built of a LRR, PYD, and NACHT domain. Nlrp10, consisting of only PYD and NACHT domains, as well as NRLP1 with its additional function to find domain (FIIND) and CARD represent exceptions to this rule (Schroder and Tschopp, 2010). Nlrp1 and Nlrc4 are the only inflammasome-inducing NLRs that express a CARD.

Another family of myeloid intracellular PRRs are the PYHIN proteins. As the name implies, they are formed of PYD and HIN200 domains with the HIN200 domain being responsible for the binding of these receptors to DNA molecules. In humans, interferon inducible protein X (IFIX), interferon gamma inducible protein 16 (IFI16), absent in melanoma 2 (AIM2), and myeloid nuclear differentiation antigen (MNDA) were identified as PYHIN family members. More paralogs seem to exist in mice (Cridland et al., 2012). AIM2 was the first PYHIN member associated with innate immune responses. The cytosolic receptor was found to induce inflammasome activation following recognition of dsDNA of viral, bacterial, or host origin (Bürckstümmer et al., 2009; Fernandes-Alnemri et al., 2009; Hornung et al., 2009; Roberts et al., 2009). IFI16 is mainly known for its ability to activate IRF3 and NF-κB causing type I interferon, proIL-1β, and IL-6 expression during viral infection (Unterholzner et al., 2010). Recently it was discovered that infection with DNA viruses can trigger an IFI16 inflammasome (Kerur et al., 2011). This finding is especially striking, as IFI16 is usually located in the nucleus.

There exists substantial interplay between the above-mentioned PRR-signaling pathways and, as described, there is also some redundancy in the recognition of certain patterns. On the one hand, this serves as a safety mechanism and on the other hand, enables subtle distinctions in the response to the same pathogen under variable conditions. Many more connections will probably be elucidated over the next years to complete our picture of innate immune signaling.

1.2 The inflammasome

The inflammasome is a multiprotein complex that was discovered in 2002 by the laboratory of Jürg Tschopp (Martinon et al., 2002). It is found in innate immune cells of the myeloid lineage. Inflammasomes consist of a cytosolic PRR, in most cases the adaptor protein ASC, and the protease Caspase-1. There exist different types of inflammasomes named after the receptor that initiates assembly of the complex. An extremely diverse set of endogenous and exogenous danger signals can be sensed by these receptors. Inflammasome

activation leads to secretion of proinflammatory cytokines (IL-1α, IL-1β, IL-18) and a certain form of programmed cell death called pyroptosis (Schroder and Tschopp, 2010).

1.2.1 Canonical inflammasome receptors

To date, the PYHIN family members AIM2 and IFI16, the RLR RIG-I, and several NOD-like receptors, like Nlrp1, Nlrp3, Nlrp6, Nlrp7, Nlrp12, and Nlrc4, have been identified as canonical inflammasome receptors. Over the past years, more and more stimuli have been linked to the activation of the individual PRRs.

AIM2 binds and responds to DNA molecules that are found in the cytoplasm during infection with *Francisella tularensis* and DNA viruses, like vaccinia virus and cytomegalovirus (Bürckstümmer et al., 2009; Fernandes-Alnemri et al., 2009; Hornung et al., 2009; Rathinam et al., 2010). This receptor can also be activated *in vitro* by transfection of a synthetic double-stranded DNA molecule of repetitive sequence (poly(dA:dT) into myeloid cells (Hornung et al., 2009). RIG-I, belonging to the family of RNA helicases, recognizes 5'-triphosphate dsRNA molecules. It causes antiviral responses by its dual mode-of-action in inducing type I interferon and Caspase-1 activation (Hornung et al., 2006; Poeck et al., 2009; Schlee et al., 2009). Human NLRP1 is activated by MDP (Faustin et al., 2007). Among the three paralogs of Nlrp1 in mice, Nlrp1a, b, and c, Nlrp1b was shown to be the key susceptibility factor for *Bacillus anthracis* lethal toxin (Boyden and Dietrich, 2006). Nlrc4 (also called Ipaf) detects bacterial type 3 secretion systems and flagellin as found, for example, in *Salmonella typhimurium (S. typhimurium)*, *Legionella pneumophila*, and *Pseudomonas aeruginosa* (Franchi et al., 2006; Miao et al., 2010; 2006). Later, it was discovered that Nlrc4 cannot sense these stimuli directly but is reliant on two NLR proteins, namely Naip2 and Naip5 (Zhao et al., 2011).

Nlrp3 represents an exception to these clear assignments between stimuli and receptors. It reacts to a broad range of not only PAMPs but also DAMPs. Among the exogenous Nlrp3-activators are viruses (e.g. influenza A, encephalomyocarditis virus, vesicular stomatitis virus) (Allen et al., 2009; Rajan

et al., 2011), fungi such as *Candida albicans* and *Aspergillus fumigatus* (Groß et al., 2009; Saïd-Sadier et al., 2010), parasites (Ritter et al., 2010), bacteria-derived pore-forming toxins as nigericin, maitotoxin, and hemolysins (Mariathasan et al., 2006; Walev et al., 1995), and crystalline structures like asbestos, aluminium salts, and silica (Dostert et al., 2008; Hornung et al., 2008). In addition, endogenous danger signals are also able to induce Nlrp3 inflammasome assembly. Monosodium urate crystals (MSU) as present in gout patients (Martinon et al., 2006), amyloid-β fibrils, the characteristic component of plaques in the brains of Alzheimer's disease patients (Halle et al., 2008), cholesterol crystals (Duewell et al., 2010), and ATP (Mariathasan et al., 2006) all fall into this group. How Nlrp3 can integrate these various signals into Caspase-1 activation remains unclear. Several mechanisms have been proposed. One hypothesis says that efflux of potassium ions from the cells, which was shown to occur in response to many Nlrp3 stimuli, is the common trigger (Muñoz-Planillo et al., 2013; Perregaux and Gabel, 1994). Other authors name the production of ROS (Cruz et al., 2007; Zhou et al., 2010) or lysosomal leakage of cathepsins (Hornung et al., 2008) as factors involved in Nlrp3 activation.

Human NLRP7 induces inflammasome assembly in response to microbial acylated lipopeptides (Khare et al., 2012) but this receptor is not expressed in mice. Nlrp6 seems to be involved in gut homeostasis and controlling infections but a distinct activating stimulus has not been identified yet (Elinav et al., 2011). The functions of Nlrp12 are only poorly defined (Arthur et al., 2010).

1.2.2 Canonical inflammasome activation

In principle, canonical inflammasome activation is a 2-step process. At first, a priming signal is needed that puts the cell in an activated state. Priming signals can for example be delivered by TLRs, like LPS on TLR4, which, engaging NF-κB, leads to upregulation of proIL-1β expression (Bauernfeind et al., 2009; Hiscott et al., 1993). Additionally, priming also has a direct influence on inflammasome activation by the induction of Nlrp3-expression. However, priming alone is not sufficient to cause processing and release of proIL-1β and

a second trigger is needed (Bauernfeind et al., 2009). Detection of a stimulus is thought to induce a conformational change in the respective inflammasome receptor, causing oligomerization. As a consequence, Caspase-1 is recruited to the inflammasome complex, usually via the adaptor protein ASC. The ASC protein consists of two domains, a CARD and a PYD (Masumoto et al., 1999). Via homotypic domain interactions ASC bridges the PYD-containing inflammasome receptors to the CARD-containing Caspase-1 (Agostini et al., 2004; Mariathasan et al., 2004; Martinon et al., 2002; Srinivasula et al., 2002). In inflammasome activated cells, ASC was visualized to concentrate in a single spot per cell by immunofluorescence imaging (Bryan et al., 2009; Fernandes-Alnemri et al., 2007). This feature has led to the term ASC “speck”.

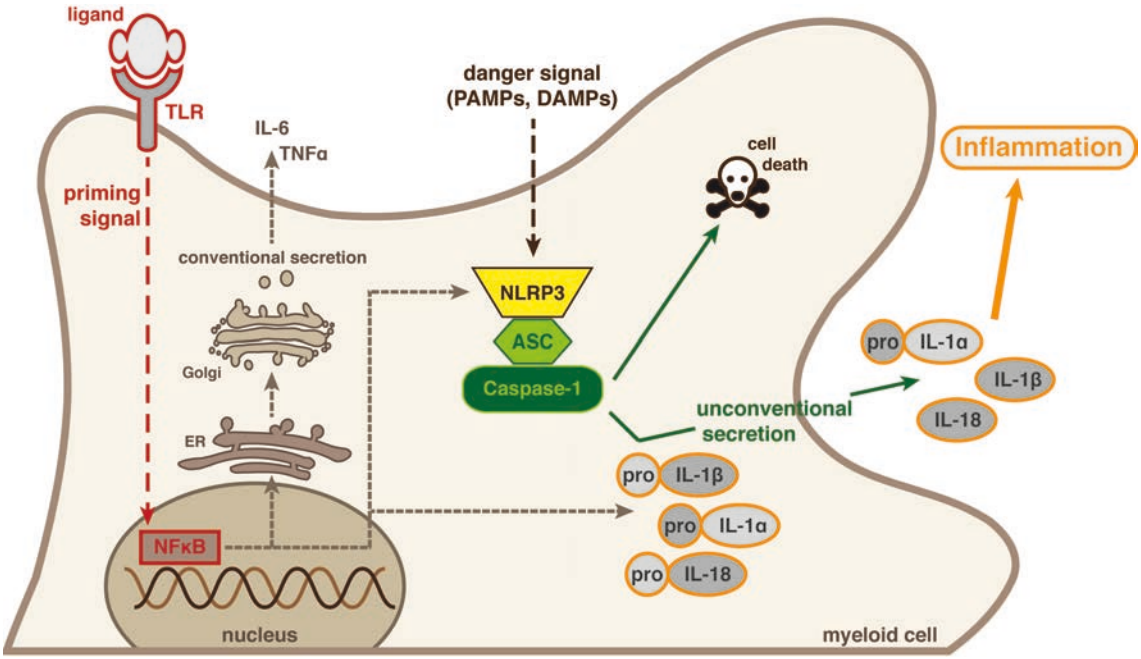

Figure 1: Model of canonical inflammasome activation
Two signals are required for canonical inflammasome activation, a priming signal and a danger signal, causing cell death and IL-1 family cytokine secretion by unconventional secretion via Caspase-1.

Enrichment of Caspase-1 on these “specks” is believed to cause activation of the protease by autocleavage due to induced-proximity. In the activated state, Caspase-1 cleaves proIL-1β and proIL-18 into their mature forms (Black et al., 1989; Gu et al., 1997; Kostura et al., 1989). ProIL-1α is not processed by Caspase-1 but by calpains (Howard et al., 1991) and is furthermore already bioactive in the full-length as well as in the mature form (Mosley et al., 1987).

Nevertheless, Caspase-1 is responsible for the secretion of all three cytokines, IL-1α, IL-1β, and IL-18 (Kuida et al., 1995). Secretion of these IL-1 family cytokines happens via poorly understood so called unconventional secretion (see 1.3.2).

Binding of IL-1α and IL-1β to their receptor interleukin-1 receptor (IL1R1) within a tissue locally leads to upregulation of chemokines and adhesion factors on endothelia. The cytokines hereby promote leukocyte attraction and retention at the site of inflammation. Systemically, IL-1 acts as an effective pyrogen (Dinarello, 2009). A third ligand of IL1R1 is interleukin-1 receptor antagonist (IL-1RA) (Hannum et al., 1990). IL-1RA binds the receptor without stimulating a cellular response and thereby serves a negative regulator of IL1R1 signaling.

IL-18 is known for its role in inducing IFNγ in NK and T helper cells (Okamura et al., 1995). Together with IL-12, it is critical for directing adaptive immune responses towards a T helper 1 (T_H1)-type development. In the absence of IL-12, IL-18 induces differentiation into T helper 2 (T_H2)-type cells (Nakanishi et al., 2001). Thus, IL-18 plays a major role in shaping suitable primary immune responses and also in generating sustained immunity.

Besides the secretion of cytokines, Caspase-1 induces a certain form of programmed cell death referred to as pyroptosis. In contrast to apoptosis, pyroptosis is not an immunological silent process but provokes an inflammatory response in the surrounding cells. One purpose of this cell death is proposed to be the elimination of the intracellular niche of a pathogen.

1.2.3 The non-canonical inflammasome

Rather recently, a new type of inflammasome was discovered featuring Caspase-11 and its human orthologues Caspase-4 and 5 as key caspases. This so-called non-canonical inflammasome is triggered by detection of Gram-negative bacteria and, like the canonical inflammasome, causes IL-1 secretion and cell death (Kayagaki et al., 2011). Interestingly, while Caspase-11 is capable of inducing cell death autonomously, it relies on interaction with the classical canonical inflammasome to evoke proIL-1β cleavage and secretion. The precise mechanism behind this interplay has not been fully elucidated.

The non-canonical inflammasome was discovered by Kayagaki *et al.* in 2011, who identified Gram-negative bacteria as stimuli for this new inflammasome (Kayagaki et al., 2011). Later LPS, an essential component of the outer membranes of Gram-negative pathogens, was found to activate Caspase-11 (Hagar et al., 2013). This is most likely achieved by direct binding of LPS to the CARD of Caspase-11 (Shi et al., 2014). In the same study, human Caspase-4 and Caspase-5 were also shown to bind LPS.

Like Caspase-1, Caspase-11 is capable of directly inducing pyroptosis. However, for proIL-1β cleavage and secretion, Caspase-11 depends on Caspase-1 (Kayagaki et al., 2011). As demonstrated in *Caspase-1* knockout cells, Caspase-11 activation alone led to the release of HMGB1 and IL-1α probably as a side effect of cell death but not to secretion of cleaved IL-1β.

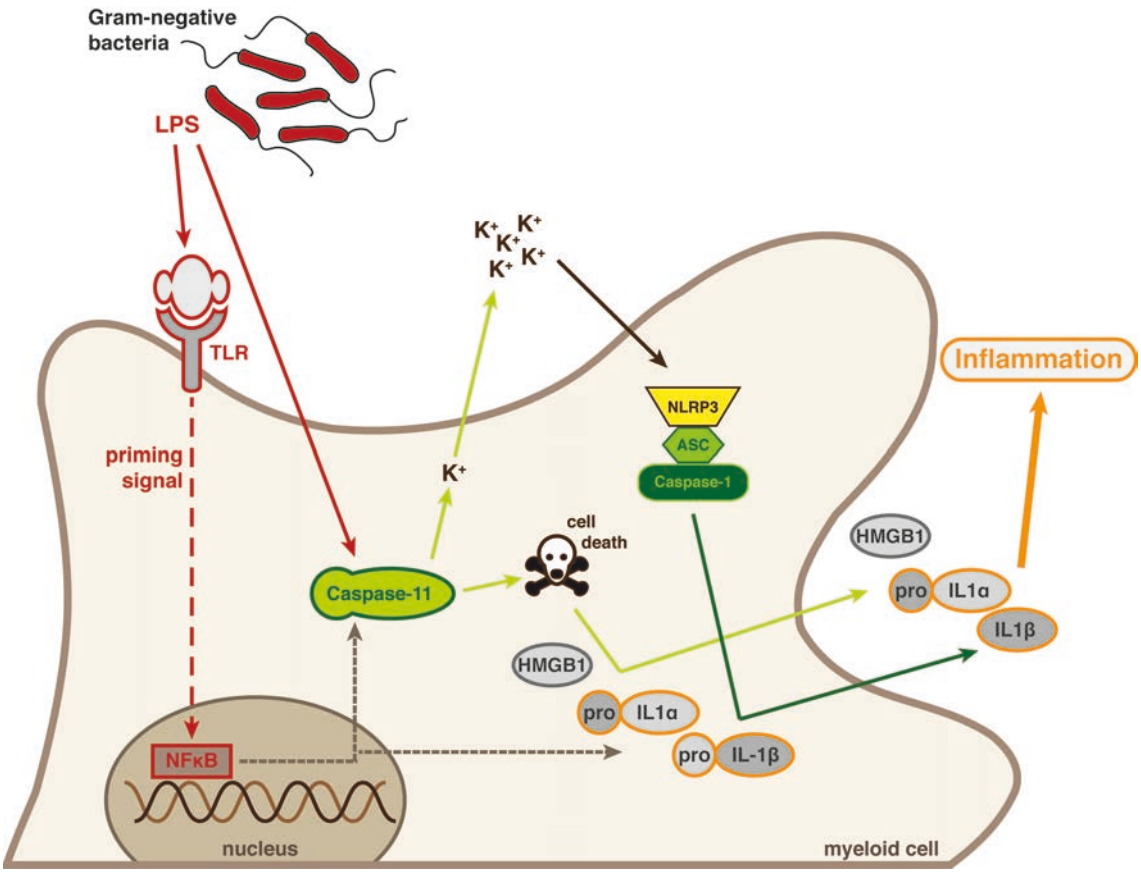

Figure 2: Model of Caspase-11 non-canonical inflammasome activation
Caspase-11 is activated by LPS as found in the outer membrane of Gram-negative bacteria. Stimulation causes cell death and IL-1α secretion. Via potassium efflux (K^+), Caspase-11 engages the canonical inflammasome thereby inducing IL-1β maturation and release.

The role of Caspase-11 in inflammasome signaling has long been underestimated. Kayagaki *et al.* uncovered the role of Caspase-11 by finding that mice of the different 129 lines do not express Caspase-11 protein. This is due to a 5 bp deletion in the *Caspase-11* gene affecting the splice acceptor junction for exon 7. Splicing of exon 6 to exon 8 leads to an aberrant premature stop codon. Caspase-11 deficiency correlated with irresponsiveness of BMDMs to *Escherichia coli* (*E. coli*), *Citrobacter rodentium* (*C. rodentium*), and *Vibrio cholerae* (*V. cholerae*) (Kayagaki et al., 2011). This result was especially notable as the original *Caspase-1* knockout was generated in 129S2/SvPas-derived embryonic stem cells (ESCs) (Kuida et al., 1995; Li et al., 1995). The *Caspase-1* and *Caspase-11* loci are in very close proximity to each other on murine chromosome 9 and therefore, cannot be segregated by backcrossing to a Caspase-11-proficient strain (Kayagaki et al., 2011). Thus, these mice represent *Caspase-1 Caspase-11* double knockouts. Since this discovery, data on these mice have been reprocessed and functions of Caspase-11 independently of Caspase-1 have been investigated extensively. It turned out that, for example, the lethality in a LPS-induced shock model was actually a consequence of Caspase-11 activity and not, as previously believed, of Caspase-1 (Kayagaki et al., 2011).

As mentioned above, Caspase-11 depends on Caspase-1 for IL-1β processing and secretion but there is controversy on which level the two caspases interact. Three potential mechanisms have been proposed: 1) Caspase-11 forms a complex with Nlrp3, ASC, and proCaspase-1; 2) Caspase-11 directly activates Caspase-1; 3) Caspase-11 regulates canonical inflammasome activation upstream of Nlrp3 (Baker et al., 2015; Broz et al., 2012; Rathinam et al., 2012). Recently it was published that Caspase-11, Caspase-4, and Caspase-5 provoke potassium efflux from the cell in response to LPS transfection and that this loss of potassium ions triggers Nlrp3 activation (Rühl and Broz, 2015; Schmid-Burgk et al., 2015). Efflux of potassium ions is a well-known stimulus of the Nlrp3 inflammasome (Muñoz-Planillo et al., 2013). Taken together, these novel findings point towards a role for Caspase-11 upstream of Nlrp3 in activation of Caspase-1. Therefore, influencing potassium homeostasis could

represent the missing connection between non-canonical and canonical inflammasomes.

1.2.4 Clinical significance

Dysregulated IL-1 production has a causal role in a number of acquired and hereditary autoinflammatory diseases. These include particle-induced sterile inflammation, as is seen in gout (Martinon et al., 2006), silicosis, and asbestosis (Dostert et al., 2008), hereditary periodic fever syndromes (Feldmann et al., 2002; Hoffman et al., 2001), inflammatory bowel diseases, like Morbus Crohn (Villani et al., 2008), and metabolic diseases such as type 2 diabetes (Masters et al., 2010). In most cases, the pathogenesis of these diseases has been linked to deregulated inflammasome activation, leading to the inappropriate activation and secretion of IL-1β.

The efficacy of IL-1R1 antagonists in conditions such as gout and periodic fever syndromes underlines the critical role of IL-1 in these diseases (Goldbach-Mansky et al., 2008; Hoffman et al., 2004). However, this treatment option is extremely expensive and elaborate. Furthermore, not only cytokine secretion but also the Caspase-1-dependent cell death may play a critical role in inflammasome-associated diseases. Thus, new approaches to control derailed inflammasome signaling are urgently needed to make effective treatments available to a broader range of patients.

1.3 Caspase-1 activation and functions

1.3.1 Caspase-1 autoprocessing

Caspase-1 belongs with Caspase-4, 5 (human), and 11 (murine) to the group of inflammatory caspases, while all other caspases belong to the families of apoptotic initiator and effector caspases (Caspase-2, 3, 7, 8, 9, and 10) (Martinon and Tschopp, 2007). Caspase-1 has initially been described under the name IL-1β-converting enzyme (ICE) (Black et al., 1989; Kostura et al., 1989). The gene for *Caspase-1* is located on the human chromosome 11 and the murine chromosome 9, respectively. Like all caspases, Caspase-1 is a

cysteine-dependent protease that requires an aspartate (Asp) residue for cleavage (Alnemri et al., 1996; Thornberry et al., 1992). The enzyme consists of three domains, a CARD, a larger (20 kDa), and a smaller subunit (10 kDa). The latter two are forming the substrate-binding pocket with the active center (Thornberry et al., 1992; Walker et al., 1994; Wilson et al., 1994). Located in the larger subunit (p20), the active cysteine is positioned at amino acid (aa) 285 in humans and aa284 in mice. Aspartate-containing linker regions separate the three domains of Caspase-1. As described above, the CARD domain is crucial for homotypic domain interaction with ASC or CARD-containing inflammasome receptors (Nlrp1, Nlrc4) (Srinivasula et al., 2002).

Cerretti *et al.* and Thornberry *et al.* were the firsts to describe autoproteolytic cleavage of Caspase-1 in its two linker regions (Cerretti et al., 1992; Thornberry et al., 1992). A bit later Gu *et al.* and Yamin *et al.* provided evidence that oligomerization of proCaspase-1 triggers this self-processing (Gu et al., 1997; Yamin et al., 1996). In non-activated cells, Caspase-1 is found as a p45 zymogen. Cleavage and formation of a p20/p10 heterotetramer greatly enhances protease activity (Yamin et al., 1996). Thus, it is assumed that agglomeration of Caspase-1 on the inflammasome triggers autoactivation of the protease by the model of induced proximity as established for the apoptotic initiator caspases (Caspase-8 and 9) (Salvesen and Dixit, 1999). Elliott *et al.* support this hypothesis by *in vitro* experiments showing that the concentration of Caspase-1 molecules on an ASC “speck” enables autocleavage within their linker regions (Elliott et al., 2009). First, Asp297 at the end of the larger subunit is cut, increasing the flexibility in the linker region between the p20 and p10 domain (Elliott et al., 2009). However, a second cut is needed for activation of Caspase-1 (Yamin et al., 1996). This takes place at position Asp316 and results in the transformation of an α-helix into antiparallel β-sheets at the newly generated ends of the p20 and p10 subunit. This rearrangement stabilizes the heterotetramer (Elliott et al., 2009). Finally, Caspase-1 cleaves its second linker between the CARD and p20 domain and thereby releases itself from the inflammasome. However, it was shown that separation of the CARD is not necessary for Caspase-1 activity (Yamin et al., 1996). Taken together, these cleavage events allow for rearrangement of the Capase-1 tertiary structure and

are important for p20/p10 heterotetramer stabilization (Elliott et al., 2009). While Caspase-1 exhibits maximal activity in this conformation, Walsh *et al.* demonstrated that processed Caspase-1 has a very short half life of only a few minutes (Walsh et al., 2011). This rapid inactivation probably serves as a safety mechanism to restrict the effects of Caspase-1.

1.3.2 Cleavage and unconventional secretion of IL-1 cytokines

The most prominent function of Caspase-1 is the proteolytic processing of proIL-1β and proIL-18 (Gu et al., 1997; Howard et al., 1991). Despite the fact that IL-1α is not cleaved by Caspase-1 (Howard et al., 1991) the dependency on Caspase-1 for secretion of both IL-1β and IL-1α has been reported (Kuida et al., 1995).

The vast majority of secreted proteins bears a signal peptide and is released from the cell via successive transport through the endoplasmic reticulum (ER) and Golgi apparatus. In contrast, some proteins use poorly defined pathways for their secretion, which are collectively called “unconventional protein secretion” (Nickel and Rabouille, 2009). This term describes a heterogeneous group of secretion mechanisms. On the one hand, some unconventionally secreted proteins display a signal peptide that leads to their translocation into the ER but they bypass the Golgi on their route to the cell’s surface. On the other hand, some proteins, like IL-1, do not possess a signal peptide and cannot be transported into the ER. Nevertheless, they have been shown to be secreted in a regulated manner (Rubartelli et al., 1990).

Although substantial research has been performed to elucidate how Caspase-1 controls IL-1 secretion, the mechanism behind the transport still remains unknown. Rubartelli *et al.* demonstrated by protease protection experiments that IL-1β is contained within a membranous compartment (Rubartelli et al., 1990), which is of endolysosomal character (Andrei et al., 1999). A more recent study suggests that IL-1 is packed into autophagosomes for autophagic degradation upon LPS priming (Harris et al., 2011). This finding questions the assumption by Rubartelli *et al.* and claims that IL-1β is present in the lysosomal compartment for catabolic reasons rather than for secretion. Another

mechanism for secretion of IL-1 was proposed by MacKenzie *et al.*, who found IL-1 contained within extracellular microvesicles that shed from the plasma membrane (MacKenzie et al., 2001). Qu *et al.* claimed that these vesicles represent exosomes that shed from multi-vesicular bodies or late endosomes (Qu et al., 2007).

As Caspase-1 activity induces membrane pores involved in the process of pyroptosis, it is furthermore debated whether IL-1 is released through these channels (Fink and Cookson, 2006). Other authors went even further and proposed release of IL-1 as a side effect of cell lysis during pyroptosis (Liu et al., 2014; Shirasaki et al., 2014).

Despite the scientific interest in elucidating the mechanisms of Caspase-1-dependent IL-1 secretion, the complexity of the pathway makes it a challenging task. To date, no satisfying model has been provided and more studies are needed to complete the picture of unconventional secretion of IL-1 cytokines.

1.3.3 Pyroptosis

Pyroptosis is a type of programmed cell death, which by definition is Caspase-1 dependent. In contrast to apoptosis, this form of cell death is a highly inflammatory event. Caspase-1 was shown to induce pore formation in the plasma membrane upon activation (Fink et al., 2008; Fink and Cookson, 2006). This leads to disturbance of the cellular ionic gradient, influx of water, and consequently osmotic cell lysis. In this process, inflammatory substances are released from the cell, inducing inflammation in the surrounding tissue (Fink and Cookson, 2006). It was shown that glycine can prevent the destabilization of the osmotic gradient following inflammasome activation and thereby block pyroptosis (Brennan and Cookson, 2000). Interestingly, it was observed that release of IL-1 and IL-18 was not impaired by glycine (Fink and Cookson, 2006). This demonstrates that the secretion mechanism for IL-1 does not use these pores directly. Furthermore, Chen *et al.* observed IL-1β secretion in neutrophils, which are resistant to pyroptosis (Chen et al., 2014). These findings imply that the cytokines are actively secreted and not simply freed from the cell as a result of cell death.

Like apoptosis, pyroptosis is characterized by DNA fragmentation. Nevertheless, both processes rely on different nucleases for execution of this feature (Fink and Cookson, 2006). A further difference between the two types of programmed cell death is the condensation of the nucleus that occurs during pyroptosis (Molofsky et al., 2006). The heterogeneity of pyroptosis and apoptosis is also reflected in the lack of participation of Caspase-1 in apoptosis (Li et al., 1995). Likewise, apoptotic caspases like Caspase-3, Caspase-6, and Caspase-8 are dispensable for pyroptosis (Brennan and Cookson, 2000). However, cleavage of Caspase-7 downstream of Caspase-1 has been reported, although the purpose of this interplay remains elusive (Akhter et al., 2009; Lamkanfi et al., 2008).

Infection models in mice revealed that Caspase-1 induced cell death plays a pivotal role in clearance of the pathogens from the organism. Mice deficient for Caspase-1 were more susceptible to bacteria than mice deficient for IL-1β and IL-18 (Henry and Monack, 2007). On the other hand, Monack *et al.* showed that neither IL-1β nor IL-18 are needed for cell death following inflammasome activation (Monack et al., 2001).

These observations highlight the importance of pyroptosis as not only a side effect of inflammasome activation, but an important mechanism in effectively fighting bacterial infections. Although many facts about Caspase-1-dependent cell death have been revealed, the precise mechanism how Caspase-1 induces cell death is still an open question. Very recently, two papers were published discovering Gasdermin D as a new cleavage target of Caspase-1 with crucial roles in pyroptosis induction (Kayagaki et al., 2015; Shi et al., 2015). The identification of novel interaction partners of Caspase-1 is a promising approach to elucidate this pathway in more detail.

1.3.4 Caspase-1 activation in the absence of ASC

As introduced above, some inflammasome receptors bear their own CARD domain (see 1.1.3.3). Human NLRP1, murine Nlrp1b, and Nlrc4 belong to this group, enabling them in principle to interact directly with Caspase-1 without the need for the adaptor protein ASC. While the Nlrp3 inflammasome is strictly

dependent on ASC for activation of Caspase-1, several studies aimed at investigating the relevance of ASC in Nlrc4 and Nlrp1 stimulation.

Broz *et al.* asked whether ASC is involved in Nlrc4 inflammasome activation and to that end, stimulated ASC-proficient and deficient immortalized BMDMs with the Nlrc4 agonists *S. typhimurium* and *Listeria monocytogenes* (Broz et al., 2010). They observed that, while ASC was dispensable for the induction of pyroptosis, it was required for optimal processing of proIL-1β and proIL-18. This was associated with absence of Caspase-1 autoproteolysis in ASC knockout cells. Retroviral reconstitution experiments using an uncleavable Caspase-1 mutant revealed that cleavage of Caspase-1 was necessary for cytokine processing but not for cell death.

Comparably, analysis of mouse macrophages stimulated with the Nlrp1b agonist *Bacillus anthracis* lethal toxin displayed that in the absence of ASC, Nlrp1b is incapable of causing Caspase-1 autoproteolysis (Van Opdenbosch et al., 2014). However, contrary to the situation with Nlrc4, the same study showed that neither pyroptosis nor IL-1β cleavage and secretion were compromised by failure of Caspase-1 cleavage. Guey *et al.* confirmed these findings in BMDMs and BMDCs and gave further insights into Nlrp1b activation (Guey et al., 2014). The group reconstituted mutants of Caspase-1 that were either uncleavable or inactive into Caspase-1-deficient cells using retroviral transduction. In their settings, protease activity of Caspase-1 was required for induction of cell death and cytokine secretion. Instead, according to the earlier results from ASC knockout cells, cleavage of Caspase-1 was not needed for cell death and cytokine secretion in response to lethal toxin. Surprisingly, the uncleavable mutant was not able to restore IL-1β secretion following Nlrp3 inflammasome activation.

The variability in the dependence of the different inflammasomes on ASC for the respective functions of Caspase-1 demonstrates the complexity of the pathway. It seems that Caspase-1 does not follow a linear activation pathway, which culminates in the full spectrum of activity, but that the activation process is finely tuned. These insights open new perspectives for analysis of how Caspase-1 controls cytokine secretion and cell death.

1.4 Caspase-1 inhibitors

Peptide-based inhibitors have been discovered to be effective on caspases more than 20 years ago (Thornberry et al., 1992). Adapted from the Caspase-1 cleavage sequence in its natural target proIL-1β, the peptide sequence Tyr-Val-Ala-Asp (Y-V-A-D) was incorporated into different inhibitors for Caspase-1. Impairment of Caspase-1 activity by these pseudo-substrates depends on covalent binding of the C-terminal group to the protease's active cysteine (Walker et al., 1994). This mode-of-action is in line with the competitive character of peptide inhibitors for Caspase-1 (Thornberry et al., 1992). As examples, the reversible inhibitor Ac-YVAD-CHO and the irreversible inhibitors Ac-YVAD-chloromethylketone (cmk) and Z-YVAD-fluoromethylketone (fmk) target Caspase-1. It was found that the kinetic properties of Caspase-1 on this polypeptide were comparable to that on proIL-1β (Thornberry et al., 1992). Later it was published that Trp-Glu-His-Asp (W-E-H-D) is actually preferred about 14-fold over YVAD by Caspase-1 as a recognition sequence (Rano et al., 1997). However, while Ac-YVAD-CHO, to some extend, also acts on caspase-4 and caspase-5, the inhibitor Ac-WEHD-CHO additionally blocked caspase-8 activity to a substantial degree (Garcia-Calvo et al., 1998). Caspase-8 belongs, in contrast to the inflammatory caspases-1, -4, and -5, to the family of apoptotic caspases. Reactivity on not only multiple caspases but also caspases of different functional groups is an important drawback of WEHD-based inhibitors. Thus, compounds employing the YVAD-motif are currently the most commonly used peptide inhibitors for Caspase-1.

More recently, several groups started developing peptidomimetic inhibitors for Caspase-1 aiming at higher specificity and potency with simultaneously offering practicable routes of administration and reasonable pharmacokinetics (Boxer et al., 2011; Hoglen et al., 2004; Rudolphi et al., 2003; Wannamaker et al., 2007). Among the tested compounds are the commercially available prodrug VX-765 and its active metabolite VRT-043198. This potent inhibitor showed a marked specificity for inflammatory caspases over apoptotic caspases and good oral availability (Wannamaker et al., 2007). Like the peptide-based inhibitors, the peptidomimetics also represent competitive inhibitors that target the active site of Caspase-1 (Stack et al., 2005).

1.5 Purpose of the study

In 2012, our group published data that served as the basis for the work at hand (Groß et al., 2012). This study described an important role for Caspase-1 in secretion of the non-substrate cytokine IL-1α in myeloid cells. It was not, as widely assumed (Dinarello, 2009), an indirect outcome of autocrine cell activation through inflammasome-dependent IL-1β. Instead, both IL-1 cytokines were shown to be released simultaneously and in an inflammasome-dependent manner. In addition, Groß *et al.* confirmed data, showing that surprisingly, while pharmacological inhibition of Caspase-1 blocked cleavage of proIL-1β, secretion of the unprocessed immature proIL-1β as well as IL-1α was not impaired. In contrast, genetic deletion of *Caspase-1* abolished secretion of both cytokines in response to different inflammasome activators. Similarly, cell death still occurred in the inhibited but not in the *Caspase-1* knockout cells. These findings suggested that Caspase-1 could control cell death and the secretion of substrate and non-substrate proteins independently of its protease activity.

The clinical relevance of impaired Caspase-1 activity has been demonstrated by Luksch *et al.* (Luksch et al., 2013). This group found several naturally-occurring genetics variants in the *Caspase-1* gene in patients suffering from unclassified autoinflammatory diseases. No alterations in other genes described to be relevant in comparable syndromes were detected. However, the different mutations identified led to a variably pronounced decrease in Caspase-1 activity. The observation that inactivation of Caspase-1 caused autoinflammation was unexpected. In addition to the *in vitro* data obtained using a Caspase-1 inhibitor, their results therefore highlight the importance of specifically investigating and distinguishing Caspase-1 activity-dependent and -independent functions *in vivo*.

To conclusively explore the processes underlying this disease-development, we decided to generate a new transgenic mouse model, expressing a catalytically inactive Caspase-1 from the native locus. This animal model had important advantages over alternative experimental approaches, like retroviral reconstitution *in vitro* or targeting into the Rosa26 locus. First, the physiological expression rates given, when modifying the native locus, were critical to avoid artifacts caused by unphysiologic expression of the mutant (or wild-type)

Caspase-1. Secondly, as it was not known which cell types were involved in the autoinflammatory pathology in patients, an animal model with expression of inactive enzyme in all cells types represented the most suitable approach.

Taken together, based on intriguing *in vitro* and *in vivo* results, the goal of this study was to explore and distinguish the protease activity-dependent functions of Caspase-1 as compared to potential, protease activity-independent functions *in vitro* and *in vivo*.

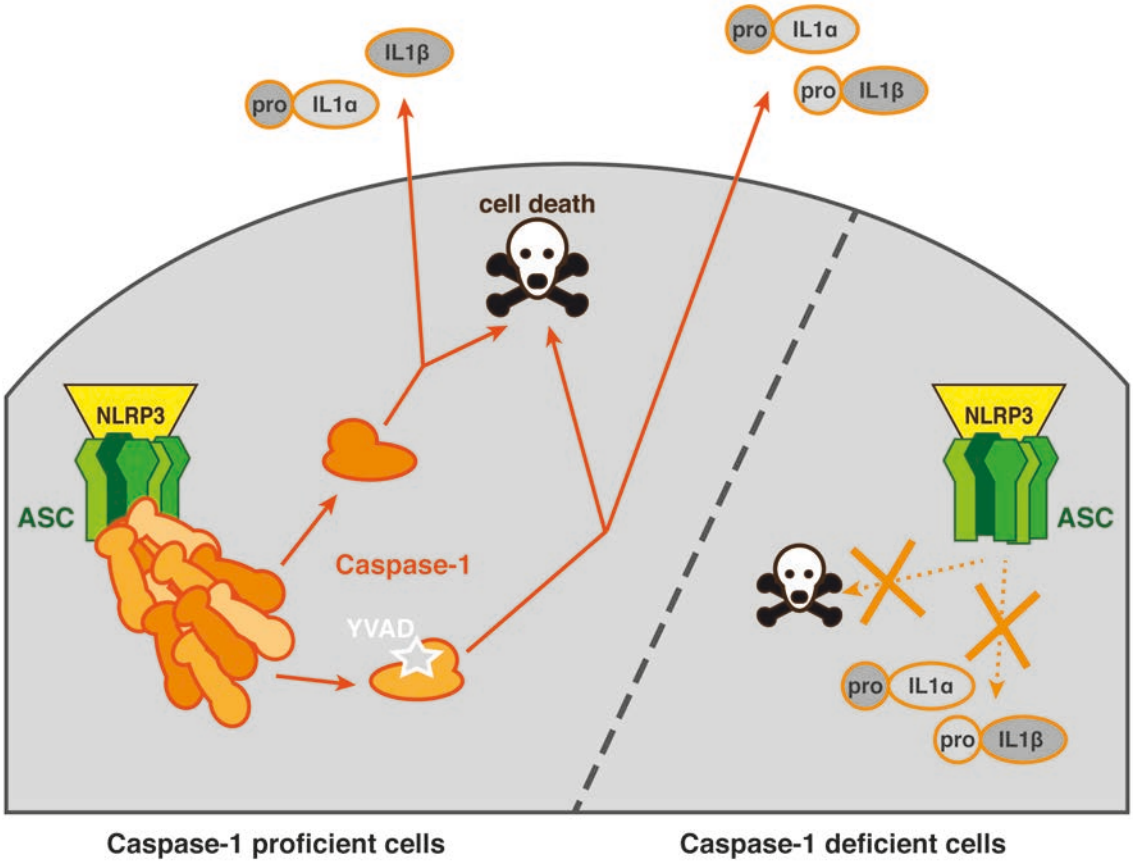

Figure 3: Caspase-1-dependent cell death and IL-1 secretion
Caspase-1 is responsible for secretion of IL-1 family cytokines and the induction of cell death following inflammsome activation as seen by comparison to Caspase-1-deficient cells. Chemical inhibition of Caspase-1 (YVAD) prevents cleavage of Caspase-1 substrates (proIL-1β) but still allows for cytokine secretion and cell death.

2 Materials and Methods

2.1 Materials

2.1.1 Primers

CL ASC-HA pcDNA3 *EcoR*I 5'	AATGAATTCATGGGGCGGGCACGAG
CL ASC-HA pcDNA3 *Xho*I 3'	ATACTCGAGAGCGTAATCTGGAACATCG TATGGGTATCCGCTCTGCTCCAGGTCC
CL C1 pcDNA3 *BamH*I 5'	TACGGGATCCTGCAAGATCTGCCACCAT GGCTG
CL C1 pcDNA3 *Not*I 3'	TACAGCGGCCGCTAGACTCGAGCGGTC ATTAATGTCC
CL Rip2 VSV-pCR3.1 *EcoR*I 5'	AACGAATTCAACGGGGACGCCATCT
CL Rip2 VSV-pCR3.1 *Xho*I 3'	ATCCTCGAGTTACAAGCTTTTATTCTGAG GGAAAATTTG
CL target. I LA fI 3'	CACTTACCTCCACGCGCTGCCTG
CL target. I LA fI 5'	GCGGCCGCACATGAAAGGAACACGCAA CTG
CL target. I LA fII 3'	GTCGACCCAGGGCCAATAAGCAGGAG
CL target. I LA fII 5'	CAGGCAGCGCGTGGAGGTAAGTG
CL target. I SA 3'	AAGCTTACCACGAGGATAAACTATGTAAC
CL target. I SA 5'	CCCGGGCATTTCCCTTCACTGGAGCATAG
CL target. I TA 3'	AAGCTTGTGGACTGCAAGAGTTCAGAAGAC
CL target. II LA fI 3'	GAATAATGATCACCTTGGGCTTGTCTTTCA AACTTGG
CL target. II LA fI 5'	CCCGGGTGTACTGGTGATATTCTGTGGT GAC
CL target. II LA fII 5'	CAAGCCCAAGGTGATCATTATTCAGGCAG CGCGTGGAG
CL target. II LA fIII 3'	AAGCTTTTCTTTCGCACCGTGAAGAC
CL target. II LA fIII 5'	CAAGCCCAAGGTGATCATTATTCAGGCAG CGCGTGGAG
CL target. II SA 3'	GTCGACGAACTAGCAAGGCTTCTGTAAC
CL target. II SA 5'	GCGGCCGCCTGAAGAACCCTGAGGCCATC
CL target. II TA 5'	GCGGCCGCCATCATTAGGGATCTCTCTGAC
CL target. III SA 3'	TCCGAAGCTTAAGCAGTTTGAAGAGCTAA AGACCA
CL target. III SA 5'	ATACCCGGGCATTTCCCTTCACTGGAGCA TAG

CL target. III TA 3'	TCGAAGCTTTTCTTTCGCACCGTGAAGAC
CL target. II LA fII 3'	GAATAATGATCACCTTGGGCTTGTCTTTC AAACTTGG
GT Casp1C284A 3'	CCAAGGGAATTATTGCTGTCTTG
GT Casp1C284A 5'	GTGATATTCTGTGGTGACTAACCGA
GT DEL Cre 3'	CGCATAACCAGTGAAACAGCAT
GT DEL Cre 5'	GAAAGTCGAGTAGGCGTGTACG
GT Neo 3'	GAAGAACTCGTCAAGAAGGCG
GT Neo 5'	ATGGGATCGGCCATTGAACAAG
GT Neodel II 3'	CACCACTCCTTGTTTCTCTTGAA
GT Neodel II 5'	ACCACTCGTACACGTCTTGC
GT Neodel III 3'	GGACTCATGGCTCCAGTTGCT
GT Neodel III 5'	CCTGCCCAGAGCACAAGACT
GT strat. II C284A 3'	CCAAGGGAATTATTGCTGTCTTG
GT strat. II C284A 5'	ATCGATCCCCGGGTGTACT
GT strat. III C284A 3'	CAGCCCAAGCTGATCCTCTAGA
GT strat. III C284A 5'	AGGAGATGGTGAAAGAGGTGAAAG
GT target. I TA 3' #4	GCATTCTTAAGCTAGAAACCTGTGGG
GT target. I TA 5' #4	AGTATAGGAACTTCCCGCTAGC
GT target. II TA 3' #1	CAGCCCAAGCTGATCCTCTAGA
GT target. II TA 5' #2	GAGACCACTAGAGTTGAATGCACC
GT target. III TA 3' #7	GGCCCAGGGATATTAGAATC
SB Casp1 3’ 3'	GAGGGTGGGGGTACAGGAAG
SB Casp1 3’ 5'	CCTTTTCTGCTGCTGTTGCC
SB Casp1 5’ 3'	TCTACACCGCAGAGCTACTGAAAC
SB Casp1 5’ 5'	TGACAGTAGATGCACACCTCTGC
SDM C1 D103N 3'	GAAGGATGTCCTCCTTTAGAATTTTCTG TAGCAACAAATGTTTCA
SDM C1 D103N 5'	TGAAACATTTGTTGCTACAGAAAATTCT AAAGGAGGACATCCTTC
SDM C1 D122N 3'	CTGGAAATGTGCCATTTTCTTTGTTCTG TTCTTCCTTTGTTTCT
SDM C1 D122N 5'	AGAAACAAAGGAAGAACAGAACAAAGAA AATGGCACATTTCCAG
SDM C1 D296N 3'	TCAGAGTCTCTTACTGAATTTTTTAACAA CACCACTCCTTGTTTC
SDM C1 D296N 5'	GAAACAAGGAGTGGTGTTGTTAAAAAATT CAGTAAGAGACTCTGA

SDM C1 D300N 3'	AATCCTCTTCAGAGTTTCTTACTGAATCTT TTAACAACACCACTC
SDM C1 D300N 5'	GAGTGGTGTTGTTAAAAGATTCAGTAAGA AACTCTGAAGAGGATT
SDM C1 D300N in D308N 3'	AATTCTCTTCAGAGTTTCTTACTGAATTTT TTAACAACACCACTC
SDM C1 D300N in D308N 5'	GAGTGGTGTTGTTAAAAAATTCAGTAAGA AACTCTGAAGAGAATT
SDM C1 D304N 3'	AAAAATTGCATCCGTTAAGAAATTCTCTTC AGAGTCTCTTACTGAAT
SDM C1 D304N 5'	ATTCAGTAAGAGACTCTGAAGAGAATTTC TTAACGGATGCAATTTTT
SDM C1 D308N 3'	CCATCATCTTCAAAAATTGCATTCGTTAAG AAATCCTCTTCAGAG
SDM C1 D308N 5'	CTCTGAAGAGGATTTCTTAACGAATGCAAT TTTTGAAGATGATGG
SDM C1 D308N in D304/313/314N 3'	CCATTATTTTCAAAAATTGCATTCGTTAAGA AATTCTCTTCAGAG
SDM C1 D308N in D304/313/314N 5'	CTCTGAAGAGAATTTCTTAACGAATGCAAT TTTTGAAAATAATGG
SDM C1 D308N in D313/314N 3'	CCATTATTTTCAAAAATTGCATTCGTTAAGA AATCCTCTTCAGAG
SDM C1 D308N in D313/314N 5'	CTCTGAAGAGGATTTCTTAAACGAATGCAAT TTTTGAAAATAATGG
SDM C1 D308N in D313N 3'	CCATCATTTTCAAAAATTGCATTCGTTAAGA AATCCTCTTCAGAG
SDM C1 D308N in D313N 5'	CTCTGAAGAGGATTTCTTAACGAATGCAATT TTTGAAAATGATGG
SDM C1 D308N in D314N 3'	CCATTCTCTTCAAAAATTGCATTCGTTAAGAA ATCCTCTTCAGAG
SDM C1 D308N in D314N 5'	CTCTGAAGAGGATTTCTTAACGAATGCAATT TTTGAAGATAATGG
SDM C1 D313/314N 3'	GGCCTTCTTAATGCCATTATTTTCAAAAATTG CATCCGTTAAGAAATCCTCTT
SDM C1 D313/314N 5'	AAGAGGATTTCTTAACGGATGCAATTTTTG AAAATAATGGCATTAAGAAGGCC
SDM C1 D313N 3'	TTCTTAATGCCATCATTTTCAAAAATTGCAT CCGTTAAGAAATCCTC
SDM C1 D313N 5'	GAGGATTTCTTAACGGATGCAATTTTTGAA AATGATGGCATTAAGAA
SDM C1 D314N 3'	GGCCTTCTTAATGCCATTATCTTCAAAAATT GCATCCGTTAAGAAAT

SDM C1 D314N 5'	ATTTCTTAACGGATGCAATTTTTGAAGATAA TGGCATTAAGAAGGCC
SQ pIRES-reverse	CCTCACATTGCCAAAAGACG
SQ pXLSN	CCCTTGAACCTCCTCGTTCGACC
SQ SP6	ATTTAGGTGACACTATAG
SQ T7	TAATACGACTCACTATAGGG
SQ targeting vector I #1	GCCTCTTCGCTATTACG
SQ targeting vector I #2	CTCCTGTAGCACACATTG
SQ targeting vector I #3	ATGCTGTCATCACTGACAG
SQ targeting vector I #4	TCTGTTCCATGCCAGAC
SQ targeting vector I #5	TGTGATCAACCCATGTG
SQ targeting vector I #6	GATGCAGTCAATATGAGTG
SQ targeting vector I #7	GACCACTAGAGTTGAATGC
SQ targeting vector I #8	TACAACCACTCGTACACG
SQ targeting vector I #9	GCACAAGACTTCTGACAG
SQ targeting vector I #10	AAGCTGATCCTCTAGAGTC
SQ targeting vector II #1	GATATTCAGGAATCAACCC
SQ targeting vector II #2	TTGAAGACAAGCCCAAG
SQ targeting vector II #3	GTAAGAGACTCTGAAGAGG
SQ targeting vector II #4	GAGCTCTGGAGGTACTG
SQ targeting vector II #5	ACAACAGACATGCATACAG
SQ targeting vector II #6	TGAACCCTAGAGTCACAC
SQ targeting vector II #7	TAGCTCTTCAAACTGCTTC
SQ targeting vector II #8	AGTATGTCATACCAATGCC
SQ targeting vector II #9	CTTTCAGACAGAACACAAG
SQ targeting vector II #10	ACTCTGGAAGCCTGGAC
SQ targeting vector II #11	TCAAGAGGCTACGAACAG
SQ targeting vector II #12	AGAAGCTGGTCGATCG
SQ targeting vector II #13	TCATAGCCTGAAGAACGAG

CL: cloning, GT: genotyping, SB: Southern blotting, SDM: site-directed mutagenesis, SQ: sequencing

All primers were obtained from Sigma-Aldrich Co. LLC.

2.1.2 Vectors

BAC RP23-424D5	Source BioScience
mNalp10-Falg-HA-pCR™ 3.1	generated by modification of pCR™ 3.1 in the group of Prof. Jürg Tschopp
Flag-pCR™ 3.1	generated by modification of pCR™ 3.1 in the group of Prof. Jürg Tschopp
gag-pol	Plasmid #14887, Addgene
pcDNA3	Invitrogen (Thermo Fisher Scientific Inc.)
pMSCV-IRES-GFP (pMIG)	Plasmid #9044, Addgene
pSPUC-DTA	was provided by Prof. Jürgen Ruland, Technical University Munich, Germany
VSV-G envelope	Plasmid #14888, Addgene
VSV-pCR™ 3.1	generated by modification of pCR™ 3.1 in the group of Prof. Jürg Tschopp

2.1.3 Kits

Mouse IL-1 alpha ELISA Ready-SET-Go! ®	eBioscience Inc.
Mouse IL-1 beta ELISA Ready-SET-Go!®	eBioscience Inc.
Mouse IL-1 beta Pro-form ELISA Ready-SET-Go!®	eBioscience Inc.
Mouse IL-6 ELISA Ready-SET-Go!®	eBioscience Inc.
Mouse TNF alpha ELISA Ready-SET-Go!®	eBioscience Inc.
NucleoBond® Xtra Midi kit	Macherey-Nagel
peqGOLD Gel Extraction Kit (C-Line)	VWR International GmbH
peqGOLD Plasmid Mini Prep Kit (C-Line)	VWR International GmbH
Promega CytoTox 96® Non-Radioactive Cytotoxicity kit	Promega Corporation
Random Primer DNA Labeling Kit	Takara Clontech Laboratories Inc.
RNeasy® Mini Kit	QIAGEN GmbH
TA Cloning® Kit, with pCR™2.1 Vector	Thermo Fisher Scientific Inc.

2.1.4 Antibodies

ASC (AL177)	rabbit	Adipogen AG
ASC (AL177 ATTO647N-conjugated)	rabbit	Adipogen AG
B220 APC-eFlour® 780-conjugated (RA3-6B2)	rat anti-mouse	eBioscience Inc.
Caspase-1 p10 (Casper-2)	mouse anti-mouse	Adipogen AG

Caspase-1 p20 (Casper-1)	mouse anti-mouse	Adipogen AG
CD11c APC-conjugated (N418)	rat anti-mouse	eBioscience Inc.
CD16/CD23 (clone 93)	rat anti-mouse	eBioscience Inc.
CD19 eFlour® 450-conjugated (1D3)	rat anti-mouse	eBioscience Inc.
CD21 FITC-conjugated (4E3)	rat anti-mouse	eBioscience Inc.
CD23 PE-Cyanine7-conjugated (B3B4)	rat anti-mouse	eBioscience Inc.
CD25 PE-conjugated (PC61.5)	rat anti-mouse	eBioscience Inc.
CD4 eFlour® 450-conjugated (RM4-5)	rat anti-mouse	eBioscience Inc.
CD8 APC-conjugated (5H10)	rat anti-mouse	Thermo Fisher Scientific Inc.
CD80 PE-conjugated (16-10A1)	rat anti-mouse	eBioscience Inc.
HA (16B12)	mouse	Abcam PLC.
HRP-conjudated anti-mouse IgG (goat)	goat	Jackson ImmunoResearch Inc.
HRP-conjugated anti-goat IgG (rabbit)	rabbit	SouthernBiotech
HRP-conjugated anti-hamster IgG (mouse)	mouse	BD Biosciences
HRP-conjugated anti-rabbit IgG (goat)	goat	Jackson ImmunoResearch Inc.
IgD APC-conjugated (11-26c)	rat anti-mouse	eBioscience Inc.
IgM PE-conjugated (II/41)	rat anti-mouse	eBioscience Inc.
IL-1α (ALF-161)	hamster anti-mouse	eBioscience Inc.
IL-1β (AF-401)	goat anti-mouse	R&D Systems Inc.
MHCII FITC-conjugated (M5/144.15.2)	rat anti-mouse	eBioscience Inc.
Nlrp3 (Cryo-2)	mouse anti-mouse	Adipogen AG
Tubulin (B512)	mouse	Sigma-Aldrich Co. LLC.
VSV Glycoprotein (P5D4)	mouse	Sigma-Aldrich Co. LLC.

2.1.5 Enzymes

Benzonase	Sigma-Aldrich Co. LLC.
*Dpn*I	New England Biolabs Inc.
FastDigest® *BamH*I	Fermentas (Thermo Fisher Scientific Inc.)
FastDigest® *Bgl*II	Fermentas (Thermo Fisher Scientific Inc.)
FastDigest® *EcoR*I	Fermentas (Thermo Fisher Scientific Inc.)
FastDigest® *Hha*I	Fermentas (Thermo Fisher Scientific Inc.)
FastDigest® *Hind*III	Fermentas (Thermo Fisher Scientific Inc.)
FastDigest® *Ndi*I	Fermentas (Thermo Fisher Scientific Inc.)
FastDigest® *Not*I	Fermentas (Thermo Fisher Scientific Inc.)
FastDigest® *Sal*I	Fermentas (Thermo Fisher Scientific Inc.)

FastDigest® *Xho*I	Fermentas (Thermo Fisher Scientific Inc.)
FastDigest® *Xma*I	Fermentas (Thermo Fisher Scientific Inc.)
*Not*I-HF	New England Biolabs Inc.
PeqGOLD Taq-DNA-polymerase	PEQLAB (VWR International GmbH)
PfuUltra High-Fidelity DNA polymerase	Agilent Technologies
Phusion® High-Fidelity DNA polymerase	Thermo Fisher Scientific Inc.
Protease from *Streptomyces griseus*	Sigma-Aldrich Co. LLC.
Proteinase K, recombinant, PCR Grade	Roche Diagnostics GmbH
SuperScript® III reverse transcriptase	Thermo Fisher Scientific Inc.
T4 ligase	Thermo Fisher Scientific Inc.

2.1.6 Reagents

[alpha-P32]dCTP	Hartmann Analytic GmbH
2-Proponal ROTIPURAN®	Carl Roth GmbH
Acetic acid (glacial)	Merck KGaA
Acrylamide/Bis Solution (30%)	Bio-Rad Laboratories GmbH
Agar-Agar	Carl Roth GmbH
Ammonium bicarbonate	Sigma-Aldrich Co. LLC.
Ammonium persulfate (APS)	Sigma-Aldrich Co. LLC.
Ampicillin sodium salt	Sigma-Aldrich Co. LLC.
BD™ CompBead (anti-rat and anti-hamster Ig κ/negative Control)	BD Biosciences
Brilliant Blue G Colloidal Concentrate	Sigma-Aldrich Co. LLC.
BSA	Sigma-Aldrich Co. LLC.
BSA, purified (20 mg/ml)	New England Biolabs Inc.
$CaCl_2$	Sigma-Aldrich Co. LLC.
Chloroform ≥99%	Sigma-Aldrich Co. LLC.
cOmplete Protease Inhibitor Cocktail	Roche Diagnostics GmbH
dATP (100mM)	Bioline GmbH
Direct PCR-Tail lysis reagent	PEQLAB (VWR International GmbH)
Disuccinimidyl suberate (DSS)	Thermo Fisher Scientific Inc.
Dithiobis(succinimidyl propionate) (DSP)	Thermo Fisher Scientific Inc.
Dithiothreitol (DTT)	Sigma-Aldrich Co. LLC.
dNTPs (100µM)	Bioline GmbH
Ethanol absolute EMSURE®	VWR International GmbH

Fixable Viability Dye eFluor® 506	eBioscience Inc.
GeneRuler™ 1kb DNA Ladder	Thermo Fisher Scientific Inc.
Glycerol	Sigma-Aldrich Co. LLC.
Glycine PUFFERAN®	Carl Roth GmbH
HCl (37%)	Sigma-Aldrich Co. LLC.
IGEPAL® CA-630	Sigma-Aldrich Co. LLC.
Illustra MicroSpin G-50 Columns	GE Healthcare Co.
Iodoacetamide	Sigma-Aldrich Co. LLC.
KCl	Sigma-Aldrich Co. LLC.
LE Agarose	Biozym Scientific GmbH
Lumigen ECL Ultra	Lumigen Inc.
Methanol ROTIPURAN®	Carl Roth GmbH
N,N,N',N-Tetramethylethylenediamine (TEMED)	Carl Roth GmbH
NaCl	Carl Roth GmbH
NaOH	Carl Roth GmbH
oligo(dT)$_{16}$	Sigma-Aldrich Co. LLC.
Paraformaldehyde (PFA)	Carl Roth GmbH
Phenol Red	Sigma-Aldrich Co. LLC.
Ponceau S	Sigma-Aldrich Co. LLC.
Precision Plus Protein™ Dual Color Standards	Bio-Rad Laboratories GmbH
Protein G Sepharose 4 Fast Flow	GE Healthcare Co.
Pyronin Y	Sigma-Aldrich Co. LLC.
Roti®-Phenol	Carl Roth GmbH
Rotiphorese® 10x TBE buffer	Carl Roth GmbH
Skim milk powder	Merck KGaA
Sodium azide	Merck KGaA
Sodium Citrate	Sigma-Aldrich Co. LLC.
Sodium dodecyl sulfate (SDS) Solution, 20 % (w/v)	Sigma-Aldrich Co. LLC.
Sodium dodecyl sulfate (SDS) Ultra Pure	Carl Roth GmbH
SYBR® Safe DNA Gel Stain	Thermo Fisher Scientific Inc.
Trichloroacetic acid	Sigma-Aldrich Co. LLC.
Tris base	AppliChem GmbH
Triton® X-100	Sigma-Aldrich Co. LLC.
Tryptone	Sigma-Aldrich Co. LLC.
Tween®-20	Sigma-Aldrich Co. LLC.
Vectashield Antifade Mounting Medium with DAPI	Vector Laboratories

Western Lightning Plus ECL	PerkinElmer Inc.
Yeast extract	Carl Roth GmbH

2.1.7 Cell culture reagents

0.05 % Trypsin-EDTA	Gibco™ (Thermo Fisher Scientific Inc.)
10x DPBS Solution -MgCl2, -CaCl2	Gibco™ (Thermo Fisher Scientific Inc.)
1x DPBS Solution -$MgCl_2$, -$CaCl_2$	Gibco™ (Thermo Fisher Scientific Inc.)
Ac-YVAD-cmk	Enzo Life Science Inc.
Plasticware	TPP Techno Plastic Products AG
DMSO	Sigma-Aldrich Co. LLC.
DMEM, high glucose, pyruvate	Gibco™ (Thermo Fisher Scientific Inc.)
EDTA	Sigma-Aldrich Co. LLC.
ESC culture plasticware	Falcon® (BD Biosciences)
FBS	Gibco™ (Thermo Fisher Scientific Inc.)
FBS ESC culture	PAN-Biotech GmbH
FuGENE HD®	Promega Co.
G-DEX™ II RBC Lysis Buffer	Intron Biotechnologies
G418 disulfate salt	Sigma-Aldrich Co. LLC.
H_2O (sterile, endotoxin-free)	B. Braun Melsungen AG
H_2O ad iniectabilia	Fresenius Kabi GmbH
Hank's Balanced Salt Solution (HBSS)	Gibco™ (Thermo Fisher Scientific Inc.)
HEPES (1M)	Gibco™ (Thermo Fisher Scientific Inc.)
L-Glutamin (200mM)	Gibco™ (Thermo Fisher Scientific Inc.)
LIF-containing cell culture supernatant	produced and provided by Prof. Thorsten Buch, University of Zurich, Switzerland
Lipofectamine® 2000	Thermo Fisher Scientific Inc.
MEM Non-Essential Amino Acids (100x)	Gibco™ (Thermo Fisher Scientific Inc.)
Millex-HV Filter, 0,45 µm, PVDF	Merck KGaA
Mitomycin C (from *S. caespitosus*)	Sigma-Aldrich Co. LLC.
Opti-MEM®	Thermo Fisher Scientific Inc.
Penicillin-Streptomycin (10,000 U/ml)	Gibco™ (Thermo Fisher Scientific Inc.)
Polybrene	Merck KGaA
rmGM-CSF	ImmunoTools GmbH
rmM-CSF	ImmunoTools GmbH
RPMI 1640 Medium, GlutaMAX™ Supplement	Gibco™ (Thermo Fisher Scientific Inc.)
β-Mercaptoethanol (50 mM)	Gibco™ (Thermo Fisher Scientific Inc.)

2.1.8 Stimuli

ATP	Sigma-Aldrich Co. LLC.
CpG oligodeoxynucleotides	InvivoGen
Curdlan	InvivoGen
E. coli K12 ultra-pure LPS	InvivoGen
MDP	Sigma-Aldrich Co. LLC.
MSU	Crystals were prepared as previously described (Martinon *et al.*, 2006)
Nigericin	Sigma-Aldrich Co. LLC.
Pam3CSK4	InvivoGen
poly(dA:dT)	Sigma-Aldrich Co. LLC.
R837	InvivoGen
R848	InvivoGen
TLR lgands	InvivoGen
Zymosan	InvivoGen

2.1.9 Cells

Embryonic feeder cells	murine embryonic fibroblasts	prepared from *Malt1+/PM* d11.5 embryos (G418-resistant) as described before (Jain *et al.*, 2014)
HEK293T	human embryonal kidney cells	originally generated by Gary Nolan, Stanford University (CRL-11268, ATCC®)
R1/E cells	embryonic stem cells, originating from a 129S1 x 129X1 mating	provided by Roland Naumann, Max Planck Institute of Molecular Cell Biology and Genetics, Dresden, Germany

2.1.10 Bacteria

NEB 5-alpha Competent *E.coli*	New England Biolabs Inc.
Salmonella enterica subspecies I Serovar *typhimurium* X3625 (ΔaroA)	provided by Prof. Bärbel Stecher, Max von Pettenkofer-Institute, University Munich, Germany
E. coli K-12 MG1655	provided by Prof. Bärbel Stecher, Max von Pettenkofer-Institute, University Munich, Germany

2.1.11 Equipment

8-chamber culture slides	BD Biosciences
Amersham Hybond-N+ membrane	GE Healthcare Co.
Amersham Protran 0.45 µm	GE Healthcare Co.
BioPhotometer plus	Eppendorf AG
Cell strainer, nylon (70 µm, 100 µm)	BD Biosciences
ChemoCam Imager	Intas Science Imaging Instruments GmbH
Eraser Screen-K	Bio-Rad Laboratories GmbH
FACS Canto II	BD Biosciences
Gene Pulser®	Bio-Rad Laboratories GmbH
Gene Pulser® Capacitane Enhancer	Bio-Rad Laboratories GmbH
Gene Pulser® Electroporation Cuvettes, 0.4 cm	Bio-Rad Laboratories GmbH
Gene Pulser® Pulse Controller	Bio-Rad Laboratories GmbH
Leica SP8 confocal microscope (63x1.40 oil objective)	Leica Microsystems
MaxiSorp® 96-well plates	Nunc (Thermo Fisher Scientifi Inc.)
Mini-PROTEAN® 3 Multi-Casting Chamber	Bio-Rad Laboratories GmbH
Mini-PROTEAN® Tetra Cell	Bio-Rad Laboratories GmbH
Mini-Trans-Blot® Cell	Bio-Rad Laboratories GmbH
MyCycler PCR cycler	Bio-Rad Laboratories GmbH
NanoDrop 2000c	Thermo Fisher Scientific Inc.
NuPAGE® 4-12% Bis-Tris Gels 1.5 mm x 15 well	Invitrogen™ (Thermo Fisher Scientific Inc.)
NuPAGE® Antioxidant	Invitrogen™ (Thermo Fisher Scientific Inc.)
NuPAGE® MES SDS Running Buffer (20x)	Invitrogen™ (Thermo Fisher Scientific Inc.)
Personal Molecular Imager™ System	Bio-Rad Laboratories GmbH
Storage Phosphor Screen BAS-MP 2040S	FujiFilm
UV Stratalinker 2400	Stratagene (Agilent Technologies)
VXR basic Vibrax	IKA®-Werke GmbH&Co KG
Widi Mini-Sub cell GT	Bio-Rad Laboratories GmbH

2.1.12 Buffers

50x TAE buffer

242 g/l Tris base
57.1 ml/l glacial acetic acid
100ml/l EDTA 0.5M (pH 8.0)

TNE buffer

50 mM Tris-HCl (pH 7.4)
100 mM NaCl
0.1 mM EDTA

20x SSC buffer

3 M NaCl
0.3 M Sodium Citrate
adjust to pH 7.0.

Wash buffer I (Southern blotting)

2x SCC buffer containing 0.2 % SDS.

Wash buffer II (Southern blotting)

0.2x SCC buffer containing 0.1 % SDS.

Neutralization Solution (Southern blotting)

1.5 M NaCl
1 M Tris pH 7.4
adjust to pH 7.4 with HCl.

Denaturation Solution (Southern blotting)

1.5 M NaCl
0.5 M NaOH

Church Buffer (Southern blotting)

1 mM EDTA
0.5 M Sodium Phosphate Buffer
7% SDS
1% BSA

ASC pellet lysis buffer

20 mM HEPES
10 mM KCl
1 % IGEPAL®
1mM DTT
1x Protease inhibitor cocktail
20 U/l Benzonase

Co-immunoprecipitation lysis buffer

50 mM Tris pH 7.4
150 mM NaCl
1 mM EDTA
1 % Triton-X100
1x cOmplete® Protease inhibitor cocktail

Imaging blocking buffer

1x DPBS containing 5 % FBS and 0.1 % Triton X-100.

PBST

PBS containing 0.1% Tween®-20.

1x Ponceau staining solution

0.05 % Ponceau S
3 % Trichloroacetic acid

3x SDS-PAGE sample buffer

187.5 mM Tris-HCl, pH 6.8
60 g/l SDS
0.03 % w/v Phenol Red
30 % w/v Glycerol
66 mM DTT

5x SDS-PAGE running buffer

15 g/l Tris base
72 g/l Glycine
5 g/l SDS

5x SDS-PAGE blotting buffer

2.5 g/l Tris base
12 g/l Glycine
15 % denatured ethanol

12 % Separating gel (SDS-PAGE)

250 ml/l Lower buffer
250 ml/l Acrylamide/Bis Solution (30%)
1.3 ml/l TEMED
10 ml APS
3 ml/l Pyronin Red
ad 1000 ml H2O

Stacking gel (SDS-PAGE)

250 ml/l Upper buffer
403 ml/l Acrylamide/Bis Solution (30%)
1.7 ml/l TEMED
5.9 ml APS
ad 1000 ml H2O

Lower buffer (SDS-PAGE)

182 g/l Tris base
4 g/l SDS
adjust to pH 8.8.

Upper buffer (SDS-PAGE)

61 g/l Tris base
4 g/l SDS
adjust to pH 6.8.

Blocking buffer

wash buffer containing 2 % skim milk powder.

FACS buffer

1x DPBS containing 2 % FBS.

2x HBS buffer

2xHBSS
280 mM NaCl
50 mM HEPES
1.5mM Na2HPO4
adjust pH to 6.95, 7.00, and 7.05 and test for best transfection efficiency.

HEK293T medium

DMEM containing 10 % FCS and 100 U/l Penicillin-Streptomycin.

BMDM medium

DMEM containing 10 % FCS, 100 U/l Penicillin-Streptomycin, and 40 ng/ml M-CSF.

BMDC medium

RPMI containing 10 % FCS, 100 U/l Penicillin-Streptomycin, 10 mM HEPES, 50 µM β-mercaptoethanol, and 20 ng/ml GM-CSF.

ESC medium

DMEM containing 20 % FBS, 100 U/l Penicillin-Streptomycin, 2 mM Glutamine, 50 µM β-mercaptoethanol, 1x MEM Non-Essential Amino Acid, and 0.5 ml LIF.

Feeder cell medium

DMEM containing 5 % FBS, 100 U/l Penicillin-Streptomycin, 2 mM Glutamine, 50 µM β-mercaptoethanol.

ESC freezing medium

ESC medium containing 10 % FBS and 10 % DMSO.

LB medium

10 g/l Tryptone
5 g/l Yeast extract
10 g/l NaCl

LB-agar

LB medium containing 15 g/l agar.

2.2 Methods

2.2.1 Generation of *Caspase-1*^{melted} mice

2.2.1.1 Cloning of the targeting vectors

The BAC clone RP23-424D5, prepared from a C57Bl/6J mouse was used as a genomic DNA template for generating the targeting vectors for the different strategies. First, the short homologous arms were amplified by PCR and successively cloned into the targeting vector. After completion, the long arms were synthesized and cloned into the targeting vectors already carrying the short arm fragments.

In detail, the obtained PCR products were analyzed by TAE agarose gel eletrophoresis and bands of the correct size were excised. DNA was purified from agarose slices using the PeqGOLD gel extraction kit according to the manufacturer's instructions. Poly(A)-tails were added to the eluted DNA by incubation with dATP and PeqGOLD Taq-DNA-polymerase (15 min at 72°C) prior to cloning into pCR™2.1-TOPO® TA vector following the standard protocol. Vectors were transformed into NEB 5-alpha Competent *E. coli*. DNA was isolated from single clone cultures using the peqGOLD Plasmid Mini Prep Kit according to the instructions. Integration of the respective inserts was investigated by restriction enzyme digestion of the prepared plasmids (targeting strategy I and III: short arm - *Xma*I and *Hind*III, long arm - *Not*I and *Sal*I; targeting strategy II: short arm - *Not*I and *Sal*I, long arm - *Xma*I and *Hind*III) and subsequent TBE agarose gel electrophoresis. Clones showing the expected band patterns were send to GATC Biotech AG for complete sequencing of the incorporated *Caspase-1* genomic sequence. When correct integration and absence of point mutations had been verified the short arms were subcloned into the targeting vector pSPUC-DTA. Inserts were excised from the pCR™2.1-TOPO® TA vector using the same restriction enzymes as for analytical digestion. The target vector pSPUC-DTA was digested with the identical enzymes. Both plasmids were run on a TAE agarose gel. Bands corresponding to the linearized vector and the inserts, respectively, were excised and DNA purified as before. Insert and vector were ligated in a 3:1 molar ratio by T4

ligase NEB 5-alpha Competent *E.coli*. Accuracy of the plasmids obtained from single clone colonies was tested by restriction digest and sequencing at GATC Biotech AG. Following positive evaluation the long arms were cloned into the targeting vector accordingly. Inserts were excised from the pCR™2.1-TOPO® TA vector and subcloned into pSPUC-DTA vectors already containing the short arms.

PCR short arm targeting vector I:

PCR conditions:		PCR program:		
0.5 µl	BAC RP23-424D5 (100 ng/ml)	98°C - 2’		
4 µl	buffer HF	98°C - 10’’		
0.4 µl	dNTPs (10 mM)	62°C - 20’’	x 30	
1 µl	primer target. I SA 5’ (10 µM)	72°C - 20’’		
1 µl	primer target. I SA 3’ (10 µM)	72°C - 2’		
0.2 µl	Phusion polymerase	4°C - ∞		
ad 20 µl	H_2O (ad injectabilia)	product: 570 bp		

PCR short arm targeting vector II:

PCR conditions:		PCR program:		
0.5 µl	BAC RP23-424D5 (100 ng/ml)	98°C - 2’		
4 µl	buffer HF	98°C - 10’’		
0.4 µl	dNTPs (10 mM)	62°C - 20’’	x 30	
1 µl	primer target. II SA 5’ (10 µM)	72°C - 20’’		
1 µl	primer target. II SA 3’ (10 µM)	72°C - 2’		
0.2 µl	Phusion polymerase	4°C - ∞		
ad 20 µl	H_2O (ad injectabilia)	product: 700 bp		

PCR short arm targeting vector III:

PCR conditions:		PCR program:		
0.5 µl	BAC RP23-424D5 (100 ng/ml)	98°C - 2’		
10 µl	buffer HF	98°C - 10’’		
2.5 µl	dNTPs (10 mM)	62°C - 30’’	x 30	
1.25 µl	$MgCl_2$ (50mM)	72°C - 50’’		
2.5 µl	primer target. III SA 5’ (10 µM)	72°C - 7’		
2.5 µl	primer target. III SA 3’ (10 µM)	4°C - ∞		
0.5 µl	Phusion polymerase	product: 1700 bp		
ad 50 µl	H_2O (ad injectabilia)			

The long arms were generated by multi-step PCRs. First, smaller fragments of the complete insert were amplified by PCR. These fragments had overlapping DNA sequences at their ends. In a second PCR two components were mixed together with external primers to obtain an enlarged fragment. The primers for the individual parts introduced, in some cases, mutations into the genomic sequence.

PCR long arm targeting vector I and III:

PCR conditions fragments I and II:	
1 µl	BAC RP23-424D5 (10 ng/ml)
10 µl	buffer HF
1 µl	dNTPs (10 mM)
2.5 µl	primer target. I LA fI 5' (10 µM)
2.5 µl	primer target. I LA fI 3' (10 µM)
	or
2.5 µl	primer target. I LA fII 5' (10 µM)
2.5 µl	primer target. I LA fII 3' (10 µM)
0.5 µl	Phusion polymerase
ad 50 µl	H_2O (ad injectabilia)

PCR program:		
98°C -	30''	
98°C -	10''	x 30
65°C -	30''	
72°C -	1'15''	
72°C -	7'	
4°C -	∞	

PCR products were purified and DNA eluted using 30 µl elution buffer.

PCR conditions overlap-PCR:	
2 µl	eluted Strat. 1 fI
2 µl	eluted Strat. 1 fII
10 µl	buffer HF
2.5 µl	dNTPs (10 mM)
1.25 µl	$MgCl_2$ (50mM)
2.5 µl	primer target. I LA fI 5' (10 µM)
2.5 µl	primer target. I LA fII 3' (10 µM)
1 µl	Phusion polymerase
ad 50 µl	H_2O (ad injectabilia)

PCR program:		
98°C -	30''	
98°C -	10''	x 8
58°C -	30''	
72°C -	1'20''	
- add primers		
98°C -	30''	
98°C -	10''	x 30
58°C -	30''	
72°C -	1'40''	
72°C -	7'	
4°C -	∞	

product: 5360 bp

PCR long arm targeting vector II:

PCR conditions fragments I - IV:	
1 µl	BAC RP23-424D5 (10 ng/ml)
10 µl	buffer HF
1 µl	dNTPs (10 mM)
2.5 µl	primer target. II LA fI 5' (10 µM)
2.5 µl	primer target. II LA fI 3' (10 µM)
	or
2.5 µl	primer target. II LA fII 5' (10 µM)
2.5 µl	primer target. II LA fII 3' (10 µM)
	or
2.5 µl	primer target. II LA fIII 5' (10 µM)
2.5 µl	primer target. II LA fIII 3' (10 µM)
0.5 µl	Phusion polymerase
ad 50 µl	H_2O (ad injectabilia)
ad 20 µl	H_2O (ad injectabilia)

PCR program:		
98°C -	30''	
98°C -	10''	x 30
64°C -	30''	
72°C -	1'10''	
72°C -	7'	
4°C -	∞	

PCR products were purified as above and two separate overlap-PCRs performed for fragment I plus fragment II and fragment II plus fragment III, respectively.

PCR conditions overlap-PCR:	
2 µl	eluted target. I fI
2 µl	eluted target. I fII
	or
2 µl	eluted target. I fII
2 µl	eluted target. I fIII
10 µl	buffer HF
2.5 µl	dNTPs (10 mM)
1.25 µl	$MgCl_2$ (50mM)
2.5 µl	primer target. I LA fI 5' (10 µM)
2.5 µl	primer target. I LA fII 3' (10 µM)
	or
2.5 µl	primer target. I LA fII 5' (10 µM)
2.5 µl	primer target. I LA fIII 3' (10 µM)
1 µl	Phusion polymerase
ad 50 µl	H_2O (ad injectabilia)

PCR program:		
98°C -	30''	
98°C -	10''	x 8
58°C -	30''	
72°C -	1'40''	
- add primers		
98°C -	30''	
98°C -	10''	x 25
58°C -	30''	
72°C -	1'40''	
72°C -	7'	
4°C -	∞	

The resulting fragments of the long arm were cloned into the pCR™2.1-TOPO® TA and transformed into NEB 5-alpha Competent *E.coli*. Resulting plasmids were digested by the restriction enzymes *Xho*I and *Ndi*I. *Ndi*I cuts within fragment II sequence and *Xho*I in the vector backbone. Afterwards the excised fragment I-II was cloned into the linearized vector carrying fragment II-III (total length LA targeting vector II: 5630 bp).

Test vectors to establish the screening PCRs for targeted stem cell clones resembled pSPUC-DTA vector containing extended short arms (test arms). As before, PCRs were performed to amplify the inserts and subsequently cloned into pCR™2.1-TOPO® TA. After sequencing, the test arms were shuttled into the final vector by use of the same enzymes as for the corresponding short arms.

PCR test arm targeting vector I:

PCR conditions:		PCR program:	
5 µl	BAC RP23-424D5 (10 ng/ml)	98°C - 2’	
4 µl	buffer HF	98°C - 10’’	x 30
0.4 µl	dNTPs (10 mM)	62°C - 20’’	
1 µl	primer target. I SA 5’ (10 µM)	72°C - 20’’	
1 µl	primer target. I TA 3’ (10 µM)	72°C - 2’	
0.2 µl	Phusion polymerase	4°C - ∞	
ad 20 µl	H_2O (ad injectabilia)	product: 890 bp	

PCR test arm targeting vector II:

PCR conditions:		PCR program:	
5 µl	BAC RP23-424D5 (10 ng/ml)	98°C - 2’	
4 µl	buffer HF	98°C - 10’’	x 30
0.4 µl	dNTPs (10 mM)	62°C - 20’’	
1 µl	primer target. II TA 5’ (10 µM)	72°C - 20’’	
1 µl	primer target. II SA 3’ (10 µM)	72°C - 2’	
0.2 µl	Phusion polymerase	4°C - ∞	
ad 20 µl	H_2O (ad injectabilia)	product: 1025 bp	

PCR test arm targeting vector III:

PCR conditions:		PCR program:		
5 µl	BAC RP23-424D5 (10 ng/ml)	98°C -	2’	
10 µl	buffer HF	98°C -	10’’	x 30
2.5 µl	dNTPs (10 mM)	65°C -	30’’	
1.25 µl	$MgCl_2$ (50mM)	72°C -	1’30’’	
2.5 µl	primer target. III SA 5’ (10 µM)	72°C -	7’	
2.5 µl	primer target. III TA 3’ (10 µM)	4°C -	∞	
0.5 µl	Phusion polymerase	product: 4300 bp		
ad 50 µl	H_2O (ad injectabilia)			

2.2.1.2 Stem cell culture and targeting of R1/E embryonic stem cells

R1/E murine embryonic stem cells (ESCs) were provided by Ronald Naumann at the Max Planck Institute of Molecular Cell Biology and Genetics in Dresden, Germany and were originally derived from mating of 129S1 to 129X1 mice. They were grown on a layer of Mitomycin C-treated embryonic fibroblasts (feeder cells). Feeder cells were prepared as described by Jain *et al.* from G418-resistant *Malt1+/PM* mice and passaged up to three times (Jain et al., 2014). When they reached confluence, mitosis was blocked by incubating the cells for 2-3 hours in feeder cell medium containing 10 µg/ml Mitomycin C. Afterwards, cells were thoroughly washed three times with 1x PBS before ESCs were plated onto them in ESC medium. The medium was changed daily and every second day ESCs were passaged onto fresh feeder cell plates (1:6). To this end, cells were incubated for 15 min with 0.05 % trypsin at 37°C. ESCs were singularized and feeder cells lysed by repeated forced pipetting.

For electroporation 300 µg targeting vector were digested overnight using 500 U *Not*I-HF. Success of the digestion was verified by agarose gel electrophoresis and the DNA extracted by phenol-chloroform-precipitation under sterile conditions. The plasmids were resuspended in sterile 1x DPBS and the concentration adjusted to 1 µg/µl as measured by NanoDrop 2000c. ESCs were harvested as described above, counted and adjusted to 6.4 $x10^6$ cells/ml in sterile 1x DPBS. An equivalent of 5 $x10^6$ cells/ml were mixed with 20 µl of the linearized vector. The mixture was transferred into Gene Pulser® Electroporation Cuvettes (0.4 cm) and electroporated using a Gene Pulser®

(340V, 250 µFD). Afterwards cells were left at room temperature for 5 min before they were plated in ESC medium on two 100 mm plates prepared with Mitomycin C-treated feeder cells. The day after the medium was replenished. On the second day post electroporation the medium was changed to ESC medium + G418 (250 µg/ml). Medium containing antibiotic was changed every second day. On day 9 surviving clones were harvested into 110 µl of ESC medium without G418. 40 % of the cell mass was seeded onto feeder cells in 96-well plates, 40 % in 96-well plates without feeder cells, and the remaining 20 % of eight clones were mixed for immediate analysis by PCR. These pooled samples were lysed by boiling in H_2O followed by and proteinase K digestion. The crude lysates were used as templates in the screening PCRs. In the same way lysates were prepared of the individual clones from sample pools, which gave a signal in the PCR, using the clone fraction that was plated without feeder cells at harvest. Positive clones were expanded on feeder cells from 96-well to 6-well format. 80 % of the ESC clones were frozen. The rest was replated without feeder cells and grown to confluence with daily medium changes. These cells were used for DNA preparation for Southern blotting.

2.2.1.3 Southern Blot analysis of R1/E stem cell clones

DNA from ESC clones was prepared by incubating the confluent cell layer (6-well) in 3 ml TNE buffer + 2U protease + 4U proteinase K overnight at 37°C. The next day DNA was purified from these lysates by a phenol-chloroform-extraction and adjusted to 1 µg/µl according to NanoDrop 2000c measurement. 15 µg DNA per sample were digested with 5 µl FastDigest *Hind*III or *EcoR*I for 14h at 37°C. Another 2 µl of enzymes were added and samples further incubated for 9h at 37°C. The reactions were loaded on a 0.7 % TAE agarose gel and run at 35 V for 20h. The gel was washed for 10 min with mild agitation in 0.25 M HCl. Prior to blotting the gel was rinsed in dH_2O, incubated 2x 20 min in denaturation solution, rinsed in dH_2O, incubated 2x 20 min in neutralization solution, and again rinsed in dH_2O. An upward transfer to Amersham Hybond-N+ membrane membrane was set up in 20x SSC buffer overnight. Transferred DNA was crosslinked to the membrane using the UV Stratalinker 2400 (70,000

µJoules x cm^2). The membranes were blocked for 1.5h at 64°C in pre-warmed Church buffer. *Caspase-1* specific probes were generated by PCR and purified using the peqGOLD Gel Extraction Kit. 50 ng of the probes were applied to [alpha-P32]dCTP-labeling using the Random Primer DNA Labeling Kit according to the instructions. Radioactively labeled probes were concentrated by the use of Illustra MicroSpin G-50 Columns. Immediately prior to addition to 12 ml of pre-warmed Church buffer the probes were boiled for 3 min at 95°C. The membranes were incubated with the probes overnight at 64°C with constant rotation. Afterwards, the membranes were successively washed for 10 min in room temperature wash buffer I, pre-warmed wash buffer I, pre-warmed wash buffer II, and finally room temperature wash buffer I. A Phosphor Screen was exposed to the membranes. After 7 days analyses were performed using a Personal Molecular Imager™ System.

Caspase-1 Southern blotting probes:

PCR conditions:		PCR program:		
2 µl	BAC RP23-424D5 (10 ng/ml)	98°C -	30''	
10 µl	buffer HF	98°C -	10''	x 30
1 µl	dNTPs (10 mM)	65°C -	30''	
2.5 µl	primer SB Casp1 5' 5' (10 µM)	72°C -	30''	
2.5 µl	primer SB Casp1 5' 3' (10 µM)	72°C -	7'	
	or	4°C -	∞	
2.5 µl	primer SB Casp1 3' 5' (10 µM)	product 5'-probe: 610 bp		
2.5 µl	primer SB Casp1 3' 3' (10 µM)	product 3'-probe: 590 bp		
0.5 µl	Phusion polymerase			
ad 50 µl	H_2O (ad injectabilia)			

2.2.1.4 PCR analysis of R1/E stem cell clones

By the use of the constructed targeting test vectors, highly sensitive screening PCRs were established. Different primer pairs and PCR conditions were tested in the presence of ESC lysate (equaling 500 cells) prepared as described under 2.2.1.2 to mimic the situation in ESC lysates. PCRs with a detection limit of three or less template copies were used for analysis of targeted ESC clone lysates.

Screening PCR targeting vector I:

PCR conditions:		PCR program:		
12 µl	ESC clone lysate (total 40 µl)	98°C - 2’		
8 µl	buffer HF	98°C - 10’’		
1.5 µl	dNTPs (10 mM)	64°C - 30’’	x 40	
0.4 µl	$MgCl_2$ (50mM)	72°C - 20’’		
2 µl	primer target. I TA 5’ #4 (10 µM)	72°C - 7’		
2 µl	primer target. I TA 3’ #4 (10 µM)	4°C - ∞		
0.4 µl	Phusion polymerase	product: 880 bp		
ad 40 µl	H_2O (ad injectabilia)			

Screening PCR targeting vector II:

PCR conditions:		PCR program:		
12 µl	ESC clone lysate (total 40 µl)	98°C - 2’		
8 µl	buffer HF	98°C - 10’’		
1.5 µl	dNTPs (10 mM)	64°C - 30’’	x 40	
2 µl	primer target. II TA 5’ #2 (10 µM)	72°C - 30’’		
2 µl	primer target. II TA 3’ #1 (10 µM)	72°C - 7’		
0.4 µl	Phusion polymerase	4°C - ∞		
ad 40 µl	H_2O (ad injectabilia)	product: 900 bp		

Screening PCR targeting vector III:

PCR conditions:		PCR program:		
12 µl	ESC clone lysate (total 40 µl)	98°C - 2’		
8 µl	buffer HF	98°C - 10’’		
0.8 µl	dNTPs (10 mM)	61°C - 30’’	x 40	
2 µl	primer target. III TA 5’ #4 (10 µM)	72°C - 1’30’’		
2 µl	primer target. III TA 3’ #7 (10 µM)	72°C - 7’		
0.4 µl	Phusion polymerase	4°C - ∞		
ad 40 µl	H_2O (ad injectabilia)	product: 1900 bp		

ESC clones showing site-specific recombination of the targeting vector were further tested for recombination of the *C284A* mutation in the *Caspase-1* gene. As the screening PCR for targeting vector I showed specificity issues only clones from targeting vector II and III were further investigated. A PCR spanning the potentially mutated site was performed. Subsequently, the PCR product was digested by the restriction enzyme *Hha*I, which specifically the mutated site.

Screening PCR *C284A* targeting vector II:

PCR conditions:

1 µl	ESC clone DNA (1 µg/µl)
8 µl	buffer HF
0.8 µl	dNTPs (10 mM)
2 µl	primer strat. II C284A 5' (10 µM)
2 µl	primer strat. II C284A 3' (10 µM)
0.4 µl	Phusion polymerase
ad 40 µl	H_2O (ad injectabilia)

PCR program:

98°C -	2'	
98°C -	10''	x 30
65°C -	30''	
72°C -	30''	
72°C -	7'	
4°C -	∞	

product: 900 bp

*Hha*I digestion:

10 µl	PCR product
2 µl	buffer
1 µl	FastDigest *Hha*I
ad 30 µl	H_2O (a.i.)

Incubated 30' at 37°C

products:
wt - 900 bp
C284A - 580 + 320 bp

Screening PCR *C284A* targeting vector III:

PCR conditions:

1 µl	ESC clone DNA (1 µg/µl)
8 µl	buffer HF
0.8 µl	dNTPs (10 mM)
2 µl	primer strat. III C284A 5' (10 µM)
2 µl	primer strat. III C284A 3' (10 µM)
0.4 µl	Phusion polymerase
ad 40 µl	H_2O (ad injectabilia)

PCR program:

98°C -	2'	
98°C -	10''	x 35
64°C -	30''	
72°C -	40''	
72°C -	7'	
4°C -	∞	

product: 1080 bp

*Hha*I digestion:

10 µl	PCR product
2 µl	buffer
1 µl	FastDigest *Hha*I
ad 30 µl	H_2O (a.i.)

Incubated 30' at 37°C

products:
wt - 1080 bp
C284A - 230 + 850 bp

2.2.1.5 Blastocyst injection of R1/E ESC clones

Injection of R1/E-derived ESC clones into C57Bl/6J blastocysts was performed by our collaboration partner Ronald Naumann at the Max Planck Institute of Molecular Cell Biology and Genetics in Dresden, Germany. Frozen ESC cell clones were send to his facility for this purpose.

2.2.1.6 Generation of *Caspase-1^{C284A}* transgenic mice in the C57Bl/6N background

C57Bl/6N ESCs were targeted using the provided targeting vector III by the PolyGene AG, Rümlang, Switzerland. Stem cell culture, PCR and Southern blotting quality control, blastocyst injection, and testing of chimeras for germline transmission were performed at PolyGene. The offspring of the chimeras, which were heterozygous for the *C284A* mutation, were sent to our facility in Munich for establishing the colony.

2.2.1.7 Genotyping PCRs of *Caspase-1^{C284A}* transgenic mice

Caspase-1^{C284A} mice of the 129- and C57Bl/6-background were genetically analyzed by the following PCR plus *Hha*I-digestion for comparison between wild-type, heterozygous, and homozygous animals. DNA from tail biopsies served as template. 1-2 mm tail biopsy were digested overnight shaking at 56°C in100 µl Direct PCR-Tail lysis reagent +0.1 U proteinase K. Samples were heat-inactivated by incubation at 85°C for 45 min.

Genotyping PCR *Caspase-1*^{C284}:

PCR conditions:		PCR program:		
1 µl	tail biopsy lysate	98°C -	2’	
4 µl	buffer HF	98°C -	10’’	x 30
0.4 µl	dNTPs (10 mM)	65°C -	30’’	
1 µl	primer GT Casp1C284A 5’ (10 µM)	72°C -	30’’	
1 µl	primer GT Casp1C284A 3’ (10 µM)	72°C -	7’	
0.2 µl	Phusion polymerase	4°C -	∞	
ad 20 µl	H_2O (ad injectabilia)	product: 880 bp		

*Hha*I digestion:

10 µl	PCR product
2 µl	buffer
0.5 µl	FastDigest *Hha*I
ad 30 µl	H_2O (a.i.)

Incubated 30' at 37°C

products:
wt - 880 bp
C284A - 380 + 500 bp

The first generation of mice, which have been crossed to the *DEL-Cre* line and afterwards to C57Bl/6J mice, were tested by a locus-specific Cre-PCR for elimination of the Cre gene from the genome. The "Neo-deleted" and "post-Cre" PCRs were applied to control for excision of the neomycin resistance cassette from the *Caspase-1* gene. The products of the latter PCR were digested by *Hha*I to distinguish between bands originating form wild-type and *melted* alleles.

Locus-specific *DEL-Cre*-PCR:

PCR conditions:		PCR program:		
1 µl	tail biopsy lysate	98°C -	2'	
4 µl	buffer HF	98°C -	10''	x 35
0.4 µl	dNTPs (10 mM)	61°C -	30''	
1 µl	primer DEL Cre 5' (10 µM)	72°C -	20''	
1 µl	primer DEL Cre 3' (10 µM)	72°C -	2'	
0.2 µl	Phusion polymerase	4°C -	∞	
ad 20 µl	H_2O (ad injectabilia)	product: 600 bp		

"Neo-deleted" PCR targeting vector II (*Caspase-1*^{C284A}-129):

PCR conditions:		PCR program:		
1 µl	tail biopsy lysate	98°C -	2'	
4 µl	buffer HF	98°C -	10''	x 30
0.4 µl	dNTPs (10 mM)	61°C -	30''	
1 µl	primer target. I TA 5' #4 (10 µM)	72°C -	40''	
1 µl	primer target. II LA 3' #1 (10 µM)	72°C -	7'	
0.2 µl	Phusion polymerase	4°C -	∞	
ad 20 µl	H_2O (ad injectabilia)	product: 730 bp		

"Neo-deleted" PCR targeting vector III (*Caspase-1*^{C284A}-B6):

Strategy 3:

PCR conditions:

1 µl	tail biopsy lysate
4 µl	buffer HF
0.4 µl	dNTPs (10 mM)
1 µl	primer target. I TA 5' #4 (10 µM)
1 µl	primer target. II LA 3' #1 (10 µM)
0.2 µl	Phusion polymerase
ad 20 µl	H_2O (ad injectabilia)

PCR program:

98°C -	2'	
98°C -	10''	x 30
66°C -	30''	
72°C -	1'30''	
72°C -	7'	
4°C -	∞	

product: 1400 bp

"Post-Cre" PCR targeting vector II (*Caspase-1*^{C284A}-129):

PCR conditions:

1 µl	tail biopsy lysate
4 µl	buffer HF
0.4 µl	dNTPs (10 mM)
1 µl	primer Neodel II 5' (10 µM)
1 µl	primer Neodel II 3' (10 µM)
0.2 µl	Phusion polymerase
ad 20 µl	H_2O (ad injectabilia)

PCR program:

98°C -	2'	
98°C -	10''	x 30
62°C -	30''	
72°C -	40''	
72°C -	7'	
4°C -	∞	

products:
wt - 1100 bp
C284A - 1200 bp
C284A-Neo - no product

*Hha*I digestion:

10 µl	PCR product
2 µl	buffer
0.5 µl	FastDigest *Hha*I
ad 30 µl	H_2O (a.i.)

Incubated 30' at 37°C

products:
wt - 1100 bp
C284A - 1000 + 200 bp

"Post-Cre" PCR targeting vector II (*Caspase-1*^{C284A}-129):

PCR conditions:

1 µl	tail biopsy lysate
4 µl	buffer HF
0.4 µl	dNTPs (10 mM)
1 µl	primer Neodel III 5' (10 µM)
1 µl	primer Neodel III 3' (10 µM)
0.2 µl	Phusion polymerase
ad 20 µl	H_2O (ad injectabilia)

PCR program:

98°C -	2'	
98°C -	10''	x 30
65°C -	30''	
72°C -	1'20''	
72°C -	7'	
4°C -	∞	

products:
wt - 1200 bp
C284A - 1300 bp
C284A-Neo - no product

*Hha*I digestion:

10 µl	PCR product
2 µl	buffer
0.5 µl	FastDigest *Hha*I
ad 30 µl	H_2O (a.i.)

Incubated 30' at 37°C

products:
wt - 1200 bp
C284A - 900 + 400 bp

2.2.2 Mice

On the basis of the original name for Caspase-1, interleukin-1β converting enzyme, short ICE, I termed the introduced inactivating *C284A* mutation *"melted" ("mlt")*. This designation is used throughout the text. Transgenic *Caspase-1* mutant mice derived from R1/E(129)- and C57Bl/6N-ESCs are referred to as *Caspase-1*$^{mlt/mlt}$*-129* and *Caspase-1*$^{mlt/mlt}$*-B6* mice, respectively. Prior to the Cre recombinase-mediated removal of the neomycin resistance cassette from the *Caspase-1* gene, the allele is called *mltNeo*. Caspase-1-melted or Caspase-1-mlt describes the protein.

Caspase-1^{melted}*-129 and Caspase-1*^{melted}*-B6, Nlrp3*$^{-/-}$ (Martinon et al., 2006), *Pycard*$^{-/-}$ *(Asc*$^{-/-}$*)* (Mariathasan et al., 2004), *ICE*$^{-/-}$ *(Caspase-1*$^{-/-}$*Caspase-4/11*$^{-/-}$*,* referred to here as *Caspase-1*$^{-/-}$*)* (Kuida et al., 1995), *B6.C-Tg(CMV-cre) 1Cgn/J (*referred to as *DEL-Cre*) (Schwenk et al., 1995), *Malt1*$^{+/PM}$ (Gewies et al., 2014) and C57Bl/6J (https://www.jax.org/strain/000664) mice were housed under specific pathogen-free (SPF) conditions at the Zentrum für Präklinische

Forschung at the Technical University Munich, Germany in accordance with local guidelines and FELASA recommendations (http://www.felasa.eu).

2.2.3 Immunophenotyping

Four 8 weeks-old *Caspase-1*$^{wt/wt}$ and *Caspase-1*$^{mlt/mlt}$*-129* mice each were sacrificed and spleens, thymi, one tibia and femur, and two cervical, two axillary, two inguinal, and one mesenteric lymph node were harvested per mouse. Mice and obtained organs were weighed. Organs were meshed through 70 µm cell strainers and red blood cell lysis performed on cells using G-DEX™ II RBC Lysis Buffer. Cells were counted using a hemocytometer and 1.5 x10^6 cells per organ and antibody-stain were plated on a 96-V-bottom plate. Following two washing steps with 1x DPBS, cells were resuspended in live/dead stain eFluor® 506 (1:1000 in 1x DPBS). After 30 min incubation at 4°C in the dark, cells were washed two times with FACS buffer before they were resuspended in antibody mixtures.

Stain I:
- CD21 FITC-conjugated
- IgM PE-conjugated
- IgD APC-conjugated
- CD23 PE-Cyanine7-conjugated
- B220 APC-eFlour® 780-conjugated
- CD19 eFlour® 450-conjugated
- CD16/CD23

Stain II:
- CD4 eFlour® 450-conjugated
- CD8 APC-conjugated
- CD25 PE-conjugated
- CD16/CD32

All antibodies were diluted 1:400 in FACS buffer except for anti-CD16/CD32, which was used at 1:200. Samples were stained for 30 min at 4°C in the dark. Prior to flow cytometry analysis by a FACS CantoII (BD Biosciences), cells were washed three times with FACS buffer. Compensation was performed using BD™ CompBeads, which had been labeled with anti-CD4 antibodies for all conjugates according to the manufacturer's protocol. DIVA software (BD Biosciences) was used for data acquisition and FlowJo (FlowJo, LLC) software for evaluation.

For differentiation analysis of BMDCs, cells of *Caspase-1$^{wt/wt}$-129* and *Caspase-1$^{mlt/mlt}$-129 mice* were harvested on day 4, 6, 7, and 8. 1x10^6 cells per well were plated on a 96-V-bottom plate. Wash steps, live/dead stain and antibody incubation was performed as described above.

Stain I: - CD11c APC-conjugated
- MHCII FITC-conjugated

Stain II: - 1c APC-conjugated
- CD80 PE-conjugated

Compensation for FACS analysis was performed using BMDCs stained individually with eFluor® 506, anti-CD11c-APC, -FITC, and -PE, before samples were measured by a FACS CantoII. As before, data analysis was carried out using DIVA and FlowJo software.

2.2.4 BMDC and BMDM culture and stimulation

BMDMs and BMDCs were prepared from the tibias and femurs of 6-30 weeks old mice as published in detail elsewhere (Schneider et al., 2013). Cells were grown in a humidified incubator at 37°C and 5 % CO_2 in the presence of recombinant murine (rm) M-CSF (BMDMs) or GM-CSF (BMDCs). After 6-9 days of differentiation, cells were harvested using 5 mM EDTA in 1x HBSS buffer. BMDCs and BMDMs were plated in 96-well plates at a density of 0.12-0.2 x10^6 cells per well in medium containing growth factor. All stimulations were performed in triplicates.

2.2.4.1 Bacterial culture for inflammasome stimulation

Overnight cultures of *E. coli* K-12 MG1655 (*E. coli*) and *Salmonella enterica* subspecies I Serovar *typhimurium* X3625 (ΔaroA) (*S. typhimurium*) were started from a glycerol stock in 3 ml sterile LB-medium without antibiotics. After 12 hours at 37°C and 250 rpm bacteria were subcultured in LB-medium diluted 1:20, 1:40, and 1:80 for another 3h at the same conditions. Samples with exponential growth rates were detected by measuring OD600 using a

BioPhotometer plus. Bacteria numbers were calculated based on a colony-forming unit (cfu) standard curve generated for the respective strain.

2.2.4.2 Inflammasome stimulation

For canonical inflammasome stimulation cells were primed with 50 ng/ml *E.coli* K12 ultra-pure LPS for 3 hours and afterwards treated with canonical inflammasome activators. Concentrations and incubation times of the stimuli were as follows: 5 mM ATP 30 min, 5 µM nigericin 30-45 min, 300 µg/ml MSU for 4h, 1 µg/ml poly(dA:dT) 3h (transfected with Lipofectamine® 2000, MOI20 *S. typhimurium* 2-3h, MOI5 *E. coli* 16h, R837 (Imiquimod) 15 µg/ml for 4h. Ac-YVAD-cmk was added to the cells at a concentration of 20 µM after 2.5 hours of priming and 30 min prior to inflammasome activation.
Cells were plated in Opti-MEM® medium for stimulation of the non-canonical inflammasome and primed with 1 µg/ml Pam3CSK4 for 4h. For LPS transfection 2 µg LPS and 0.5 µl FuGENE HD® were diluted in 100 µl Opti-MEM®. After 15 min of incubation the reaction was added to the well. The experiment was stopped after 16h.

2.2.4.3 TLR and MDP stimulation

For stimulation of TLRs cells were treated for 6h with the following concentrations of agonists: 20 ng/ml LPS, 10 µg/ml CpG DNA, 1 µg/ml R848, 0.1 µg/ml Pam3CSK4, 0.1 mg/ml Zymosan, 0.1 mg/ml Curdlan.
Prior to stimulation of Nod2 cells were primed with 20 ng/ml LPS or left untreated for 3h. Subsequently MDP was added at a concentration of 10 µg/ml and incubated with the cells for 16h. Nigericin was used as a control for inflammasome activation at 5 µM for 40 min.

2.2.4.4 Analysis of BMDM and BMDC stimulations

Cell-free supernatants were analyzed by ELISA. ELISA kits from eBioscience for murine cytokines were used according to the manufacturer's instructions to

quantify concentrations of TNFα, IL-6, IL-1α, proIL-1β, and IL-1β. Values are given as mean ± standard error of the mean (SEM).

For Western blot analysis triplicates of cell-free supernatants were pooled and combined with 3x sample buffer. Cell lysates were prepared by lysing the cells on the plate in 1x sample buffer and triplicates were pooled. Supernatants and lysates were subjected to SDS-PAGE and afterwards blotted to a nitrocellulose membranes according to the protocol in Schneider *et al.* (Schneider et al., 2013). Primary antibodies were diluted 1:2000 in 2% skim milk powder in PBST + 0.05 % azide. They comprise anti-mouse caspase-1 p20, anti-mouse caspase-1 p10, anti-mouse IL-1β, anti-mouse IL-1α, anti-mouse Nlrp3, anti-ASC, anti-HA, anti-VSV-Glycoprotein, and mouse anti-α-tubulin.

Cell death was determined by measuring LDH using the Promega CytoTox 96® Non-Radioactive Cytotoxicity kit according to the protocol. Medium served as blank value and was subtracted from the sample values. Results were plotted in a ratio of 100 % dead cells in comparison to freeze-thaw-lysed cycles.

2.2.5 Mass spectrometry analysis

BMDCs were plated at 1.5 x10^7 cells per 100 mm plate and primed with 20 ng/ml LPS for 3h. Afterwards, four plates per genotype were treated with 5 µM nigericin for 40 min and one plate was left untreated. Replicates were kept individually at all times. Cells were lysed on the plates in lysis buffer. Cell lysates were harvested into tubes and homogenized on a VXR basic Vibrax (2000 rpm, 15 min, 4°C). A sample of cell lysate was taken prior to centrifugation (3000 x g, 10 min, 4°). The supernatant (soluble fraction) was collected, while the pellet was washed with lysis buffer, and spun at 13,000 x g, 10 min, 4°C. The wash buffer was aspirated and the pellet resuspended in 1x DPBS. Samples of cell lysates, soluble fraction, and pellet were mixed with 3x sample buffer and Western blot analysis was preformed.

For the crosslinker approach, cells were carefully washed two times with 1x DPBS after 25 min of nigericin stimulation. Subsequently dithiobis(succinimidyl propionate) (DSP) was added at 1 mM in 1x DPBS. The reaction was stopped by addition of Tris pH 7.4 to a final concentration of 10 mM. Samples were

prepared as before but omitting DTT from the lysis buffer to prevent premature cleavage of crosslinked proteins.

Pellet samples were run on a SDS-PAGE together with a BSA-dilution series. Following electrophoresis, the gel was placed in 2% acetic acid in 40% methanol for 1h. Afterwards, proteins were visualized by incubation of the gel in Coomassie blue staining solution (16% Brilliant Blue G Colloidal Concentrate in 20% methanol) for 10 min. Background signal was destained by several washing steps (1.5 % acetic acid in 25 % methanol, 5 min; 2.-5. 25 % methanol, 30 min). The amount of protein per sample was estimated from a comparison to the signal intensities of the BSA-standard.

An equivalent of 8 µg protein were subjected to alcylation of the pellet samples in preparation for mass spectrometry. First, samples were diluted in 1x sample buffer +DTT. Iodoacetamide in ammonium bicarbonate buffer (50 mM) was added in double the concentration of DTT. Samples were incubated in the dark at room temperature for 30 min. Immediately afterwards the reactions underwent SDS-PAGE. NuPAGE® 4-20% Bis-Tris gels and NuPAGE® MES SDS Running Buffer were used and electrophoresis was stopped as soon as the samples had entered the separating gel. Coomassie staining was performed as described above and the gel stored in 1 % acetic acid at 4°C.

Mass spectrometry analysis was done by our collaboration partner Guillaume Médard in the group of Prof. Bernhard Küster at the Chair of Proteomics and Bioanalytics at the Technical University Munich. An Orbitrap Velos mass spectrometer (Thermo Fisher Scientific Inc.) was used and Data analysis performed using MaxQuant (version 1.5.1.0) with the integrated search engine Andromeda.

2.2.6 Immunofluorescence imaging

Immunofluorescence staining and imaging were performed by Dr. Ritu Mishra from our group. BMDMs were seeded at 8 $\times 10^5$ cells/well in 8-chamber culture slides for immunofluorescence imaging. Cells were primed for 2h with 50 ng/ml LPS. Afterwards, they were stimulated with nigericin at 10 µM for 45 min or left untreated. For chemical inhibition of Caspase-1, Ac-YVAD-cmk (20 µM) was

applied to the cells after 1.5h of priming and 30 min prior to nigericin-stimulation. Subsequently, the cells were washed with 1x DPBS, fixed for 10 min in 4 % paraformaldehyde, and extracted in DPBS + 0.1 % (v/v) Triton® X-100 for 5 min. Inflammasome formation was stained for by anti-ASC antibody conjugated to ATTO 647 and anti-Caspase-1 p10 antibody diluted 1:200 in blocking buffer (1x DPBS + 5 % FBS + 0.1 % Triton® X-100). Staining was completed by incubation with an anti-mouse secondary (coupled to Alexa 488). Finally, slides were mounted in Vectashield containing DAPI (Vector Laboratories). Images of the immunostained cells were taken with constant laser setting on a Leica SP8 confocal microscope equipped with a 63×/1.40 oil objective. To observe all the specks in the region, a z-stack of a region of interest was obtained. The depicted images are a maximum projection of the respective z-stacks.

2.2.7 Cloning of expression vectors

Coding sequence of murine *Caspase-1*, *ASC*, and *Ripk2* were amplified from cDNA. First, RNA was prepared from BMDCs of wild-type mice using the RNeasy® Mini Kit according to the manufacturer's instructions. 1 µg of RNA was transcribed into cDNA based on oligo$(dT)_{16}$ primers by SuperScript® III reverse transcriptase according to the manufacturer's instructions. The resulting cDNA served as template for PCRs. Sites for restriction enzymes were incorporated into the primer sequences and thereby added to the coding sequences for the different proteins. In some cases a Kozak sequence was also included or start and stop codons deleted or mutated. Following PCR, the PCR product as well as the target vector were cleaved by the respective restriction enzymes and afterwards purified by the peqGOLD Gel Extraction Kit according to the instructions. Ligated plasmids were transformed into NEB 5-alpha Competent *E.coli*. Correct insertion was confirmed by restriction digestion and sequencing at GATC Biotech AG.

Caspase-1-pcDNA3:

1 µl	BMDC cDNA
10 µl	buffer HF
2.5 µl	dNTPs (10 mM)
1.25 µl	$MgCl_2$ (50mM)
1.5 µl	primer C1 pcDNA3 *BamH*I 5' (10 µM)
1.5 µl	primer C1 pcDNA3 *Not*I 3' (10 µM)
0.5 µl	Phusion polymerase
ad 50 µl	H_2O (ad injectabilia)

PCR program:

98°C -	2'	
98°C -	10''	x 30
65°C -	30''	
72°C -	30''	
72°C -	7'	
4°C -	∞	

product: 1200 bp

Restriction enzymes: FastDigest *BamH*I, FastDigest *Not*I

Target vector: pcDNA3

ASC-Flag-pCR™ 3.1:

1 µl	BMDC cDNA
10 µl	buffer HF
1 µl	dNTPs (10 mM)
2.5 µl	primer ASC-HA pcDNA3 *EcoR*I 5' (10 µM)
2.5 µl	primer ASC-HA pcDNA3 *Xho*I 3' (10 µM)
0.5 µl	Phusion polymerase
ad 50 µl	H_2O (ad injectabilia)

PCR program:

98°C -	2'	
98°C -	10''	x 30
63°C -	30''	
72°C -	40''	
72°C -	7'	
4°C -	∞	

product: 590 bp

Restriction enzymes: FastDigest *BamH*I, FastDigest *Xho*I

Target vector: pcDNA3

Ripk2-VSV-pCR™ 3.1:

10 µl	BMDC cDNA
10 µl	buffer HF
1 µl	dNTPs (10 mM)
2.5 µl	primer Rip2 VSV-pCR3.1 *EcoR*I 5' (10 µM)
2.5 µl	primer Rip2 VSV-pCR3.1 *Xho*I 3' (10 µM)
0.5 µl	Phusion polymerase
ad 50 µl	H_2O (ad injectabilia)

PCR program:

98°C -	2'	
98°C -	10''	x 35
60°C -	30''	
72°C -	1'15''	
72°C -	7'	
4°C -	∞	

product: 1620 bp

Restriction enzymes: FastDigest *BamH*I, FastDigest *Xho*I

Target vector: pcDNA3

The different mutants of *Caspase-1* were designed by site-directed mutagenesis of *Caspase-1*^{wt}-pcDNA3 or *Caspase-1*-pcDNA3 mutants. To this end, complementary, HPLC-purified primers containing the desired mutation were used in a PCR, which copied the complete plasmid. Subsequently, parental DNA was digested by the restriction enzyme *Dpn*I and the remaining plamids were transformed into NEB 5-alpha Competent *E.coli*. Successful mutation was confirmed by sequencing at GATC Biotech AG.

Caspase-1 site-directed mutagenesis:	
1.5 µl	*Caspase-1*-pcDNA3 (10 ng/µl)
2.5 µl	buffer
0.5 µl	dNTPs (10 mM)
0.7 µl	HPLC-purified primer 5' (10 µM)
0.7 µl	HPLC-purified primer 3' (10 µM)
0.5 µl	Pfu Ultra HF polymerase
ad 25 µl	H_2O (ad injectabilia)

PCR program:		
95°C -	1'	
95°C -	30''	x 14
65°C -	1'	
72°C -	7'30''	
72°C -	10'	
4°C -	∞	

The *Caspase-1*^{nc}-pcDNA3 mutant was subcloned into the pMSCV-IRES-GFP vector. *Caspase-1*^{nc} was excised from pcDNA3 and pMSCV-IRES-GFP was linearized by incubation with the FastDigest restriction enzymes *Bgl*II and *Xho*I. Both components were purified using the peqGOLD Gel Extraction Kit, ligated and transformed into NEB 5-alpha Competent *E.coli*. Sequencing at GATC Biotech AG proved accuracy of the generated plasmid.

Tagged Caspase-1-mlt was generated by amplification of *Caspase-1*^{mlt} form *Caspase-1*^{mlt}-pcDNA3 using a primer containing the sequence of a HA-tag. The PCR product was digested by the FastDigest restriction enzymes PstI and *Xho*I. The target vector Flag-pCR™ 3.1 was prepared accordingly. peqGOLD Gel Extraction Kit -purified DNA was ligated and transformed into NEB 5-alpha Competent *E.coli*. Correct insertion of the insert into the plasmid and in-frame orientation of the 5-prime HA-tag and the 3-prime Flag-tag were demonstrated by sequencing at GATC Biotech AG.

2.2.8 Plasmid preparation from bacteria using mini und midi preps

For cloning purposes, transformed bacteria were streaked out onto LB-agar plates containing 100 µg/ml ampicillin. Plates were incubated at 37°C. 3 ml LB-medium were inoculated with single colonies and propagated at 37°C with shaking. Plasmids were prepared using the peqGOLD Plasmid Mini Prep Kit according to the manufacturer's protocol. For larger amounts of plasmid, bacteria were grown in 200-300 ml LB-medium and DNA purified using the NucleoBond® Xtra Midi kit from Macherey-Nagel.

2.2.9 Transfection of HEK293T cells

HEK293T cells were plated to a confluence of 70-90% at the time of transfection. Where various amounts of plasmids were transfected into different samples, total DNA concentrations were normalized among all samples by addition of empty vector (pcDNA3). Plasmids were diluted in H_2O a.i. and mixed with $CaCl_2$ to a final concentration of 25 mM (transfection mix + medium). The same volume of 2x HBS buffer was pipetted dropwise to the DNA while vortexing. Following 15 min incubation, the mixture was added to the cells. The medium was changed after 5-6 hours and cell lysates were generated by resuspending the cells in 1x sample buffer 24-36 hours post transfection.

2.2.10 Retroviral transduction

HEK293T cells were used for retrovirus production. On two successive days cells were plated on a 100 mm dish to a confluence of 70-90% and transfected with *Caspase-1*^{nc}-pMSCV-IRES-GFP, gag-pol, and VSV-G envelope using Lipofectamine® 2000. After 24 hours the medium was changed to BMDM-medium without M-CSF. Additional 24 hours later the supernatant containing the viral particles was harvested and filtered through a 45 µm filter. Polybrene was added to a final concentration of 4 µg/ml. Day 1 BMDMs of *Caspase-1*$^{-/-}$ and *Caspase-1*$^{mlt/mlt}$*-129* mice were harvested, counted, and 7 x10^6 cells mixed with half the volume of viral supernatant. Cells were plated in 6-well plates and spun for 2h at 35°C and 1000 x g. After that, BMDM-medium +M-CSF was

added to the cells. 24 hours later the transduction was repeated using virus harvested from the second set of transfected HEK293T cells. During the medium change on the following day a few cells were removed from the culture. These cells were analyzed for successful transduction by assessing GFP-expression via FACS analysis. On day 8, BMDMs were harvested and subjected to inflammasome activation as described in 2.4. Samples were analyzed by Western blotting.

2.2.11 Co-immunoprecipitation

HEK293T cells were transfected (see 2.10) with combinations of *Caspase-1*^{wt}-pcDNA3, *Caspase-1*^{nc}-pcDNA3, *Caspase-1*^{mlt}-pcDNA3, or *mNalp10*-Falg-HA-pCR™ 3.1 with *Ripk2*-VSV-pCR™ 3.1. 30h after transfection cells were washed and harvested using ice-cold 1x DPBS. The cell pellet was resuspended in lysis buffer and homogenized using the VXR basic Vibrax (2000 rpm, 15 min, 4°C). Samples of the cell lysates were taken and mixed with 3x sample buffer for Western blot analysis. The rest of the samples was centrifuged (13,000 x g 10 min, 4°C) and the supernatant used for immunoprecipitation. An aliquot of the supernatant was also kept for Western blotting. 1 µg anti-VSV glycoprotein antibody was mixed with the supernatants and rotated at 4°C. After 1h, Protein G Sepharose 4 Fast Flow beads, which previously had been washed three times with lysis buffer, were resuspended in the solutions. Binding of the antibody-protein-complexes to the bead was allowed overnight at 4°C. Afterwards, the beads were washed four times with lysis buffer. 1x sample buffer was added to the beads and samples were boiled for 5 min at 95°C to elute proteins. Cell lysates, supernatants, and bead fractions were analyzed by Western blotting.

3 Results

3.1 Generation of *Caspase-1^{melted}* transgenic mice

3.1.1 Targeting and Screening of R1/E (129S1/X1) embryonic stem cells

Three different targeting vectors were generated for introducing the inactivating *C284A* (*melted*, *mlt*) point mutation into exon 6 of the murine *Caspase-1* genomic locus. The mutation introduced was a change from the sequence GCATGCCGT to GCAGCGCGT, which translates into the amino acid (aa) sequence AAR instead of ACR. At the same time, the introduced mutation generated a *Hha*I restriction site (GCG^C) that is used for screening purposes (see below). Wilson *et al.* showed that mutation of the active site cysteine completely abolished Caspase-1 activity (Wilson et al., 1994). The *C284A* mutation was introduced into the long homology arms of the targeting constructs close to the neomycin restriction cassette (Figure 4A, B). The three different vectors were based on two different targeting strategies. Strategy I/III and strategy II differed in the orientation of the long and short homology arms relative to the neomycin resistance cassette and the point mutation. As a result, the *loxP* site remaining in the genome is located either in the intron between exon 5 and 6 or in the intron between exon 7 and 8 (Figure 4B). Targeting vector I and III only varied in the length of their short homology arm. Figure 4B shows the results of recombination of the different targeting vectors with the murine *Caspase-1* locus. *Not*I-linearized targeting vectors I - III were used for electroporation into R1/E (129S1/X1) embryonic stem (ES) cells. Electroporation of all three targeting vectors resulted in G418-resistant ESC clones.

Prior to starting ESC culture, screening PCRs were established to analyze clones for recombination of the targeting vectors with the *Caspase-1* gene. These screening PCRs were optimized for sensitivity and have a detection limit of 3-10 copy numbers of template DNA. Sensitivity was assessed using test plasmids carrying the PCR template sequence (data not shown).

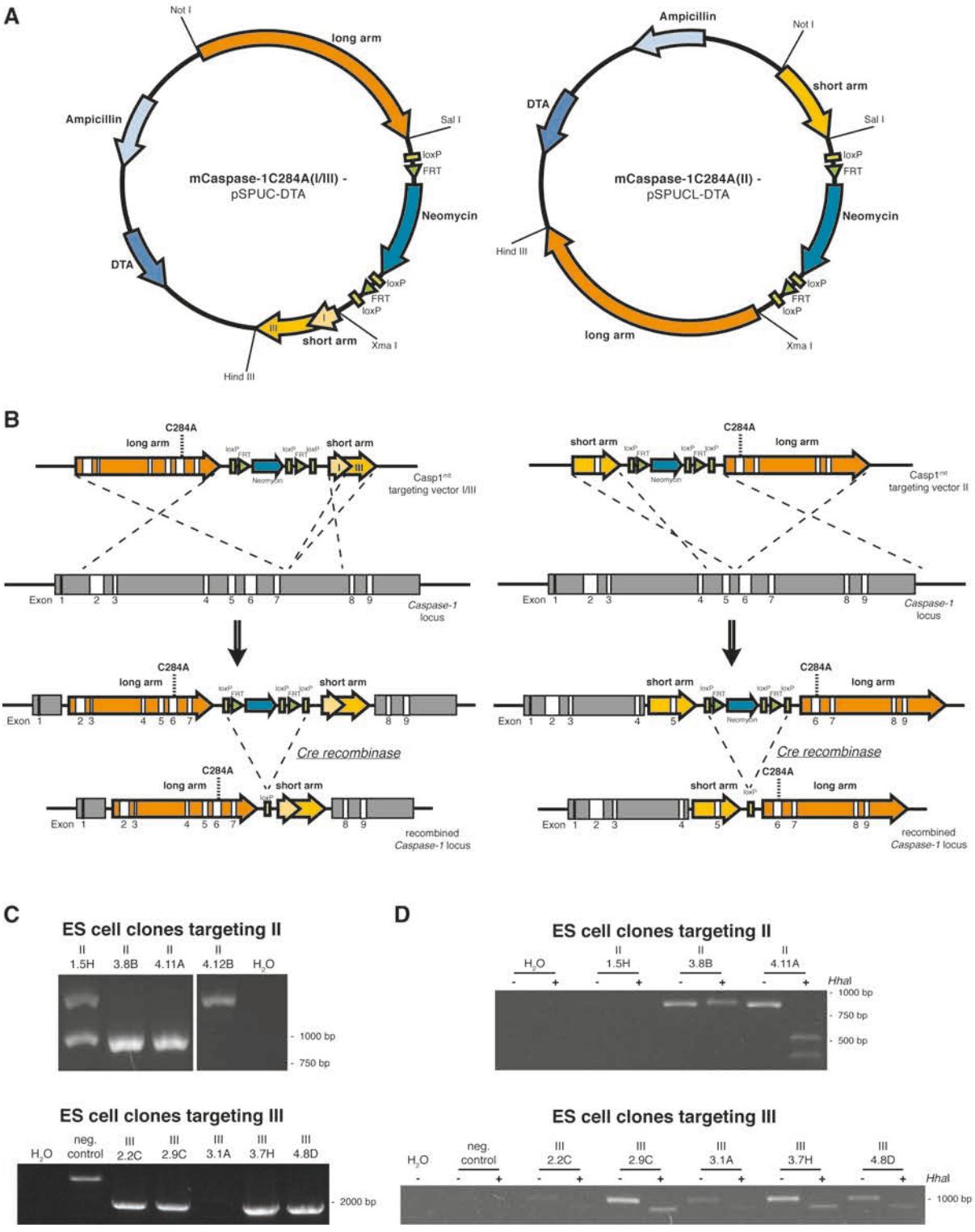

Figure 4: *Caspase-1*^{melted} targeting strategies
(A) Three different targeting vectors (I-III) were generated for introduction of the *melted* mutation (*C284A*) into the murine *Caspase-1* gene. Targeting vectors I and III differ in the lengths of their short homologous arms (570 bp and 1700 bp, respectively). (B) Different integration strategies between vectors I/III (left) and vector II (right). Cre-mediated removal of the resistance-cassette results in the final *Caspase-1*^{melted} loci (B, bottom panel). (C) ESC clones were tested for site-specific recombination by PCR (positive clones vector II= 0.9 kb; vector III= 1.9 kb. (D) ESC clones were analyzed by PCR for integration of the *C284A* point mutation into the *Caspase-1* locus. *C284A* mutation was confirmed by specific *Hha*I restriction digestion (vector II: wt= 800 bp, mlt= 530 + 380 bp; vector III: wt= 1080 bp, mlt= 850 bp + 230 bp (smaller fragment not shown)).

I screened crude cell lysates of 400 G418-selected stem cell clones per targeting vector for integration into the *Caspase-1* gene by PCR. Two clones positive for the PCR product of 900 bp were detected by the screening PCR for electroporation of vector II (II-3.8B, II-4.11A) (Figure 4C, top). Four clones originating from electroporation of vector III (III-2.2C, III-2.9C, III-3.7H, III-4.8D) showed PCR signals at 1.9 kb and were therefore considered as correctly targeted (Figure 4C, bottom). The screening PCR for ESC clones resulting from electroporation with vector I proved to lack specificity under real conditions (data not shown). Therefore, clones from this electroporation cycle could not be further investigated.

ESC clones positive in these screening PCRs, were tested for introduction of the desired point mutation into the *Caspase-1* gene (*C284A*) by PCR *C284A*. The genomic region around the mutation was amplified by PCR and the product was digested using the restriction enzyme *Hha*I, which specifically recognizes and cleaves the mutated site. The PCR products of one clone obtained from vector II (II-4.11A) and of all four clones from vector III (III-2.2C, III-2.9C, III-3.7H, III-4.8D) were cut by *Hha*I, indicating presence of the *C284A* mutation (Figure 4D). These ESC clones were expanded and high quality DNA was prepared for Southern blot analysis. Two different probes binding at the 5-prime and 3-prime end of the *Caspase-1* gene, respectively, were used to evaluate the integrity of the *Caspase-1* genomic locus. Clone II-4.11A showed the expected band pattern for the 5-prime probe (Figure 5A, left: wt= 6 kb, mlt= 17 kb) and 3-prime probe (Figure 5A, right: wt= 9 kb, mlt= 17 kb). In addition, this clone exhibited a good (1:1) ratio of the band intensities of the *wild-type* over the recombined allele, proving its clonal origin and purity. The different probes also detected bands of the correct sizes for clones III-2.9C and III-3.7H (Figure 5A left: wt and mlt= 6 kb; right: wt= 9 kb, mlt= 11 kb) as well as a 1:1 ration between *wild-type* and mutant allele. Based on the results from the two screening PCRs and Southern blot analysis these three clones (II-4.11A, III-2.9C, III-3.7H) were sent for blastocyst injection of the ESC to Roland Naumann at the Max Planck Institute of Molecular Cell Biology and Genetics in Dresden, Germany.

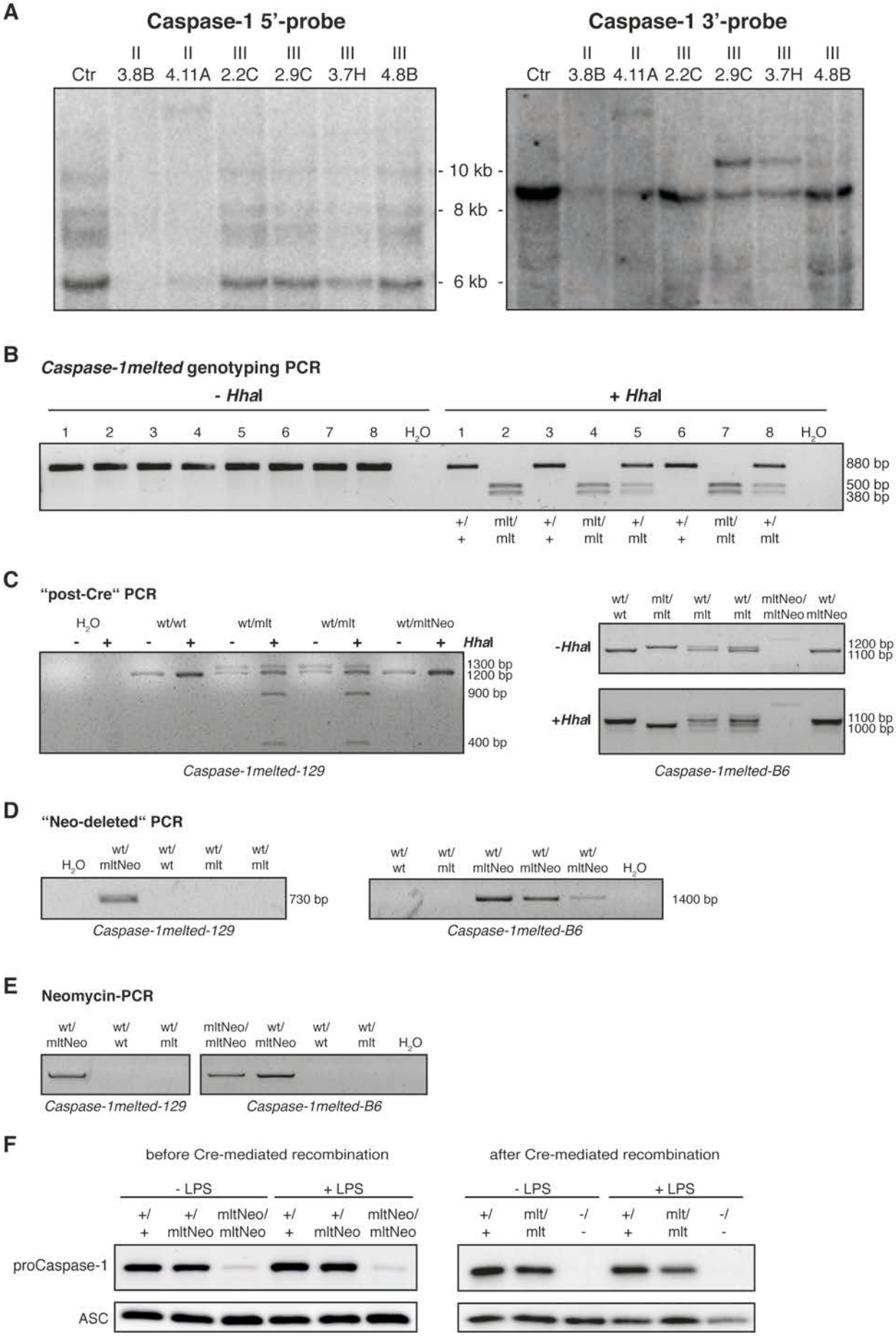
A
Caspase-1 5'-probe
Caspase-1 3'-probe
Ctr
II 3.8B
II 4.11A
III 2.2C
III 2.9C
III 3.7H
III 4.8B
10 kb
8 kb
6 kb
B
Caspase-1melted genotyping PCR
- HhaI
+ HhaI
1 2 3 4 5 6 7 8 H2O
880 bp
500 bp
380 bp
+/+ mlt/mlt +/+ mlt/mlt +/mlt +/+ mlt/mlt +/mlt
C
"post-Cre" PCR
H2O wt/wt wt/mlt wt/mlt wt/mltNeo
HhaI
1300 bp
1200 bp
900 bp
400 bp
Caspase-1melted-129
wt/wt mlt/mlt wt/mlt wt/mlt mltNeo/mltNeo wt/mltNeo
-HhaI
+HhaI
1200 bp
1100 bp
1100 bp
1000 bp
Caspase-1melted-B6
D
"Neo-deleted" PCR
H2O wt/mltNeo wt/wt wt/mlt wt/mlt
730 bp
Caspase-1melted-129
wt/wt wt/mlt wt/mltNeo wt/mltNeo wt/mltNeo H2O
1400 bp
Caspase-1melted-B6
E
Neomycin-PCR
wt/mltNeo wt/wt wt/mlt mltNeo/mltNeo wt/mltNeo wt/wt wt/mlt H2O
Caspase-1melted-129
Caspase-1melted-B6
F
before Cre-mediated recombination
after Cre-mediated recombination
- LPS
+ LPS
+/+ +/mltNeo mltNeo/mltNeo +/+ +/mltNeo mltNeo/mltNeo
+/+ mlt/mlt -/- +/+ mlt/mlt -/-
proCaspase-1
ASC

Figure 5: Analysis of *Caspase-1^{melted}-129* ESC clones and *Caspase-1^{melted}* transgenic mice
(A) Southern blot analysis with two different probes was used to investigate integrity of the *Caspase-1* locus from selected ESC clones. Clone II-4.11A (5-prime probe: wt= 6 kb, mlt= 17 kb; 3-prime probe: wt= 9 kb, mlt= 17 kb) and clones III-2.9C and III-3.7H (5-prime probe: wt= 6 kb, mlt= 6 kb; 3-prime probe: wt= 9 kb, mlt= 11 kb) showed the expected band patterns and comparable signal intensities for the *wild-type* and mutant allele. (B) Genotyping of *Caspase-1^{melted}* mice was performed by a PCR (880 bp) covering the mutated site (*C284*). Restrcition enzyme *Hha*I specifically cleaves the *C284A* mutation (530 + 330 bp) in the PCR product. (C) Confirmation of Cr-mediated recombination. In the "post-Cre" PCR, a 1.2 and 1.3 kb band is expected for *melted* alleles in the C57Bl/6 and 129 background, respectively. *Wild-type* alleles resulted in bands of 1.1 kb and 1.2 kb, respectively. The *melted* PCR product is cleavable by *Hha*I into two fragments (1.0 kb + 0.2 kb and 0.9 + 0.4 kb). *MltNeo* alleles were not amplified. (D) In the "Neo-deleted" PCRs a product is only generated prior to Cre-mediated recombination. (E) Cell lysates of unstimulated or LPS-primed BMDCs from *wild-type*, *Caspase-1$^{-/-}$* , *Caspase-1^{mltNeo}-129*, and *Caspase-1^{mlt}-129* (heterozygous and homozygous) mice were analyzed by Western blotting using the Caspase-1 p20 antibody.

3.1.2 Blastocyst injection, 129S1/X1 chimeras and genotyping of *Caspase-1^{melted}* mice

Blastocysts from C57Bl/6 mice were used for injection of ESC of II-4.11A and III-2.9C. Clone III-3.7H was not used in this first round of blastocyst injection. Ten highly chimeric males (+/- 80%) were born from ESC of clone II-4.11A. Offspring resulting from clone III-2.9C looked less promising in terms of chimerism and was not used for further breeding. The ten II-4.11A chimeras were shipped to our facility and mated to C57Bl/6J females. Four of them showed germline transmission of the transgenic *Caspase-1* allele as proven by screening PCR and the *Caspase-1^{melted}* genotyping PCR (data not shown).

The Cys284 to Ala point mutation was designed in such a way that a new restriction enzyme site was introduced into the *Caspase-1* locus. This feature could be conveniently used not only to screen stem cell clones but also in genotyping analysis of the mice. The *Caspase-1^{melted}* genotyping PCR was established with forward and reverse primers binding in *Caspase-1* genomic sequence spanning the mutated site. After the amplification reaction the PCR product was digested using the restriction enzyme *Hha*I. *Hha*I specifically detects and cleaves the *melted* mutation. This genotyping protocol therefore allowed to easily distinguish between wild-type, heterozygous or homozygous animals (Figure 5B).

3.1.3 Generation of *Caspase-1^{melted}* in the C57Bl/6 background

In addition to targeting the *Caspase-1* gene in 129 ESCs, I also obtained *Caspase-1^{melted}* transgenic mice in the C57Bl/6 background.

Mice of the 129 line carry a naturally occurring, inactivating mutation in the *Caspase-11* gene. *Caspase-1* and *Caspase-11* lie in too close proximity on chromosome 9 for segregation by backcrossing to a different background (Kayagaki et al., 2011). Therefore, the *Caspase-1^{melted}* mice originating from R1/E ESCs are always deficient for Caspase-11. Since a role for Caspase-11 has been described for inflammasome activation by certain stimuli, I planned to dissect the roles of Caspase-1 proteolytic activity and Caspase-11 by comparing *Caspase-1^{melted}* in Caspase-11-deficient (129 background) and Caspase-11-proficient (C57Bl/6) *Caspase-1^{melted}* mice. To this end, PolyGene AG was commissioned to generate *Caspase-1^{melted}* C57Bl/6 ES cell clones using my targeting vector III (Figure 4A).

Targeting in C57Bl/6 ES cells was apparently much more demanding and time-consuming and by the point when the first ESC clones carrying the *Caspase-1^{melted}* mutation in the C57Bl/6 background were generated, transgenic mice in the 129 background derived from clone II-4.11A were already at the heterozygous state (*+/mltNeo*). As mentioned above, targeting vector II and III feature a different orientation of the homologous arms. Therefore, after recombination and Cre recombinase-mediated removal of the neomycin resistance cassette, the *loxP* site left over in the genome is located in intron 5 and 7, respectively. To prepare for the unlikely event that this remaining vector sequence interferes with Caspase-1 expression, C57Bl/6 ESCs were electroporated using vector III to generate two differentially targeted transgenic mouse lines. PolyGene AG performed all PCR and Southern blot analyses as described above and reported the results of every step. In the end, I was provided with heterozygous *Caspase-1$^{+/mltNeo}$* C57Bl/6 animals and proceeded with Cre recombinase-mediated removal of the neomycin resistance cassette as for *Caspase-1$^{+/mltNeo}$-129*.

3.1.4 Cre-mediated recombination of the *Caspase-1$^{melted-Neo}$* locus

To remove the neomycin resistance cassette from the genome of *Caspase-1$^{+/mltNeo}$* mice by Cre recombinase-mediated genomic rearrangement in the germ line, heterozygous male descendants of the chimeras were crossed to female mice of the *DEL-Cre* line. As Cre recombinase can cause genome instability *Caspase-1$^{+/mlt}$Cre^{tg}* males were crossed to C57Bl/6J females to delete the X-chromosome-linked *Cre* gene from the genome. Males originating from these breedings were again mated with C57Bl/6J females to obtain *Caspase-1$^{+/mlt}$Cre^{-}* mice of both genders.

Removal of the neomycin resistance cassette from the *Caspase-1* genomic locus was verified by Western blot and two different PCRs. Figure 5C-E show these results. The primers of the "postCre-PCRs" bind left and right of the neomycin cassette but within genomic sequence. Only in the *wild-type* and *Caspase-1^{melted}* Cre-recombined allele, the distance between the primer pair is close enough to allow for amplification of the target sequence (Figure 5C: *Caspase-1^{melted}-129* wt= 1.2 kb, mlt= 1.3 kb; *Caspase-1^{melted}-B6* wt= 1.1 kb, mlt= 1.2 kb). As the PCR includes Cys284, *Hha*I-digestion resulted in cleavage of the PCR product for the *Caspase-1^{melted}* allele (Figure 5C, *Caspase-1^{melted}-129* wt= 1.2 kb, mlt= 0.9 + 0.4 kb; *Caspase-1^{melted}-129* wt= 1.1 kb, mlt: 1 kb + 0.2 kb).

In the "Neo-deleted-PCRs", one primer binds within the genomic sequence but the other primer binds within the neomycin resistance cassette. In this case a PCR product is only obtained for the *Caspase-1^{mltNeo}* allele prior to Cre-mediated recombination. As shown in Figure 5D *+/mlt* mice originating from a *Caspase-1^{melted}Cre^{tg}* father had successfully recombined the *Caspase-1^{melted}* allele resulting in absence of signal. Figure 5E shows a PCR amplifying the *neomycin* gene. Again, absence of signal for animals derived from *Cre^{tg}* parents proved successful recombination of the *Caspase-1* gene (Figure 5E).

For analysis of Caspase-1-melted expression by Western blotting, cell lysates were prepared from BMDCs of *wild-type*, *Caspase-1$^{mltNeo/mltNeo}$* and *Caspase-1$^{mlt/mlt}$* mice that were left untreated or LPS-primed. As shown in Figure 5F presence of the neomycin resistance cassette in the *Caspase-1* gene almost completely abolished Caspase-1 expression (left panel). Cre-mediated

recombination and deletion of the neomycin cassette restored normal Caspase-1 expression levels (Figure 5F, right panel). Comparison of three mice per genotype (wild-type, heterozygous, and homozygous) of the *Caspase-1*^{melted}*-129* line revealed similar expression levels of wild-type and mutant Caspase-1 (Figure 6E). No Caspase-1 cleavage and secretion was observed in *Caspase-1*$^{mlt/mlt}$ samples following inflammasome activation.

Caspase-1$^{+/melted}$*Cre*$^{-}$ mice were bred with each other to obtain experimental animals and littermate *wild-type* control mice.

3.2 Basic phenotype analysis of *Caspase-1*^{melted} mice

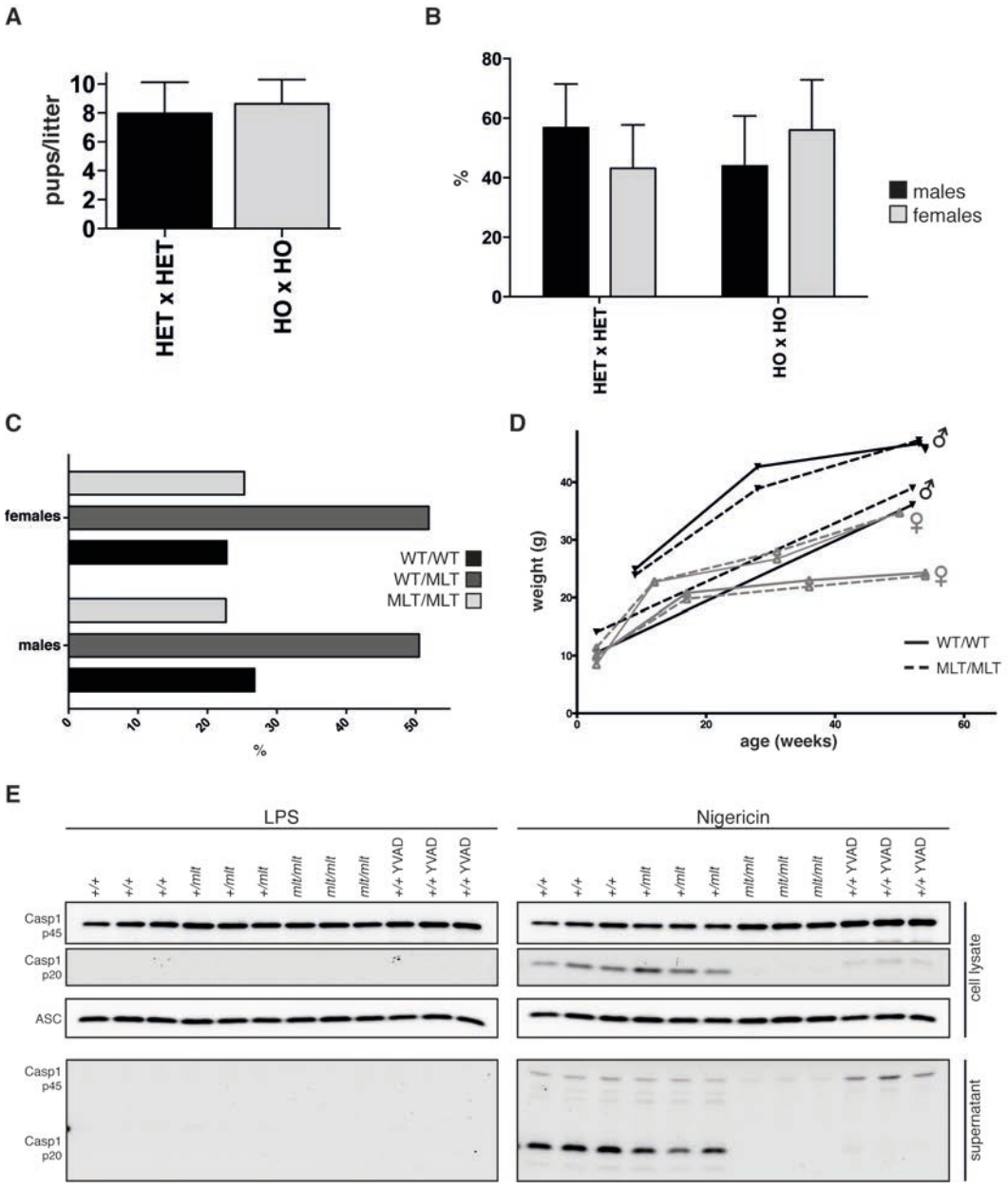

Figure 6: Basic phenotype analysis of *Caspase-1^{melted}* mice
(A) Heterozygous and homozygous *Caspase-1^{melted}* breeding pairs produced litters of comparable sizes with (B) an equal distribution of male and female pups (HETxHET: litters n=23, pups n=183 ;HOxHO: litters n=8, pups n=69). (C) Percentage of the different genotypes of the offspring of heterozygous breeding pairs (males n=100, females n=83). (D) Weight development of four pairs of *Caspase-1$^{+/+}$* and *Caspase-1$^{mlt/mlt}$* littermates over 12 month. Two male (♂) and two female pairs (♀) are shown. (E) Expression levels of Caspase-1 in cell lysates of BMDCs (+LPS or +LPS/Nigericin) of 3 different mice per genotype (*wild-type*, heterozygous, and homozygous). *Caspase-1$^{+/+}$* cells were additionally treated with Caspase-1 inhibitor Ac-YVAD-cmk (YVAD). All data originated from *Caspase-1^{melted}-129* line.

3.2.1 Weight, growth, health, fertility, mendelian ratios

Mice homozygous for the *C284A* mutation in the *Caspase-1* gene did not differ in weight development from their *wild-type* littermates. Under SPF conditions, the mice were healthy and did not show any signs of immunosuppression. A group of *Caspase-1^{melted}-129* and *-B6* mice was observed up to an age of twelve and six month, respectively and within that time, did not develop spontaneous forms of cancer, inflammatory disorders, or other diseases.
Homozygous *Caspase-1$^{mlt/mlt}$* males and females were fertile and had litters of sizes common for their genetic backgrounds. Heterozygous and homozygous breeding pairs produced on average 50 % female and male pups. Matings between heterozygous males and females resulted in a ratio of *+/+*, *+/mlt* and *mlt/mlt* mice according to the expected mendelian ratios (Figure 6A-D).

3.2.2 Immunophenotype analysis of *Caspase-1^{melted}* mice

Different lymphatic organs of 8 weeks-old *Caspase-1$^{+/+}$* and *Caspase-1$^{mlt/mlt}$* littermates were analyzed for the presence and frequency of different immune cell entities by FACS. Likewise, the development of *in vitro*-generated bone marrow-derived, inflammasome-competent myeloid cells was investigated.
Bone marrow cells were stained for B220 and IgM to distinguish between the different developmental stages of B cells (Figure 7A). *Caspase-1$^{mlt/mlt}$* mice displayed equal percentages of pro- and pre-B cells (Figure 7A, B220^{low}IgM^{-}), immature B cells (Figure 7A, B220^{low}IgM^{+}) and recirculating B cells (Figure 7A, B220^{high}IgM^{+}) as compared to *wild-type* littermates. To analyze B cells within the spleen, splenocytes were gated for B220 and CD19. These cells were subsequently investigated for IgM and IgD surface expression (Figure 7B).

Immature B cells were identified as IgM^+IgD^- cells, transitional B cells as IgM^+IgD^+ and mature recirculating B cells as IgM^-IgD^+. Numbers of the different subgroups did not differ significantly between *wild-type* and *mlt/mlt* animals. B220-CD19-gated splenocytes were additionally examined for the presence of marginal zone B cells, by staining for CD21 and CD23 (Figure 7C). No differences between the two genotypes were detected. Thymocytes were tested for CD4 and CD8 expression to follow the differentiation process of T cells within that organ. FACS analysis revealed comparable situations in *Caspase-1*$^{+/+}$ and *Caspase-1*$^{mlt/mlt}$ mice (Figure 7D). Cells isolated from lymph nodes were analyzed accordingly, demonstrating equal distributions of cytotoxic ($CD8^+$) and helper ($CD4^+$) T cells between *wild-type* and transgenic animals (Figure 7E). CD4-gated lymph node cells were further plotted for CD25. $CD4^+CD25^+$ cells represent regulatory T cells and were found in similar amounts in animals of both genotypes (Figure 7F). The cellularity of the organs was comparable between the groups (Figure 7G).

For the *in vitro* experiments presented within this study, bone-marrow-derived dendritic cells (BMDCs) were used. To make sure that *Caspase-1*$^{mlt/mlt}$ BMDCs differentiated normally, bone-marrow progenitors of *wild-type* and *Caspase-1*$^{mlt/mlt}$ mice were cultured in the presence of recombinant murine GM-CSF. The state of differentiation of these cells was assessed by FACS analysis on day 4 as an early time-point and on days 6, 7, and 8, representing the days cells were used for experiments. Plotted against MHC class II as a marker for antigen-presenting cells, CD11c was used as a marker for differentiation of the progenitor cells into the DC lineage and CD80 as a marker for DC maturation. Figure 7H and 7I display that *Caspase-1*$^{mlt/mlt}$ BMDCs exhibited normal differentiation and maturation as compared to *wild-type* cells.

To conclude, I did not observe any differences in the percentages of various immune cells between *wild-type* and transgenic animals in lymph nodes, spleen, bone marrow, and thymus. *Caspase-1*$^{mlt/mlt}$ mice therefore did not exhibit defects in the development of the adaptive immune system. Furthermore, BMDCs of *Caspase-1*$^{mlt/mlt}$ mice differentiated normally in the presence of GM-CSF *in vitro*.

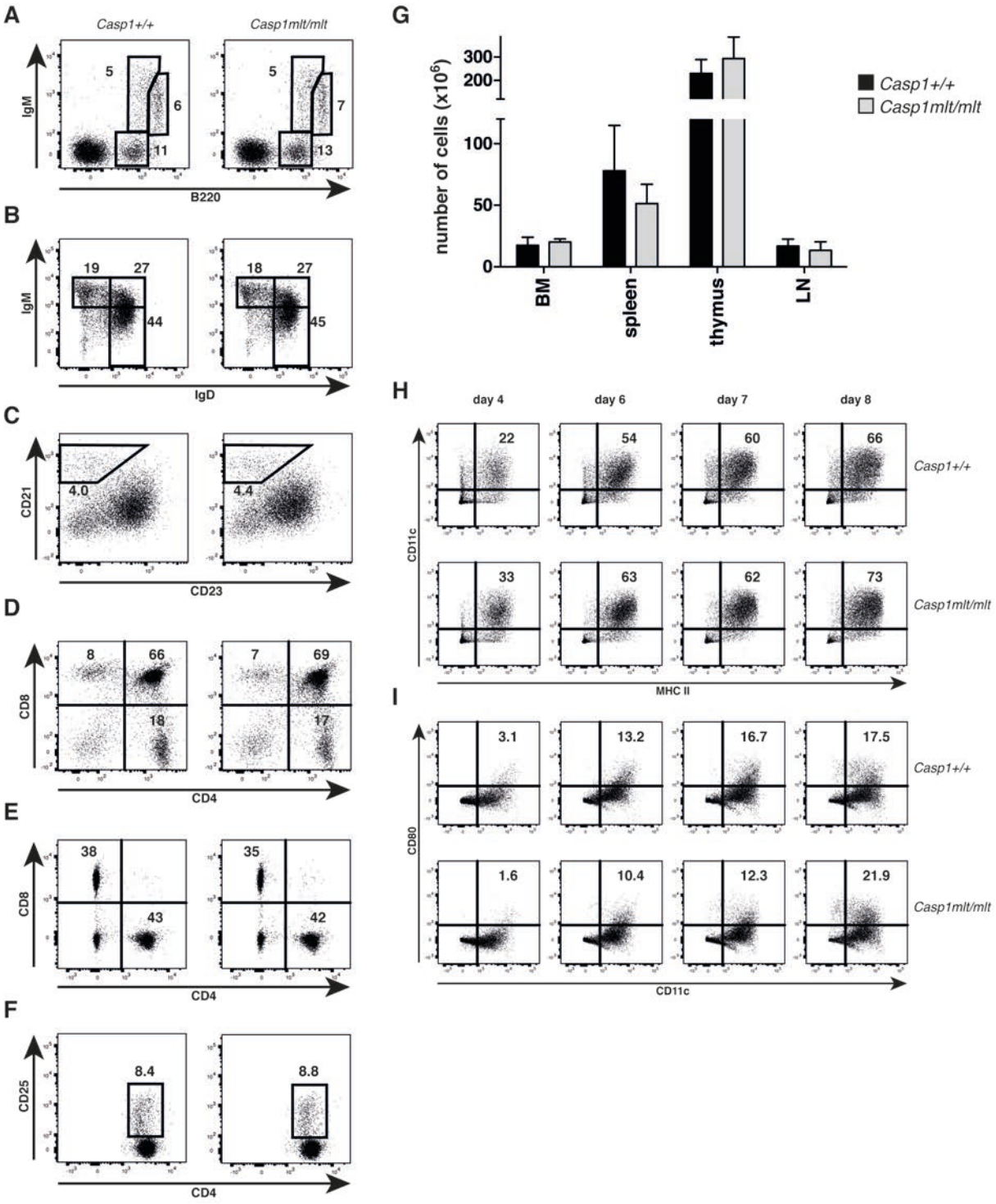

Figure 7: FACS analysis of different lymphatic organs and *in vitro*-differentiated BMDCs
(A-F) Cells of different lymphatic organs of *wild-type* and *mlt/mlt* mice of the *Caspase-1*^{melted}*-129* line were analyzed for distribution of various cell types. (A) Bone marrow cells were stained for B220 and IgM. (B, C). Expression of IgD and IgM (B) or CD21 and CD23 (C) was determined in CD19- and B220-gated splenocytes. (D, E) Thymocytes (D) and lymph node cells (E) were analyzed for presence of CD4 and CD8. (F) CD4-gated $CD4^+CD25^+$ lymph node cells represent regulatory T cells. Data is representative of four mice per genotype. (G) Cellularity of the in (A-F) analyzed organs of four mice is shown as mean ±SEM.(H, I) *In vitro* GM-CSF-differentiated bone-marrow progenitor cells were analyzed by FACS. Antibodies for MHC class II, CD11c (G) and CD80 (H) were used as markers for DC differentiation and maturation.

3.3 *In vitro* analysis of *Caspase-1^{melted}* mice

3.3.1 Canonical inflammasome activation in BMDCs of *Caspase-1^{melted}* mice

BMDCs derived from *wild-type* (*Caspase-1$^{+/+}$*) and *Caspase-1$^{mlt/mlt}$* mice were analyzed for inflammasome activation. I used IL-1β, proIL-1β, and IL-1α secretion as read-outs for inflammasome activation. Cytokine levels were measured by ELISA and by Western blot analysis. Release of LDH served as an indicator of cell death. Nigericin, MSU, and R837 were selected as stimuli for the Nlrp3 inflammasome, *S. typhimurium* for the Nlrc4 inflammasome and poly(dA:dT) for the Aim2 inflammasome.

Comparison of *Caspase-1$^{+/+}$* BMDCs to *Caspase-1$^{+/+}$* cells treated with a Caspase-1-specific inhibitor (AC-YVAD-cmk) showed that inhibition of Caspase-1 activity blocked the secretion of IL-1β as seen in ELISA and Western blots for IL-1β (Figure 8A, top, Figure 8D, bottom). In contrast, IL-1α secretion was comparable in both conditions (Figure 8A, bottom). Analysis of proIL-1β secretion (ELISA and WB) revealed that more unclevaed IL-1β was secreted in YVAD-treated cells than in untreated cells (Figure 8A, middle, Figure 8D, bottom). Taken together, the results for IL-1α and IL-1β secretion indicated that pharmacological inhibition of Caspase-1 interferes with protease activity and cleavage of proIL-1β but not with cytokine secretion. Furthermore, inhibition of Caspase-1 protease activity by YVAD was insufficient to prevent cell death induced by inflammasome stimuli as measured by LDH release from the cells (Figure 8C).

In accordance to the results for *Caspase-1$^{+/+}$* samples +YVAD, no IL-1β was secreted in *Caspase-1$^{mlt/mlt}$* BMDCs (Figure 8A, top, Figure 8D, bottom). Contrasting the findings in cells where Caspase-1 protease activity was pharmacologically inhibited, I did not detect any IL-1α or proIL-1β in the supernatants of *Caspase-1$^{mlt/mlt}$* cells by ELISA or Western blot analysis (Figure 8A, bottom, Figure 8D, bottom). Furthermore, Caspase-1 was not secreted (not even in the full-length form, compare to *Caspase-1$^{+/+}$* +YVAD) in *Caspase-1$^{mlt/mlt}$* samples (Figure 8D, bottom). *Caspase-1$^{mlt/mlt}$* BMDCs were protected from cell

death following inflammasome activation and did not release LDH (Figure 8C). Thus, *Caspase-1*$^{mlt/mlt}$ cells resembled the phenotype of *Caspase-1*$^{-/-}$ cells and not of *Caspase-1*$^{+/+}$ +YVAD.

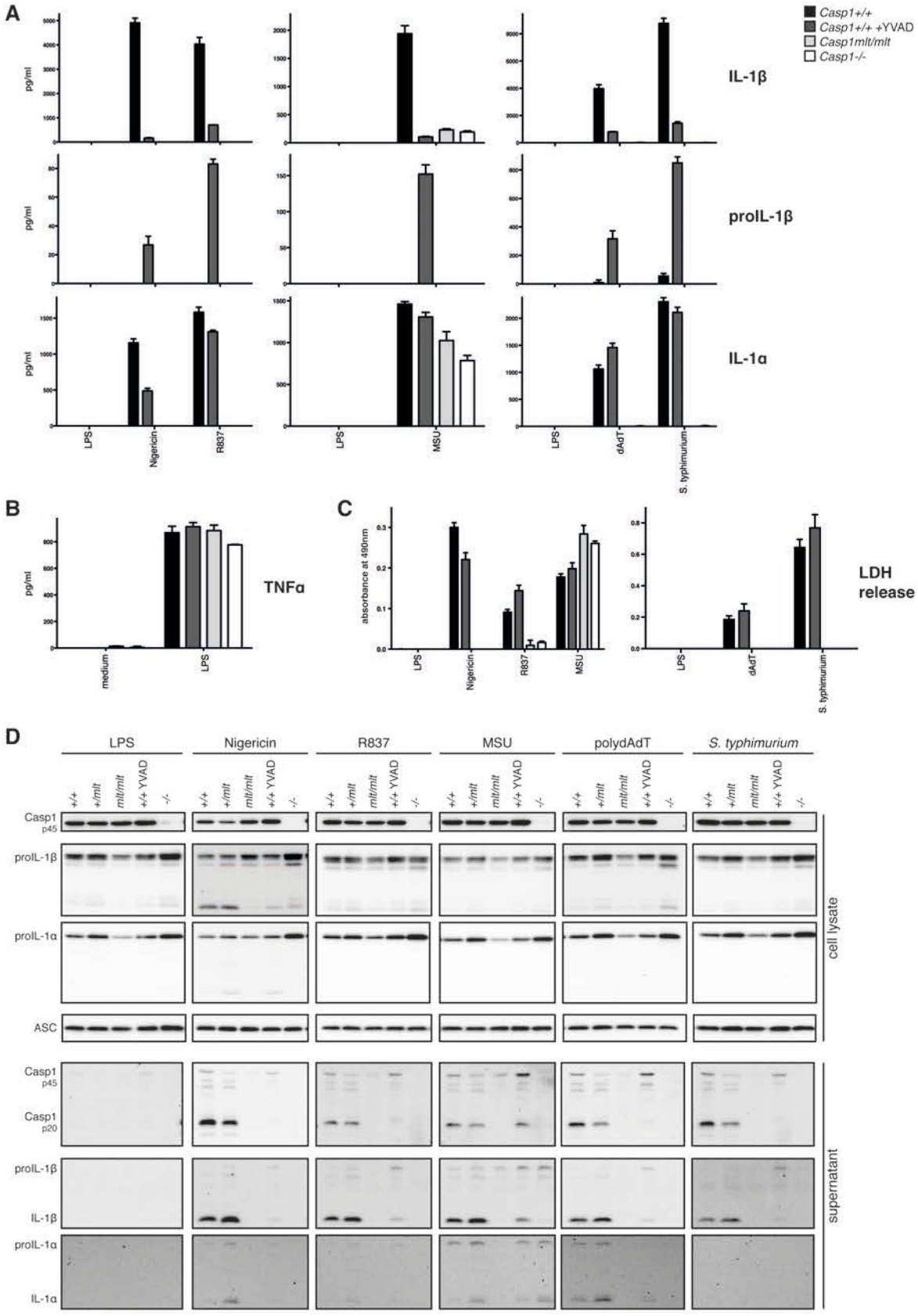

Figure 8: Inflammasome activation in BMDCs of *Caspase-1^{melted}-129* mice
(A-D) *Wild-type* BMDCs treated without (*Caspase-1$^{+/+}$*, *+/+*) or with Caspase-1 inhibitor (*Caspase-1$^{+/+}$* +YVAD, *+/+* +YVAD) and BMDCs derived from *Caspase-1$^{-/-}$* (*-/-*) and *Caspase-1$^{mlt/mlt}$* (*mlt/mlt*) animals were LPS-primed and stimulated with agents activating the Nlrp3 (nigericin, R837, MSU), Aim2 (poly(dAdT)) and Nlrc4 (Salmonella) inflammasome. (B) LPS-induced TNFα was measured by ELISA as an indicator for equal cell numbers and responses to the priming stimulus among samples. (C) LDH release was analyzed as an indicator of cell death. (A, D) Secretion of (pro)IL-1β and IL-1α were analyzed by ELISA (A) and Western blot (D). Caspase-1 expression, cleavage, and secretion were determined using Western blotting (D). (A-C) Results are depicted as mean ±SEM and are representative of at least four comparable experiments.

Our group published that MSU crystals can induce Caspase-1-independent IL-1 secretion and cell death (Groß et al., 2012). I confirmed these observations in my assays with YVAD-inhibited, *Caspase-1$^{-/-}$*, and *Caspase-1$^{mlt/mlt}$* BMDCs (Figure 8A, bottom, Figure C).

Taken together, these experiments showed that genetically inhibiting Caspase-1 protease-activity interferes with Nlrp3-, Nlrc4- and Aim2-inflammasome activation in terms of IL-1α and (pro)IL-1β secretion and cell death. This is contrary to inflammasome activation in cells, in which Caspase-1 activity has been blocked by a specific inhibitor.

3.3.2 TLR stimulation in BMDCs and BMDMs of *Caspase-1^{melted}* mice

To investigate whether the homozygous *Caspase-1$^{mlt/mlt}$* mutation has an influence on other pathways important in innate immune responses, I stimulated *Caspase-1$^{+/+}$*, *Caspase-1$^{mlt/mlt}$* and *Caspase-1$^{-/-}$* BMDCs and BMDMs with a panel of activators for different membrane-bound PRRs. In response to PRR activation, immune cells will induce the production and secretion of cytokines through inflammasome-independent mechanisms, involving transcription factors, including NF-κB, and ER-Golgi-dependent secretion. Among these are IL-6 and TNFα. Engagement of TLR4 (LPS), TLR9 (CpG), TLR7/8 (R848), TLR1/2 (Pam3CSK4), and Dectin-1 (Curdlan, Zymosan) led to comparable amounts of IL-6 and TNFα in the supernatants of stimulated BMDCs and BMDMs irrespective of the genotypes as measured by ELISA (Figure 9A).

This confirmed existing data on *Caspase-1* knockout animals, in that Caspase-1 is required for inflammasome activation but not for TLR signaling. It further

showed that the defective IL-1 secretion observed in *Caspase-1*$^{mlt/mlt}$ BMDCs is most likely not due to insufficient priming but a non-functional inflammasome.

3.3.3 *Caspase-1*^{melted} and Ripk2

Heymann *et al.* proposed an enhanced interaction between inactive Caspase-1 and Ripk2, culminating in sustained NF-κB activation (Heymann et al., 2014). Using the new *Caspase-1*^{melted} mouse model, I investigated this interaction in a more physiological system as compared to their *in vitro* studies.

I started with co-transfection experiments in HEK293T cells using expression vectors for Ripk2 and wild-type or mutant Caspase-1. I observed that Caspase-1-mlt was more strongly enriched in immunoprecipitations of Ripk2 as compared to wild-type (wt) or non-cleavable (nc) Caspase-1 (Figure 9B, bead fraction). Analysis of the input fraction showed that the levels of Ripk2 protein varied between cells that had been co-transfected with *Caspase-1*^{mlt} or with *Caspase-1*^{wt} and *Caspase-1*^{nc} (Figure 9B, cell lysates). This suggests that wild-type and non-cleavable Caspase-1 can dampen the expression or force the degradation of Ripk2 protein. The more efficient co-immunoprecipitation of Caspase-1-mlt with Ripk2 could therefore either result from higher Ripk2 input levels in this sample or from a stronger interaction between Ripk2 and Caspase-1-mlt.

To test the effect of Caspase-1-mlt on Ripk2 in primary cells, I stimulated BMDCs with muramyl-dipeptide (MDP), an agonist of the Nod2 receptor. Activation of Nod2 leads via Ripk2 to NF-κB activation and thereby to an inflammatory response. Stimulation with MDP did not lead to hyperactivation of *Caspase-1*$^{mlt/mlt}$ cells compared to *Caspase-1*$^{+/+}$ cells as measured by secretion of IL-6 and TNFα as NF-κB-dependent factors by ELISA (Figure 9C). Furthermore, in inflammasome stimulation experiments (Figure 8B) TNFα levels in *Caspase-1*$^{mlt/mlt}$ cells were also not increased over *wild-type* controls.

To conclude, my data showed that proteolytically inactive Caspase-1 did not cause an overshooting immune response via Ripk2 in BMDCs, although Ripk2 expression or stability seems to be influenced by Caspase-1 in an overexpression system.

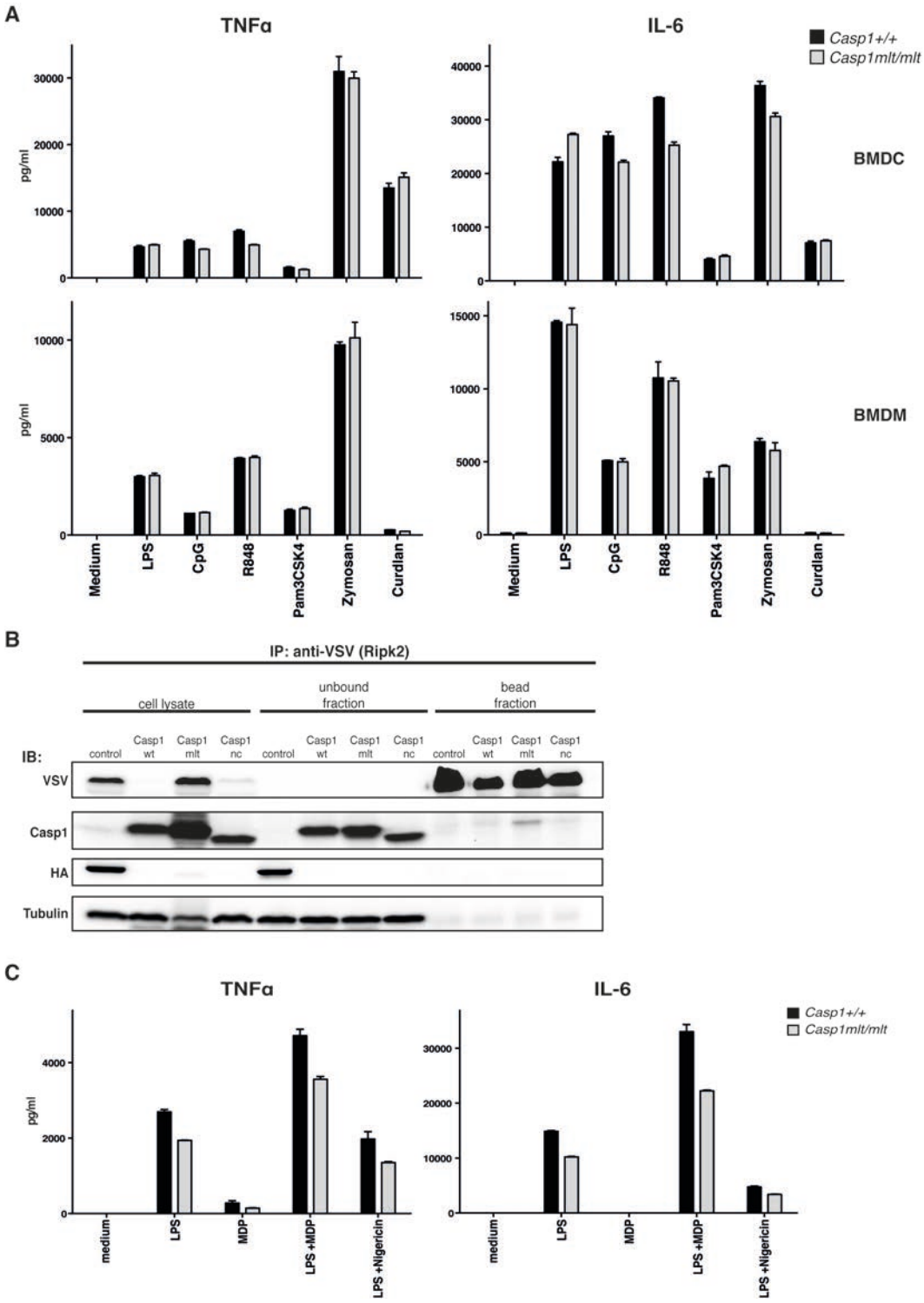

Figure 9: TLR signaling in *Caspase-1^{melted}-129* BMDCs and BMDMs and interaction between Ripk2 and Caspase-1

(A) Different TLR and Dectin-1 agonists were used to stimulate BMDCs and BMDMs of *Caspase-1$^{+/+}$* and *Caspase-1$^{mlt/mlt}$* mice. Measurement of IL-6 and TNFα secretion by ELISA served as read-outs for PRR activation. Data representative of 3 independent experiments is shown as mean ±SEM. (B) VSV-tagged Ripk2 was expressed in HEK293T cells together with wild-type (wt), melted (mlt), non-cleavable (nc) Caspase-1 or an unrelated HA-tagged protein as negative control. Using an anti-VSV antibody, Ripk2 was immuno-precipitated from cell lysates. Cell lysates, bead fractions, and unbound fractions were compared by Western blotting and analyzed for co-precipitated Caspase-1 protein. (C) BMDCs of *Caspase-1$^{+/+}$* and *Caspase-1$^{mlt/mlt}$* mice were treated with the Nod2 activator MDP. Ripk2-dependent cell activation was assessed by secretion of IL-6 and TNFα into the cells' supernatants.

3.3.4 Non-canonical inflammasome activation in BMDCs of *Caspase-1^{melted}* mice

Besides canonical inflammasome activation, I tested LPS transfection and *E. coli* infection as established stimuli for the Caspase-11-dependent, non-canonical inflammasome. BMDCs of *Caspase-1$^{mlt/mlt}$-129* and *-B6* mice were compared in these experiments.

Accuracy of the targeting strategy for *Caspase-1$^{mlt/mlt}$-B6* mice was proven by detection of comparable Caspase-1 expression in *wild-type* and *melted* cells. Furthermore, Western blotting of cell lysates revealed Caspase-11 expression in C57Bl/6-derived transgenic mice (Figure 10C, D). For stimulation with canonical inflammasome activators, I observed no difference in the *Caspase-1$^{mlt/mlt}$-129* (Caspase-11-deficient) and *-B6* (Caspase-11-proficient) mice. As shown by ELISA and Western blotting, IL-1α and IL-1β secretion were abolished in cells from *Caspase-1$^{mlt/mlt}$* mice of both genetic backgrounds following Nlrp3 (nigericin), Aim2 (poly(dA:dT)), and Nlrc4 (*S. typhimurium*) activation (Figure 10A-D). In addition, cell death as measured by LDH release did not occur in response to these stimuli in cells with inactive Caspase-1. Accordingly, no Caspase-1 was detected in the supernatants of these samples (Figure 10C, D). In conclusion, these experiments document the independence of these inflammasomes from Caspase-11.

In line with expression of Caspase-11 in *Caspase-1$^{mlt/mlt}$-B6* but not *-129* mice, activation of Caspase-11 by LPS-transfection resulted in IL-1α secretion and cell death only in BMDCs of mice of the C57Bl/6 background (Figure 10B, D). Both effects were irrespective of Caspase-1 proteolytic activity as C57Bl/6 *wild-type* and *mlt/mlt* behaved the same. However, IL-1β release was substantially detected only in C57Bl/6 *wild-type* cells, confirming the role of Caspase-1 activity for IL-1β cleavage and secretion downstream of Caspase-11 (Kayagaki et al., 2011) (Figure 10B). More pronounced than in the ELISA measurement, a long exposure of the Western blot showed a low residual release of IL-1β in the *Caspase-1$^{mlt/mlt}$-B6* and 129 *wild-type* samples. This finding implies that the dependence of Caspase-11 on Caspase-1 in this process is incomplete.

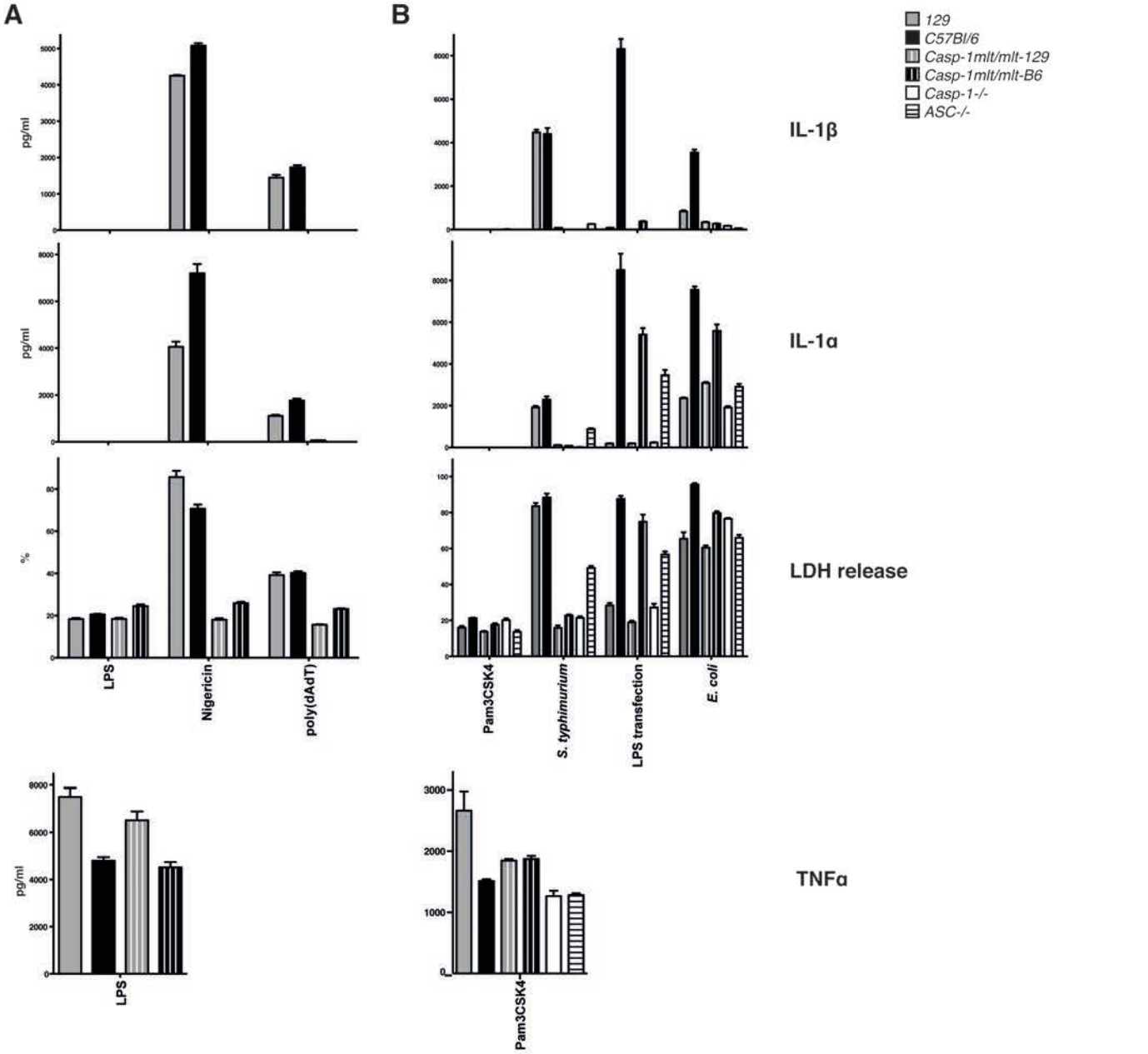
A
B
129
C57Bl/6
Casp-1mlt/mlt-129
Casp-1mlt/mlt-B6
Casp-1-/-
ASC-/-
pg/ml
%
IL-1β
IL-1α
LDH release
TNFα
LPS
Nigericin
poly(dAdT)
Pam3CSK4
S. typhimurium
LPS transfection
E. coli

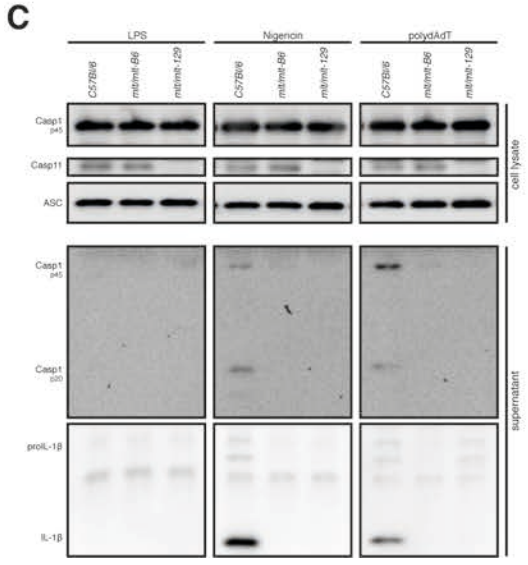
C
LPS
Nigericin
polydAdT
C57Bl/6
mlt/mlt-B6
mlt/mlt-129
Casp1 p45
Casp11
ASC
cell lysate
Casp1 p20
proIL-1β
IL-1β
supernatant

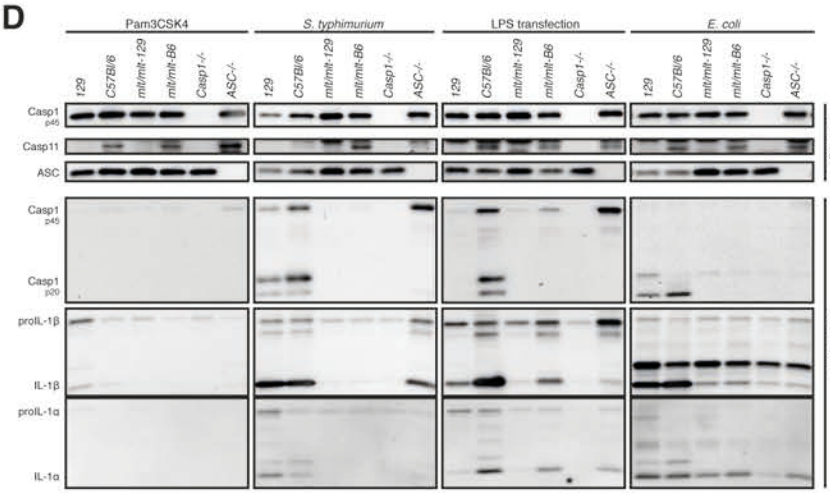
D
Pam3CSK4
S. typhimurium
LPS transfection
E. coli
129
C57Bl/6
mlt/mlt-129
mlt/mlt-B6
Casp1-/-
ASC-/-
Casp1 p45
Casp11
ASC
cell lysate
Casp1 p20
proIL-1β
IL-1β
proIL-1α
IL-1α
supernatant

Figure 10: Inflammasome activation in BMDCs of *Caspase-1^{melted}-B6* and *-129* mice
(A-C) BMDCs of *wild-type* C57Bl/6 and 129, *Caspase-1$^{mlt/mlt}$-B6*, *Caspase-1$^{mlt/mlt}$-129*, *Caspase-1$^{-/-}$*, and *ASC$^{-/-}$* mice were LPS-primed and stimulated with activators of the (A) Nlrp3- (nigericin), Aim2- (poly(dA:dT)), (B) Nlrc4- (*S. typhimurium*), and non-canonical (LPS transfection, *E. coli*) inflammasome. (A, B) Secretion of IL-1β, IL-1α, and TNFα was assessed by ELISA. Measurement of LDH-release served as read-out for cell death and is depicted as a ratio of 100 % as compared to freeze-thaw lysed cells. Results are shown as mean ±SEM. (C, D) Caspase-1 processing and secretion as well as release of IL-1β and IL-1α were investigated by Western blot analysis. Data is representative of four comparable experiments.

Upon LPS transfection, ASC was dispensable for IL-1α secretion and LDH release but not for IL-1β secretion, underlining the crosstalk of Caspase-11 with the canonical inflammasome for this purpose. The absence of cleaved Caspase-1 in the supernatant of LPS-transfected samples of *Caspase-1$^{mlt/mlt}$-B6* mice is in congruency with this data (Figure 10D). The release of full-length Caspase-1 was likely due to cell death.

E. coli infection reflected the phenotype of LPS transfection only partially. IL-1β secretion was most prominent in C57Bl/6 *wild-type* cells (Figure 10B). However, some secretion was also detected in Caspase-11-deficient 129 *wild-type* cells by ELISA and Western blotting (long exposure) (Figure 10B, D). The detection of cleaved Caspase-1 in the supernatant of these cells by Western blotting, is indicative of Caspase-1 activation by the microorganisms (Figure 10B). Inhibition of catalytic activity of Caspase-1 abolished this secretion almost completely (Figure 10B, D). IL-1α levels in the supernatants followed the same trend as with LPS transfection, although background levels in cells of all mice from a 129 background were increased (Figure 10 B). This could be due to Caspase-11-independent cell death caused by the bacteria. LDH measurement showed similar signals for all genotypes. Possible explanations could be, as mentioned, unspecific, inflammasome-independent cell death induced by the bacteria or production of an enzyme that has LDH activity by the bacteria themselves (Figure 10B).

Independent of Caspase-1, I was able to confirm data by Broz *et al.* showing that ASC is dispensable for induction of cell death following activation of the CARD-containing Nlrc4 receptor by *S. typhimurium* (Broz et al., 2010). IL-1β and IL-1α secretion in contrast, relied fully or partially on the adaptor protein (Figure 10B, D).

3.3.5 Immunofluorescence microscopy of ASC "specks" in *Caspase-1^{melted}* cells

In addition to measuring the effects and outcome of inflammasome activation in myeloid cells of *Caspase-1$^{mlt/mlt}$* mice - like IL-1 secretion and cell death - I wanted to follow the initial steps after stimulation within these cells by microscopy. To this end, my colleague Dr. Ritu Mishra performed immunofluorescence microscopy analysis using *Caspase-1$^{+/+}$*, *Caspase-1$^{mlt/mlt}$* and *Caspase-1$^{-/-}$* BMDCs. The cells were LPS-primed and the inflammasome activated by the Nlrp3-agonist nigericin. In addition, *Caspase-1$^{+/+}$* BMDCs were treated with the Caspase-1-specific inhibitor Ac-YVAD-cmk. After stimulation, the cells were stained with antibodies directed against ASC and Caspase-1 p10 subunit as well as DAPI to visualize nuclei (Figure 11).

Stimulation with nigericin led to the formation of so-called ASC "specks" in the cytoplasm of all cells. In Caspase-1-expressing cells (C57Bl/6*, C57Bl/6* +YVAD and *Caspase-1$^{mlt/mlt}$*), Caspase-1 was also detected at these platforms. *Caspase-1$^{-/-}$* BMDCs served as a control for the specificity of the Caspase-1 antibody staining and no signal was detected in these cells. Interestingly, Caspase-1 was more strongly enriched on the ASC "specks" in *Caspase-1$^{mlt/mlt}$* cells. A similar but slightly reduced increase in Caspase-1 signal was seen in wild-type cells treated with YVAD. It is also noteworthy that no condensation of the nuclei (DAPI) as a sign for cell death was observed in *Caspase-1$^{mlt/mlt}$* and *Caspase-1$^{-/-}$* samples. This was in contrast to C57Bl/6 BMDCs -/+ YVAD.

The finding that Caspase-1 was enriched in inflammasome-complexes of *mlt/mlt* versus *wild-type* cells suggested that potential (non-substrate) interaction partners of Caspase-1 would also be concentrated on these "specks". To identify such interaction partners, I therefore continued with mass spectrometry analysis of samples prepared from *Caspase-1$^{mlt/mlt}$* mice.

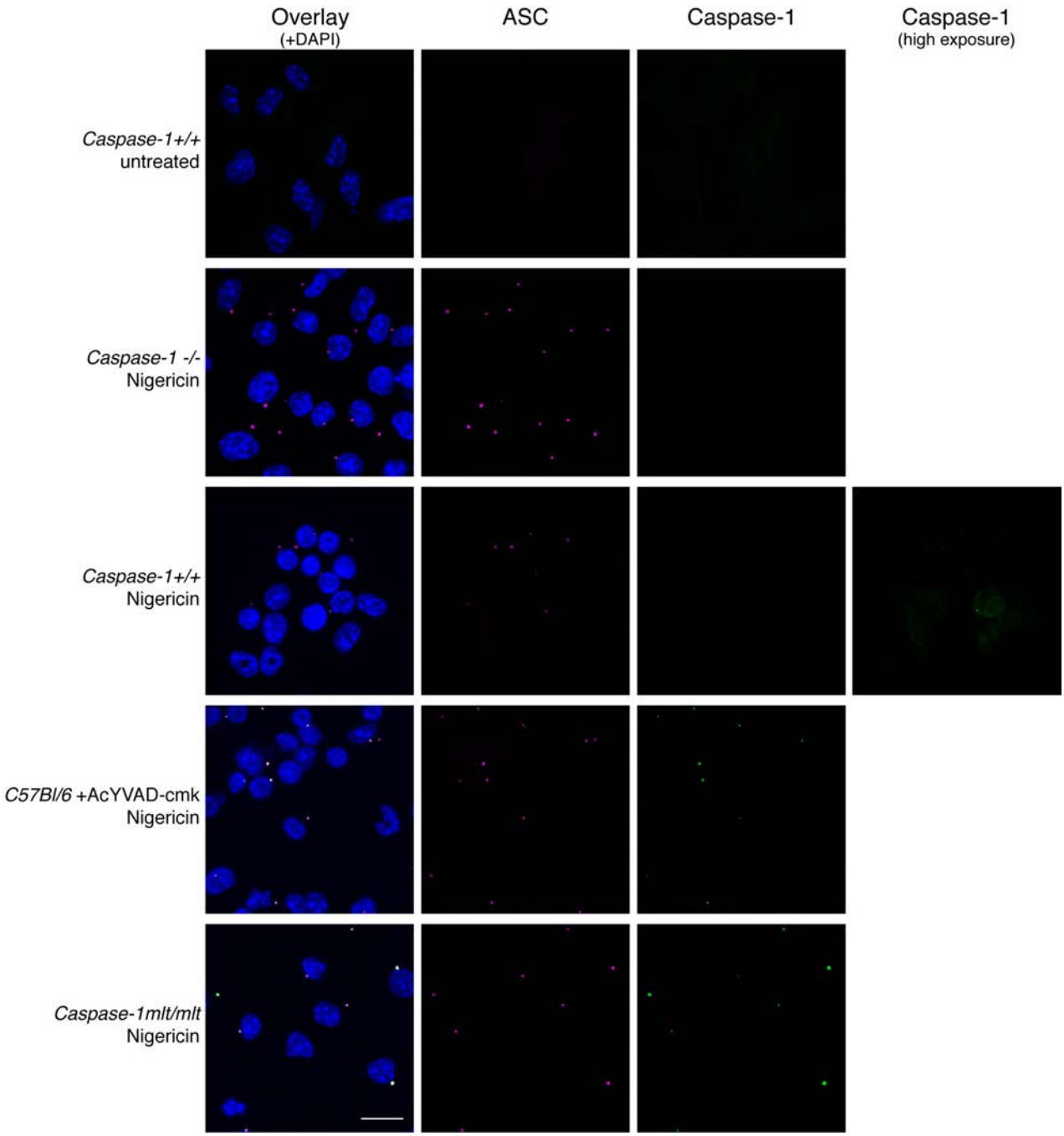

Figure 11: Immunofluorescence analysis of ASC "specks"
BMDCs derived from C57Bl/6, *Caspase-1*$^{-/-}$, and *Caspase-1*$^{mlt/mlt}$*-129* mice treated with or without the Caspase-1 inhibitor Ac-YVAD-cmk (YVAD) were LPS-primed and nigericin-stimulated for inflammasome activation. Cells were fixed and antibodies against ASC and Caspase-1 p10 were used to visualize inflammasome assembly (ASC "specks"). DAPI stained the nuclei of the cells. The experiment was performed by Dr. Ritu Mishra. The scale bar represents 15 µm.

3.4 Mass spectrometry analysis

3.4.1 Measurement of ASC "speck" enriched cell fractions by label-free mass spectrometry

BMDCs of *Caspase-1*$^{+/+}$, *Caspase-1*$^{mlt/mlt}$*-129*, *Caspase-1*$^{-/-}$ and *Nlrp3*$^{-/-}$ mice were either LPS-primed only or primed and nigericin-stimulated to induce Nlrp3-inflammasome assembly. After activation and ASC "speck" formation had been completed, I prepared whole cell lysates of the cells. These lysates were further processed into an insoluble pellet fraction containing an assembled inflammasome complex and a soluble supernatant fraction. The samples were analyzed by Western blotting to confirm the success of the experiment before I prepared the samples for mass spectrometry (Figure 12A). The mass spectrometry analysis as well as the evaluation of the raw data was performed by our collaboration partner Dr. Guillaume Médard in the group of Prof. Bernhard Küster at the Chair of Proteomics and Bioanalytics at the Technical University Munich.

3.4.2 Cross-linker-free approach

Western blot analysis of BMDCs treated as explained above revealed signal-specific enrichment of inflammasome components in the insoluble fraction: ASC in *Caspase-1*$^{-/-}$ cells and ASC and Caspase-1 in *Caspase-1*$^{+/+}$ and *Caspase-1*$^{mlt/mlt}$ cells, respectively (Figure 12B, pellet fraction). Missing the upstream signal, *Nlrp3*$^{-/-}$ cells were unable to recruit ASC and Caspase-1 to an inflammasome complex and the proteins therefore remained in the soluble fraction. Much more Caspase-1 is found in the insoluble fraction in *Caspase-1*$^{mlt/mlt}$ than in *Caspase-1*$^{+/+}$ samples (Figure 12B, pellet fraction). As seen in Figure 11, inhibition of its protease activity seemed to prevent release of Caspase-1 from the inflammasome. Western blot analysis showed the expected results in terms of the behavior of the known components of the complex for the different genotypes. Thus, the samples were used for mass spectrometry analysis.

For each genotype, experimental quadruplets of the pellet samples were measured by label-free mass spectrometry. Analysis of the obtained results revealed that this label-free setup enhanced the specificity as compared to analyzing single samples per condition and that the repetitive measurements allowed for elimination of unspecific background signal. Comparing the mean amounts of proteins, identified between samples obtained from *Caspase-1*$^{mlt/mlt}$ cells to *Nlrp3*$^{-/-}$ cells, I found ASC and Caspase-1 to be specifically enriched (Figure 12C, purple group). This comparison served as a proof-of-principle for the assay. Since no signal can be transmitted after nigericin-stimulation in *Nlrp3*$^{-/-}$ BMDCs and no inflammasome can form in these cells, proteins involved in downstream signalling should be enriched in Nlrp3-proficient over Nlrp3-deficient cells.

To identify interaction partners of Caspase-1, I compared the mean protein amounts measured for the *Caspase-1*$^{mlt/mlt}$ group to the *Caspase-1*$^{-/-}$ group (Figure 12B, orange group). Caspase-1 was the only protein, found to be differentially recruited to the inflammasome between these two groups. No other proteins were consistently enriched in the *Caspase-1*$^{mlt/mlt}$ samples.

3.4.3 Mass spectrometry analysis using crosslinker

As the first mass spectrometry approach was unsuccessful in identifying inflammasome-dependent interaction partners of Caspase-1, I repeated the experiment including the amine-reactive crosslinker dithiobis(succinimidyl propionate) (DSP). Weaker or more transient interactions between Caspase-1 and (non-substrate) downstream targets are supposed to be covalently linked by DSP and will thereby become enriched in the ASC pellet fraction. Although this approach should also lead to an increase in the background signal, since my read-out is based on recruitment to the insoluble fraction, I deemed it feasible as the quadruplet measurement was successful in eliminating unspecific hits.

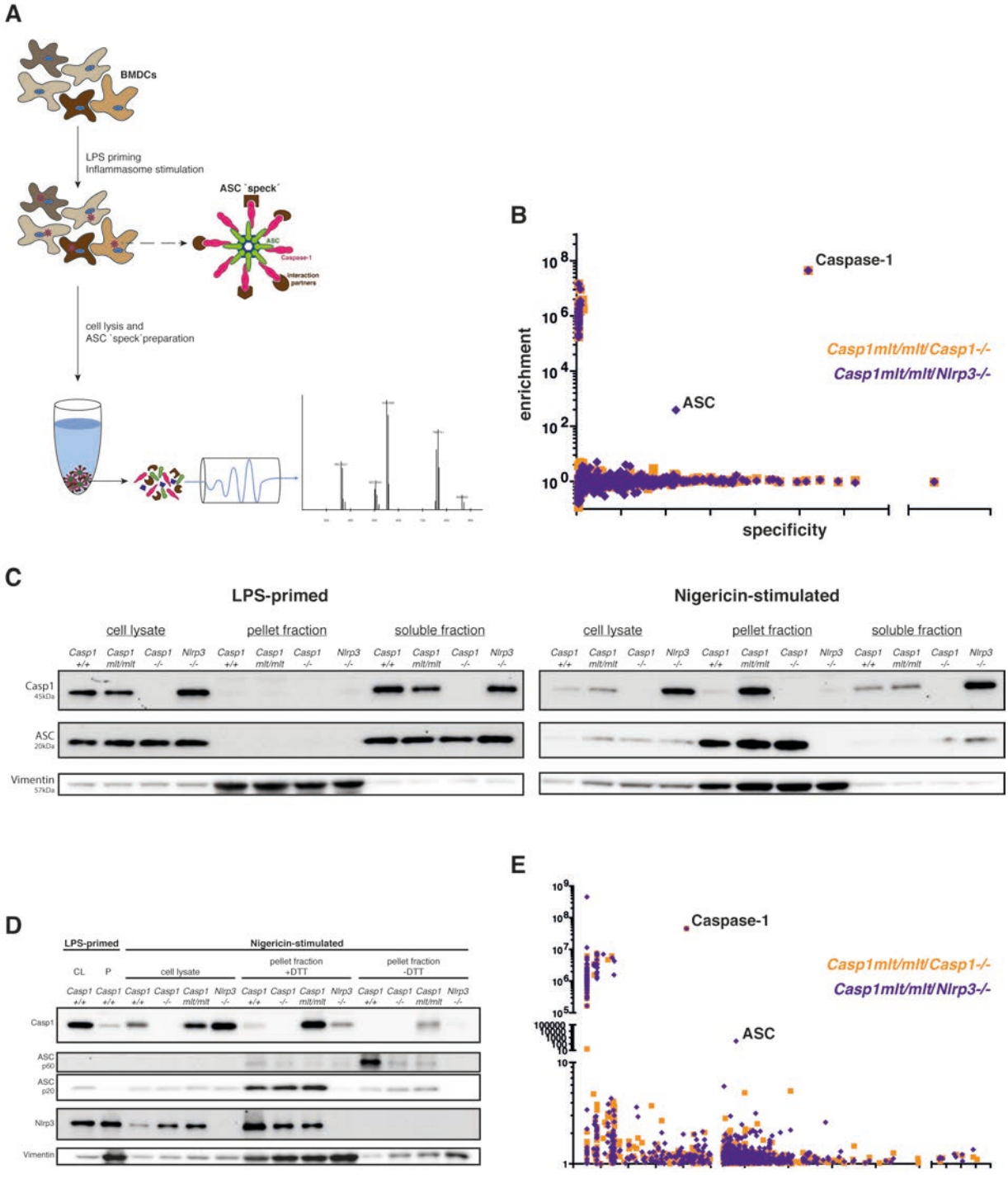

Figure 12: Mass spectrometry analysis of ASC "speck" preparations
(A) Experimental setup of label-free mass spectrometry analysis. BMDCs were primed and inflammasome-stimulated to induce ASC "speck" formation. Specks were isolated by centrifugation and processed for Western blot and mass spectrometry analysis. (B) Western blot results of the crosslinker-free approach are shown. Cell lysates, insoluble/pellet fractions, and soluble fractions were analyzed for presence of the inflammasome components ASC and Caspase-1. Four replicates of the pellet samples as shown in (B) were analyzed by mass spectrometry. (C) Abundance of proteins in *Nlrp3*$^{-/-}$ or *Caspase-1*$^{-/-}$ cells compared to *Caspase-1*$^{mlt/mlt}$ samples. Variation of the four *Caspase-1*$^{mlt/mlt}$ replicates determined the specificity (mean/SD). (D) Western blot analysis of samples prepared as in (B) with additional DSP-crosslinking. Presence of Nlrp3, ASC and Caspase-1 were investigated under crosslinked (-DTT) and DTT-cleaved crosslinked (+DTT) conditons. One of four identically prepared samples of each condition is shown. (E) Graphic presentation of the mass spectrometry results (as in (C)) for DSP-linked DTT-cleaved pellet samples. (B, D) Vimentin served as fractionation control.

DSP is cell-permeable and cleavable by DTT. I divided each cell lysate into two replicates. The pellet fraction from one these replicates was treated with DTT, to cleave the crosslinker, whereas the other was left DTT-free. In line with the experiment under 4.4.2, stimulation of BMDCs of *Caspase-1*$^{+/+}$, *Caspase-1*$^{-/-}$, *Nlrp3*$^{-/-}$, and *Caspase-1*$^{mlt/mlt}$ mice with nigericin caused recruitment of ASC into the insoluble pellet in all genotypes except for *Nlrp3*$^{-/-}$. The presence of ASC in the pellet fraction only after inflammasome stimulation and only in Nlrp3-proficient cells, proved the specificity of the assay under cross-linked conditions (Figure 12D, pellet fraction). Comparison of the DTT-free to the DTT-treated pellet samples showed that DTT cleaved DSP successfully as indicated by the loss of ASC multimers in the ASC Western blot and the simultaneous increase in monomeric ASC (Figure 12D, pellet fraction +/- DTT). Caspase-1 was also recruited to the pellet fractions in a signal- and genotype-specific manner (Figure 12D, pellet fraction). As seen before, inhibiting its protease-activity (*Caspase-1*$^{mlt/mlt}$) led to a significant enrichment of Caspase-1 in the insoluble fraction as compared to wild-type Caspase-1. Interestingly, upon cross-linking, Caspase-1 was detected in all quadruplicates of the pellet fractions of *Nlrp3*$^{-/-}$ cells as well as of unstimulated *wild-type* cells (Figure 12D, pellet fraction, 1 out of 4 replicates shown), indicating that at least parts of the Caspase-1 pool are in close contact to factors that are recruited the pellet even in the absence of inflammasome activation. The amount of protein was in between *Caspase-1*$^{mlt/mlt}$ and *Caspase-1*$^{+/+}$ samples. As mentioned above, no ASC was found in the pellet fraction of *Nlrp3*$^{-/-}$ cells indicating that this recruitment of Caspase-1 is independent of the adaptor protein.

After I had confirmed the success of the experiment by Western blotting, the DTT-treated pellet samples were prepared for mass spectrometry analysis. Cleavage of DSP prior to investigation by mass spectrometry is critical for identification of individual proteins. As in 4.4.2, label-free measurement of quadruplet samples resulted in conclusive results. Only hits that were measured in a minimum of three out of four replicates of the *Caspase-1*$^{mlt/mlt}$ samples were considered reliable and were used for analysis. Mass spectrometry studies with and without DSP (Figure 12B, E) detected ASC and Caspase-1 under the expected conditions. However, the use of crosslinker lowered the specificity for

Caspase-1 in relation to ASC. The results were further analyzed to distinguish between Caspase-1-dependent hits and Nlrp3-dependent hits. I supposed that interaction partners of Caspase-1 should be enriched comparably in *Caspase-1$^{mlt/mlt}$* samples over *Caspase-1$^{-/-}$* and *Nlrp3$^{-/-}$* samples, respectively. The proteins that fulfilled this criterion unfortunately did not show consistent results in the overall measurements and were therefore not considered as promising hits. Caspase-1 itself was the only exception, proving the principle of the assay. For Nlrp3-dependent interacting proteins, I searched the data for proteins that were highly enriched in *Caspase-1$^{mlt/mlt}$* over *Nlrp3$^{-/-}$* samples but not in *Caspase-1$^{mlt/mlt}$* over *Caspase-1$^{-/-}$* samples. Besides ASC as an internal control for the assay, 4 proteins fell into this class and in addition showed plausible overall results.

Taken together no interaction partners of Caspase-1 could be identified using the crosslinker DSP in sample preparations for mass spectrometry analysis. Nevertheless, 4 proteins detected could play a role in inflammasome signaling upstream of Caspase-1.

3.5 Caspase-1 autoprocessing

3.5.1 Analysis of Caspase-1 cleavage mutants in HEK293T cells

The murine Caspase-1 protein contains eight aspartate residues within its two linker regions between the CARD and p20 domain (linker-I) and the p20 and p10 domain (linker-II), respectively, that could serve as autocleavage sites (Figure 13A). Autoprocessing might be involved in IL-1 secretion and cell death independent of substrate cleavage. Therefore, I wanted to systematically compare the effect of destroying protease activity, by mutating the catalytically active cysteine, to the elimination of the autocleavage sites. Broz *et al.* have investigated the use of the different aspartate sites in autocleavage of Caspase-1 (Broz et al., 2010). On the basis of this work, I generated expression vectors for murine Caspase-1 carrying aspartate to asparagine mutations in the 8 potential Caspase-1 autocleavage sites in various combinations. The plasmids were transfected into HEK293T cells and expression and cleavage of Caspase-1 was investigated by Western blot analysis. Probing the membranes with

antibodies directed against the CARD, the p20, or p10 domains of Caspase-1 allowed to dissect the different cleavage events and the composition of the arising Caspase-1 fragments.

I found that in this model, Caspase-1 cleaved itself even in the absence of an additional inflammasome stimulus. Overexpression of the protein alone was sufficient to induce autoprocessing as soon as a certain concentration of Caspase-1 protein was reached (Figure 13B). As HEK293T cells are deficient for ASC, this Caspase-1 cleavage occurred independently of the adaptor protein (Hasegawa et al., 2005). Nevertheless, co-transfection of an *ASC* expression vector together with *Caspase-1* lowered the threshold for Caspase-1 autoprocessing (Figure 13C). These findings showed that ASC serves as a catalyst in Caspase-1 processing in overexpression studies. Importantly, the pattern of Caspase-1 cleavage was not changed in the presence of ASC, indicating that the autoprocessing mechanisms of Caspase-1 are identical whether they are induced by ASC or by increasing the concentration of Caspase-1.

3.5.2 Caspase-1 CARD-p20-linker mutants

I started my analysis of Caspase-1 autoprocessing investigating the cleavage of Caspase-1 between the CARD and p20 domain. In line with Broz *et al.*, I confirmed that positions D103 and D122 are used as cleavage sites in this first linker (Broz et al., 2010). In Western blots of cell lysates of HEK293T cells transfected with a wild-type Caspase-1 expression construct, the anti-Caspase-1 p20 antibody detected the full-length protein and two bands at around 20 kDa (Figure 13D, middle). These bands were absent when the Caspase-1-mlt mutant was expressed. This finding demonstrates that the observed cleavage events were a result of autoprocessing, not of cleavage by endogenous proteases active in HEK cells or of high protein-turnover during overexpression. Comparison to Caspase-1 mutants D103N, D122N, and D103N+D122N allowed to identify the described bands as two fragments of the p20 domain, cleaved at different sites in linker-I. The upper of the two bands represents the p20 domain cut at D103 since it is gone in the D103N mutant (a different slightly

bigger band appeared here), whereas the lower one has been cut at D122 (gone in the D122N mutant). The existence of the bigger fragment of the p20 domain (Figure 13D, middle, Casp1-wt) indicates that cleavage at position 103 and 122 was not a sequential but an either-or event, at least under overexpression conditions. My experiments also showed that Caspase-1 exhibited a preference for autoprocessing at D103 over D122 as indicated by the stronger signal for the upper p20 domain band. The finding that mutation of D103N - as compared to D122N did not only abolish generation of the respective p20 fragment but had an influence on the overall processing of Caspase-1, further suggested that position D103 plays a role in regulating Caspase-1 autocleavage (Figure 13D, middle, Casp1 D103N). In addition to the p20 domain fragment that was still generated by cleavage at D122 in the Caspase-1 D103N mutant, three new cleavage fragments were detected by the anti-Caspase-1 p20 antibody for this mutant. These additional bands were identical to the cleavage pattern of the Caspase-1 D103N+D122N double mutant (Figure 13D, middle, compare Casp1 D103N and Casp1 D103N+D122N). The biggest of these bands also appeared in the anti-Caspase-1 CARD Western blot, showing that this band represents a CARD-linker-I-p20 fragment (Figure 13D, left). Cleavage between the p20 and p10 domains was not affected by any of the mutations between the CARD and the p20 domain as all mutants still gave rise to a Caspase-1 p10 fragment (Figure 13D, right).

3.5.3 Caspase-1 p20-p10-linker mutants

In the second linker region between the p20 and p10 domains of Caspase-1, I targeted all six aspartate residues (D296, D300, D304, D308, D313, and D314) for mutation and cloned expression vectors carrying these mutations in various combinations. In line with Broz *et al.*, I found that D300 and D304 are not used in autocleavage of Caspase-1. There was no difference in the cleavage pattern between the quadruple mutant D296N+D308N+D313N+D314N and the sextuple mutant D296N+**D300N**+**D304N**+D308N+D313N+D314N (Figure 13E, left and right panel, lanes 12 and 13). In both mutants, the p10 domain could

not be separated from the p20 subunit anymore and instead two new bands appeared in the blots with both antibodies at around 35kDa. These bands were detected by antibodies directed against the p20 and the p10 subunit. They therefore represented Caspase-1 fragments consisting of the p20 and p10 domain plus their linker. The different sizes of these two fragments presumably stem form split-off of the CARD at either D103 or D122 as demonstrated in 4.5.2. Thus, under overexpression, either of these two sites can be used, but cleavage does not necessarily proceed to D122 after D103 has been used. The presence of these p20-linker-II-p10 fragments showed that cleavage between the CARD and p20 domain is not prevented by blockage of cleavage between the p20 and p10 domains. Together with the results from 4.5.2, my findings therefore revealed that cleavage in one linker of Caspase-1 is not required for cleavage at the other linker in an overexpression system.

In contrast to D300 and D304, these overexpression studies demonstrated that the other four aspartate residues in linker-II (D296, D308, D313, D314) were used in Caspase-1 autocleavage. By transfecting *Caspase-1* expression vectors containing Asp (D) to Asn (N) mutations at these sites in different combinations, I was able to prove D296, D308, D313, and D314 as relevant in Caspase-1 processing (Figure 13E, lanes 3-11). Compared to the *Caspase-1* wild-type construct, the two p20 domain fragments described above shifted to a higher molecular weight in the Caspase-1 D296N mutant (Figure 13E, lane 6). This effect of the mutation showed that D296 is used for autoprocessing in wild-type Caspase-1. Additional mutation of D308 to N in the D296N background further increased the size of the bands for the p20 domain, demonstrating the additional physiological relevance of D308 in Caspase-1 cleavage (Figure 13E, lane 9). Only mutation of four Asp residues (D296N+D308N+D313N+D314N) abolished the separation of the p20 from the p10 domain and led to the above-mentioned p20-linker-II-p10 bands (Figure 13E, lane 12).

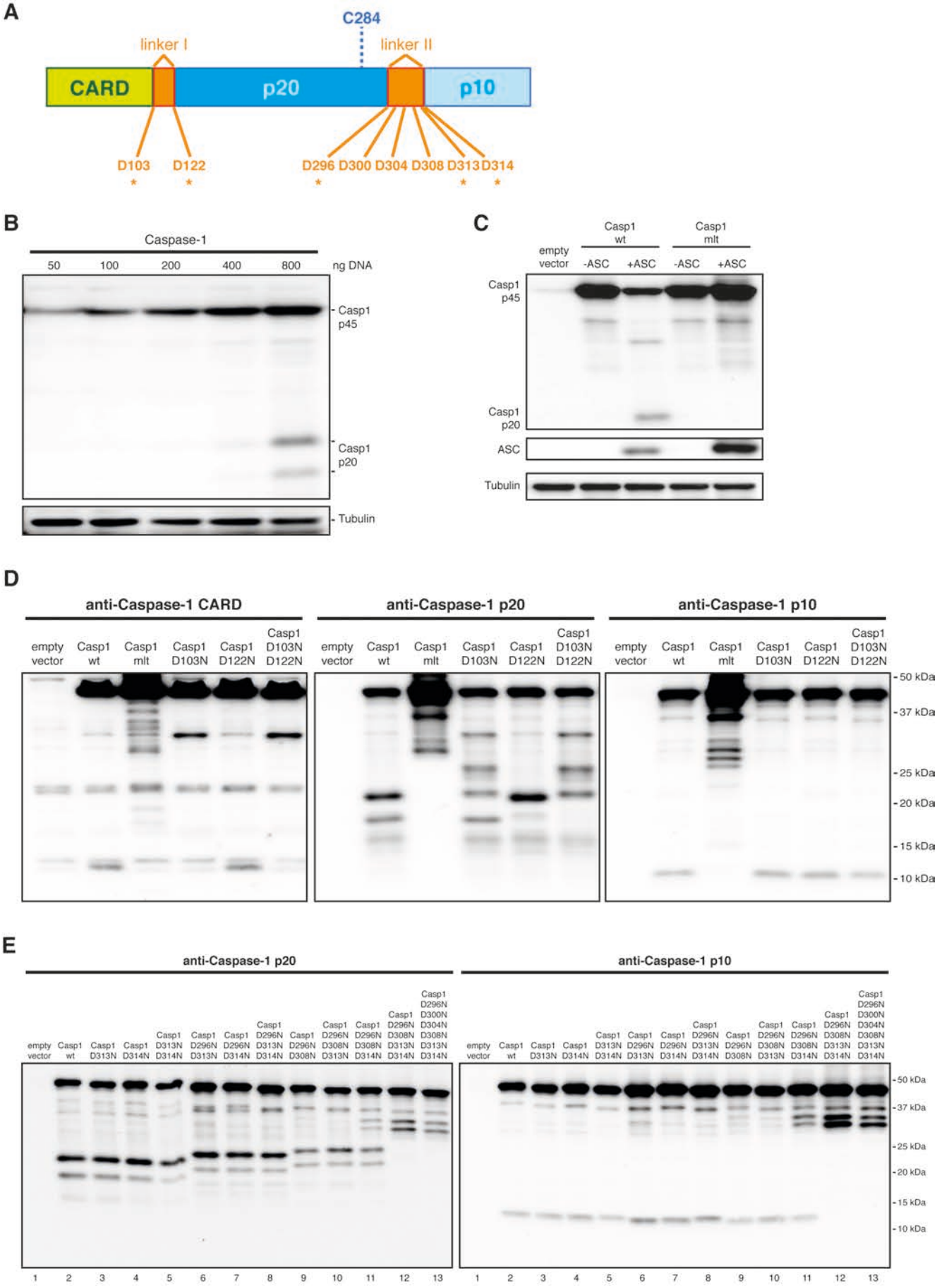
A
C284
linker I
linker II
CARD
p20
p10
D103
D122
D296 D300 D304 D308 D313 D314
B
Caspase-1
50
100
200
400
800
ng DNA
Casp1 p45
Casp1 p20
Tubulin
C
empty vector
Casp1 wt
Casp1 mlt
-ASC
+ASC
-ASC
+ASC
Casp1 p45
Casp1 p20
ASC
Tubulin
D
anti-Caspase-1 CARD
anti-Caspase-1 p20
anti-Caspase-1 p10
empty vector
Casp1 wt
Casp1 mlt
Casp1 D103N
Casp1 D122N
Casp1 D103N D122N
50 kDa
37 kDa
25 kDa
20 kDa
15 kDa
10 kDa
E
anti-Caspase-1 p20
anti-Caspase-1 p10
empty vector
Casp1 wt
Casp1 D313N
Casp1 D314N
Casp1 D313N D314N
Casp1 D296N D313N
Casp1 D296N D314N
Casp1 D296N D308N
Casp1 D296N D313N D314N
Casp1 D296N D308N D313N D314N
Casp1 D296N D300N D304N D308N D313N D314N
1 2 3 4 5 6 7 8 9 10 11 12 13
50 kDa
37 kDa
25 kDa
20 kDa
15 kDa
10 kDa

Figure 13: Autocleavage of murine Caspase-1
(A) Graph of murine Caspase-1 protein consisting of 3 subunits - CARD, the p20, and the p10 domain - separated by two linker regions containing in total eight (two + six) aspartate (D) residues that could potentially serve as autocleavage sites. D-residues marked with an asterisk (*) are conserved in mouse and human Caspase-1. Cysteine at position 284 represents the active site. (B) Overexpression of Caspase-1 wild-type (wt) resulted in spontaneous auto-activation and dose-dependent processing of Caspase-1. Caspase-1 activity was assessed by detection of cleaved Caspase-1 p20 fragments. (C) Caspase-1 cleavage in the presence of adaptor protein ASC. (D) Role of D103 and D122 in Caspase-1 autolceavage. After overexpression, Western blots of cell lysates of HEK293T cells were probed with antibodies against Caspase-1 CARD, p20, and p10 domains, respectively, to detect cleavage products. (E) HEK293T cells were transfected with *Caspase-1* constructs carrying various mutations at potential autocleavage sites in linker-II. Relevance of individual cleavage sites in Caspase-1 autoprocessing were addressed by Western blotting of cell lysates. The membranes were probed with antibodies directed against the Caspase-1 p20 and p10 domain.

To more thoroughly investigate the influences of mutating aspartate residues towards the end of linker-II, I probed these samples with an antibody directed against the Caspase-1 p10 domain (Figure 13E, right panel). Although the changes in size were smaller and therefore more difficult to resolve, I could visualize that position D313 and D314 play a role in Caspase-1 cleavage. Exchange of D314 to N generated a bigger p10 domain fragment compared to wild-type Caspase-1 (Figure 13E, right panel, lanes 4, 7 and 11). Additional mutation of D313 further added to the p10 fragment (Figure 13E, right panel, lanes 5 and 8). Thus, the use of two antibodies, directed against the different domains of Caspase-1, allowed me to comprehensively follow the autocleavage processes happening within the Caspase-1 linker-II.

In contrast to cleavage in linker-I, separation of the p10 domain from the p20 domain was a sequential process. In cells transfected with *Caspase-1* wild-type, of the possible cleavage sites in linker-II, the ones closest to the respective domains (D296 and D314) were invariably used, resulting in only two bands for the p20 domain and 1 for the p10 domain as final products (Figure 13E, lane 2).

3.5.4 Proteolytic activity of uncleavable Caspase-1

To test if inhibiting processing of Caspase-1 by mutating all relevant autocleavage sites has an effect on its activity, I did co-transfection experiments in HEK293T cells. I overexpressed different combinations of wild-type, melted, and non-cleavable Caspase-1. As demonstrated in 4.5.1, wild-type Caspase-1 underwent spontaneous auto-proteolysis if a certain protein threshold was

reached (400 ng plasmid transfected per 6-well). As expected, the non-cleavable mutant (Casp1-nc; D103N+D122N+D296N+D308N+D313N+ D314N) and the proteolytically inactive Caspase-1 mutant (Casp1-mlt) did not undergo fragmentation into p20 domain fragments at any expression level (Figure 14A, Casp1-wt, Casp1-nc, Casp1-mlt 400 ng). The differential migrating behavior of Caspase-1-nc compared to Caspase-1-wt in SDS-PAGE is explained by the change in the charge of the Caspase-1 protein due to the exchange of several aspartate (acidic) to asparagine (neutral) residues (Figure 14, compare Casp1-wt to Casp1-nc).

Co-transfection of Caspase-1-mlt together with Caspase-1-wt at doses that alone are suboptimal for autoprocessing (200 ng plasmid), resulted in the generation of p20 domain fragments at levels comparable to 400 ng transfected Caspase-1-wt (Figure 14A, second lane from the right). This showed that an increase in the amount of Caspase-1 protein is sufficient to activate wild-type Caspase-1, even in the absence of protease activity in a large part of the Caspase-1 protein pool.

In view of this finding, I transfected *Caspase-1*^{mlt} simultaneously with non-cleavable *Caspase-1* to investigate whether Caspase-1-nc still exhibits protease activity. Co-expression of these two mutants did not result in cleavage of Caspase-1 and indicated that Caspase-1-nc exhibits reduced protease activity compared to wild-type Caspase-1 (Figure 14A, right lane).

To assess whether cleavage of Caspase-1 in one of the two linkers is sufficient to reconstitute normal activity of non-cleavable Caspase-1, I repeated the co-transfection experiments with the different partially non-cleavable Caspase-1 mutants (Figure 14B). As these mutants bear an active site but are unable to cleave themselves due to the D to N mutations, I co-expressed them together with HA-tagged Caspase-1-mlt. The melted mutant is inactive at any concentration but can be cleaved by co-expressed, active Caspase-1 proteins. Consequently, any p20 fragments detected in this assay must result from cleavage of Caspase-1-mlt by the cleavage mutants. In contrast to Caspase-1-wt, the Caspase-1 variants defective in cleavage in linker-I (Casp1 D103N+D122N) or linker-II (Casp1 D296N+D308N+D313N+D314N) were unable to cleave Caspase-1-mlt and produce a p20 domain product (Figure

14B, 4 rightest lanes). However two higher molecular weight bands appeared in co-expression of Caspase-1-mlt with Caspase-1 D103N+D122N (Figure 14B, third lane from right). These bands might correspond to CARD-p20 or p20-p10 fragments and indicate limited activity of the linker-I mutant.

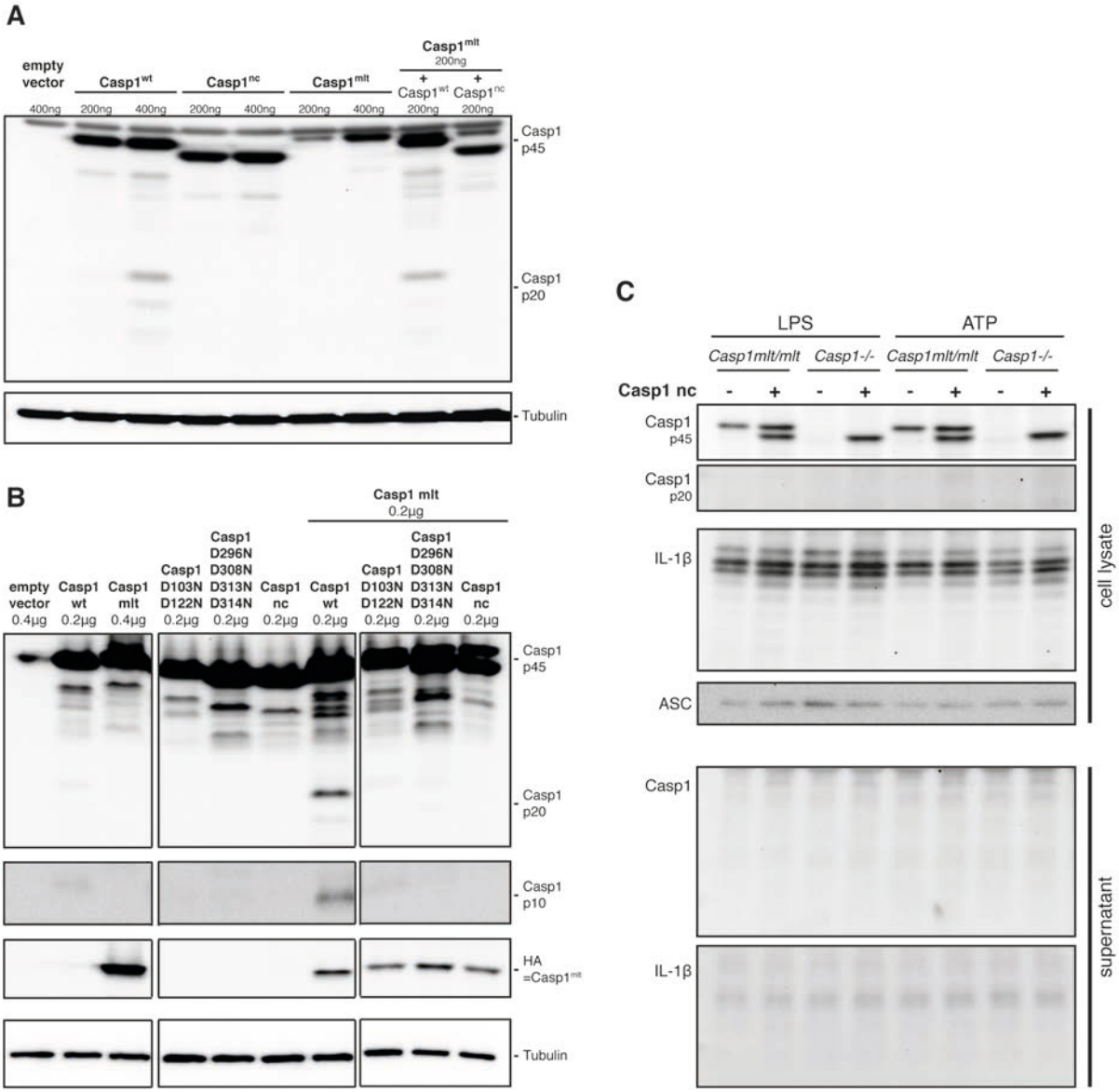

Figure 14: Activity of Caspase-1 cleavage mutants
(A) *Caspase-1 wild-type*, *mlt*, or *nc* mutants were transfected into HEK293T cells alone or in combination in different concentrations. Whole cell lysates were analyzed by Western blotting for generation of Caspase-1 p20 cleavage fragments as a read-out for Caspase-1 activity. (B) HEK293T cells were transfected with *Caspase-1 wild-type*, *melted* and different *Caspase-1* cleavage mutants alone or in combination. Caspase-1 activity was monitored by appearance of Caspase-1 p20 cleavage products in cell lysates. Anti-HA antibody detected HA-tagged Caspase-1-mlt. (C) BMDMs of *Caspase-1*$^{mlt/mlt}$ or *Caspase-1*$^{-/-}$ mice were retrovirally transduced with the *Caspase-1*^{nc} mutant. Cell lysate and supernatant samples were analyzed for Caspase-1 expression and cleavage and for proIL-1β cleavage and secretion by Western blotting.

3.5.5 Retroviral reconstitution of Caspase-1 mutants in BMDMs

After investigating the Caspase-1 non-cleavable mutant in HEK293T overexpression systems, I went on to evaluate its role in cells of the myeloid lineage. To this end, I transduced BMDMs from *Caspase-1*$^{mlt/mlt}$ or *Caspase-1*$^{-/-}$ mice with retroviral particles carrying a vector for *Casp1*^{nc}. Successful transduction was confirmed by FACS analysis for GFP-positive cells (data not shown). Transduced BMDMs were then LPS-primed or primed and Nlrp3-inflammasome stimulated (ATP). I used Western blot analysis of cell lysates and supernatant samples of these cells to examine inflammasome-competence of these cells. Western blots of the cell lysates showed that I achieved an expression level of Caspase-1-nc comparable to endogenous Caspase-1-mlt (Figure 12C). The differential migration behavior of Caspase-1-nc made it easily distinguishable from Caspase-1-mlt protein (Figure 14C, compare *Caspase-1*$^{mlt/mlt}$ +Casp1-nc to *Caspase-1*$^{-/-}$ +Casp1-nc). Despite the good expression of Caspase-1-nc, the mutant was not able to restore proIL-1β cleavage and IL-1β secretion in *Caspase-1*$^{mlt/mlt}$ or *Caspase-1*$^{-/-}$ BMDMs (Figure 14C, supernatant). In line with previous co-expression experiments introduction of the non-cleavable Caspase-1 mutants into *Caspase-1*$^{mlt/mlt}$ cells also did not lead to Caspase-1 cleavage (Figure 14C, cell lysate).

4 Discussion

4.1 Basic phenotype of *Caspase-1^{melted}* mice

Comprehensive analysis by Southern blotting and diverse PCRs at each milestone verified the successful generation of the knock-in *Caspase-1^{melted}* lines in two different genetic backgrounds. As a final verification of successful generation of the model, expression of the mutant Caspase-1 protein was investigated by Western blotting of BMDC-lysates obtained from mice before and after Cre recombinase-mediated removal of the neomycin resistance cassette from the *Caspase-1* genomic locus. The comparison between cells of neomycin-carrying, *melted,* and *wild-type* mice showed that deletion of the resistance cassette restored physiological Caspase-1 protein expression in the final transgenic lines in both backgrounds. This fact is critical for reasonable comparison of inflammasome signaling in *melted* to *wild-type* animals.

Caspase-1$^{mlt/mlt}$ mice derived from C57Bl/6N and 129S1/X1 stem cells were viable, fertile, and healthy under SPF conditions. Up to an age of 12 and 6 month, respectively, *Caspase-1^{melted}-129* and *Caspase-1^{melted}-B6* mice showed no differences in development, appearance, and body weight as compared to wild-type littermates. Furthermore, within that time, no spontaneous pathologies were observed in the animals. Breeding pairs of heterozygous parents resulted in the expected mendelian ratios of wild-type, heterozygous, and homozygous offspring. Accordingly, males and females each represented approximately 50% of the offspring. In view of the described autoinflammatory phenotype of inactivating Caspase-1 variants in humans (Luksch et al., 2013), these findings were surprising. However they are in line with publications on Caspase-1-deficient animals (Kuida et al., 1995; Li et al., 1995).

Besides the general phenotype, I also investigated the development of the adaptive immune system in *Caspase-1^{melted}* mice. In agreement with the authors of the first Caspase-1 null mice (Kuida et al., 1995; Li et al., 1995), I did not observe any abnormalities in the distribution of $CD4^+$, $CD8^+$, and $CD4^+CD8^+$ T-lymphocytes in thymus and lymph nodes. This fits to the established view that apoptosis plays a pivotal role in negative selection of T cells but that Caspase-1-dependent pyroptosis is not involved in this process (Surh and Sprent, 1994).

In addition, neither the development of other specific types of T cells (regulatory T cells) nor the maturation and activation state of effector B cells was affected by mutant Caspase-1. These results, together with the normal overall health of the animals, argued against immunopathologies in the transgenic animals. Thus, I revealed that *Caspase-1^{melted}* mice possess a normal and functional adaptive immune system and confirmed that absence or mutation of Caspase-1 does not interfere with a normal embryonic and adult development. Because the *in vitro* differentiation of bone marrow-derived myeloid cells was also indistinguishable from wild-type cells, transgenic *Caspase-1^{melted}* mice were considered as suitable models to investigate the effect of inflammasome activation in the presence of protease-dead Caspase-1.

The data shown for immunophenotyping analysis and *in vitro* differentiation of BMDCs originated from *Caspase-1^{melted}-129* mice. Prior to analysis, the mice had been backcrossed to the C57Bl/6 background for 5 generations, rendering their genome largely identical to that of the acceptor strain. The main difference between *Caspase-1^{melted}-B6* and *Caspase-1^{melted}-129* mice at this stage was therefore, the expression of functional Caspase-11 in only the C57Bl/6 ESC-derived animals. However, *Caspase-11* knockout animals have been created and did not present any major health issues (Kayagaki et al., 2011). Thus, it can be assumed that *Caspase-1^{melted}-B6* mice show the same immunophenotype as 129S1/X1-derived transgenic mice. Availability of both *Caspase-1^{melted}* strains allowed to univocally distinguish between features of Caspase-1 and Caspase-11 activity without the need for Caspase-11-deficient controls.

4.2 The role of Caspase-1 proteolytic activity in canonical inflammasome activation

I tested BMDCs of *Caspase-1^{melted}* mice for inflammasome activation using stimuli of various inflammasome receptors. Myeloid cells expressing a proteolytically inactive Caspase-1 did not secrete mature IL-1β in response to Nlrp3, Aim2, and Nlrc4 stimulation. This was in line with our hypothesis and data obtained from wild-type cells treated with a specific Caspase-1 inhibitor (Ac-YVAD-cmk). As proIL-1β is a target of Caspase-1, it was expected that

abolishment of this cleavage was accompanied by absence of secreted mature IL-1β. Interestingly, BMDCs from *wild-type* animals exposed to Ac-YVAD-cmk were still able to release proIL-1β and IL-1α. This phenomenon has already been made in the first descriptions on *Caspase-1* knockout mice (Kuida et al., 1995) and, together with the observations from our group (Groß et al., 2012), built the basis for generating the transgenic, protease-dead Caspase-1 mouse lines. In cells of *Caspase-1*$^{mlt/mlt}$ *mice* however, secretion of IL-1α and any form of IL-1β was completely eliminated. The dependence on Caspase-1 for IL-1 family cytokine secretion was demonstrated in the beginning of Caspase-1 research (Kuida et al., 1995; Li et al., 1995). Later, Charles Dinarello suggested control of IL-1α by released IL-1β in an autocrine way (Dinarello, 2009). He therefore assumed that absence of Caspase-1 influenced IL-1α secretion only indirectly via IL-1β. However, Groß *et al.* disproved this hypothesis and demonstrated Caspase-1-dependent IL-1α secretion in IL-1β knockout cells following inflammasome activation.

Further discrepancies between cells with differential inhibition of Caspase-1 activity were observed in terms of pyroptotic cell death. While chemical blockade of protease activity did not affect the extend of cell death as compared to uninhibited cells, genetic ablation of Caspase-1 protease activity prevented cell death entirely as was measured by LDH release. Taken together, my results revealed that *Caspase-1*$^{mlt/mlt}$ cells copy the inflammasome phenotype of Caspase-1 knockout cells in terms of IL-1β and IL-1α cleavage and release. In contrast, they differed from cells with specific chemical Caspase-1 inhibition. An explanation for these findings is incomplete suppression of Caspase-1 activity by Ac-YVAD-cmk.

The possibility of imperfect inhibition of Caspase-1 as a reason for the remaining secretory activity of Caspase-1 was of course considered prior to this study. The inconsistency in the efficacy of chemical inhibition is also reflected in the literature in the form of contradictory publications on the requirement of Caspase-1 activity for IL-1α secretion and cell death (Guey et al., 2014; Keller et al., 2008; Kuida et al., 1995; Li et al., 1995; Van Opdenbosch et al., 2014). However, the earlier observation from our lab that proIL-1β cleavage was thoroughly abolished by Ac-YVAD-cmk but secretion was not, led to the

assumption that downstream cleavage activity was indeed blocked (Groß et al., 2012). Thus, it implied protease-independent functions of Caspase-1. In contrast, my results suggest that minimal residual activity of Caspase-1 in the presence of inhibitor is responsible for cytokine secretion and cell death as the absence of any protease activity in *Caspase-1*$^{mlt/mlt}$ samples eliminated all these effects.

It was intriguing to find inhibited Caspase-1 to be capable of performing some unknown kind of proteolysis while it did not cleave its best-known substrate proIL-1β. Therefore, I hypothesize that compromised Caspase-1 still cleaves certain substrate proteins that play a role in the secretion pathway or in induction of cell death. Three explanations are possible. First, although full-length Caspase-1 has been shown to be only weakly active (Yamin et al., 1996), this marginal activity might have crucial functions during IL-1 family cytokine secretion and pyroptosis (but not proIL-1β cleavage). Caspase-1 might be able to process substrates after recruitment to the ASC "speck" but prior to autocleavage. Secondly, inhibition of Caspase-1 by the pseudo-substrate Ac-YVAD-cmk depends on and occurs after autocatalytic cleavage and activation of the protease, because it allows access and covalent binding to the enzyme's active site (Walker et al., 1994). Such a competitive mechanism harbors the statistical risk that Caspase-1 cleaves other substrates before it becomes silenced by Ac-YVAD-cmk. Therefore, target proteins, for which only fractional cleavage of the protein pool by Caspase-1 is sufficient to activate full downstream signaling, could continue the cascade under these circumstances. In both mentioned scenarios, preference of uncleaved or minimally active Caspase-1 for substrates other than proIL-1β could be due to a higher ratio of enzyme to substrate and/or a greater specificity of the protease for this substrate. Gasdermin D, a protein that has been described to be a substrate of Caspase-1 and was very recently discovered to have critical functions in pyroptosis induction downstream of Caspase-11 and/or -1, could represent such a target (Agard et al., 2010; Kayagaki et al., 2015; Shi et al., 2015).

An increase in inhibitor concentration was unable to block IL-1α and proIL-1β secretion as well as cell death as previously demonstrated (Groß et al., 2012) and independently verified in our lab (data not shown). Furthermore, at all

inhibitor doses tested, Caspase-1 was still processed into a p20 fragment. Caspase-1 linked to Ac-YVAD-cmk can be distinguished from active Caspase-1 by Western blotting due to a shift towards a higher molecular weight of the conjugated form. Under all inhibitory conditions, the whole fraction of p20 fragments was found to migrate at the size of p20 +Ac-YVAD-cmk, demonstrating a complete inhibition of the protease at the end-point of the experiment. Simultaneously, this showed the inability of the inhibitor to block the first event of Caspase-1 autoprocessing. In line with this, full-length Caspase-1 did not shift in Western blot analysis, implying that only cleaved Caspase-1 is able to bind the inhibitor. These findings do not speak against the aforementioned possibility of residual Caspase-1 protease activity but rather confirm formation of an active enzyme before the peptide-inhibitor was bound.

Additionally, this discovery allows to draw a conclusion in terms of the activation mechanism of Caspase-1. In the presence of inhibitor, a part of the Caspase-1 pool still undergoes processing into the p20 fragment following inflammasome activation, indicating, as mentioned, that the inhibitor cannot prevent this event. However, the majority of Caspase-1 protein is still found in the full-length (p45) form. This in turn, lets one speculate that activation of the bulk of the Caspase-1 protein pool does not rely on autoprocessing but that a few processed Caspase-1 molecules cut other p45 proteins intermolecularly, thereby starting an proteolytic cascade. While the initial inflammasome-dependent activation of some Caspase-1 proteins remains possible under inhibitor treatment, the progression of the activation cascade is blocked at this point because the compound attacks as soon as active enzymes have formed. Taken together, these results suggest a two-step process in which Caspase-1 would be its own initiator caspase. The exact activation mechanism of Caspase-1 remains to date elusive and is of great interest to the field. Thus, further investigating this hypothesis might advance our understanding of Caspase-1 regulation.

As a last aspect, the differing phenotypes of *Caspase-1*$^{mlt/mlt}$ and inhibitor-treated samples might result from the inability of inactive Caspase-1 to leave the inflammasome. Following activation, Caspase-1 is thought to concentrate on the ASC “speck”, undergo autoprocessing, and by that, disconnect itself from the complex again. Protease-dead Caspase-1 is incapable of cleaving itself off

from the “speck”. Thus, any function of Caspase-1, which requires separation from the inflammasome complex, is prevented. Actions of Caspase-1 that would require disconnection from the ASC “speck” could involve processing of target proteins, which are spatially inaccessible to inflammasome-incorporated Caspase-1, as for example membrane-bound proteins. Alternatively, Caspase-1 might drag non-substrate binding proteins with it when leaving the ASC “speck”, acting like a transporter or scaffold protein. In this case, protease activity would only be indirectly involved in downstream effects. In contrast to Caspase-1-melted, peptide inhibitors, as discussed in the previous paragraph, do not fully prevent autocleavage. Indeed, we observed a stronger signal for Caspase-1 within the speck by immunofluorescence staining in the *melted* mutants than in cells treated with inhibitor. Lu *et al.* recently gave new, imaging-based, insights into the structure of inflammasome complexes (Lu et al., 2014). They described the formation of Caspase-1 polymer fibers radiating from an ASC core multimer. With regard to this model, it is conceivable that, in the presence of Ac-YVAD-cmk, the residual activity of individual Caspase-1 molecules is sufficient to cause destabilization and maybe breaking of the fibers. This scenario would explain the different immunofluorescence signals observed for Caspase-1-melted as compared to inhibited Caspase-1 and speak for (partial) release of inhibited Caspase-1 from the “speck”. This event might also be sufficient to initiate protease activity-independent functions of Caspase-1 that would require its release from the ASC speck.

To conclude, all three proposed models give reasonable explanations for the differences between *Caspase-1*$^{mlt/mlt}$ and Ac-YVAD-cmk-treated samples. Potentially, even a combination of the mentioned points is responsible for the observed phenomenon.

The knowledge obtained from *Caspase-1*^{melted} mice also shed new light on the debate about the route of IL-1 cytokine secretion. As myeloid cells of *Caspase-1*^{melted} mice were defective for both, pyroptosis and cytokine secretion, a link between the two pathways could be argued. However, studies showing that pore formation, which is to date assumed to be the executioner step in pyroptosis induction, is not required for IL-1 release as well as data demonstrating IL-1β secretion in pyroptosis-incompetent neutrophils stand in

contrast to this idea (Brennan and Cookson, 2000; Chen et al., 2014; Fink and Cookson, 2006). Further studies are needed to dissect the underlying mechanisms but I could prove that Caspase-1 proteolytic activity is indispensable for both processes. Whether Caspase-1 attacks a common molecular target, which subsequently diverges into cell death or unconventional secretion or whether Caspase-1 triggers two unrelated pathways will be the content of future investigations.

4.3 Caspase-1 catalytic activity in non-canonical inflammasome activation

Direct comparison of BMDCs from *Caspase-1^{melted}-B6* and *-129* mice in Nlrp3-, Aim2-, and Nlrc4-inflammasome activation revealed no difference between the two transgenic lines in IL-1α and IL-1β secretion as well as cell death. As expected, a differential phenotype was only observed in response to stimuli targeting Caspase-11 (LPS transfection, *E.coli*). Under these conditions, Caspase-11-proficient *Caspase-1$^{mlt/mlt}$-B6* mice showed substantial release of IL-1α and LDH. Interestingly, IL-1α secretion was diminished in *Caspase-1$^{mlt/mlt}$-B6* and *ASC$^{-/-}$* samples as compared to C57Bl/6 wild-type samples, indicating a role for the canonical inflammasome in Caspase-11-initiated responses. Based on the recent publications by Rühl *et al.* and Schmid-Burgk *et al.* I favor the idea that Caspase-11 activation causes assembly of an Nlrp3-inflammasome via potassium efflux (Rühl and Broz, 2015; Schmid-Burgk et al., 2015). This contribution of Caspase-1 appears to be required for full-blown secretion of IL-1α.

Strikingly, Caspase-11 activation by LPS transfection and *E. coli* infection presented with some differences. While for LPS transfection, IL-1α and LDH release coincided, infection with live bacteria caused comparable LDH values in all cells irrespective of the genotype. The possibility that *E. coli* themselves produce an enzyme with LDH activity needs to be excluded before further conclusions can be drawn. However, IL-1α release of infected cells followed the same pattern as with LPS transfection, although the background in the Caspase-11-deficient cells was comparably higher. An explanation for this

release might be Caspase-11-independent cells death induced by the bacteria. In principle, my results indicated a certain overlap and redundancy of Caspase-1 and -11 in response to Gram-negative bacteria. While Caspase-11 is clearly critical for inflammasome activation in response to the bacteria, I also noticed Caspase-1 cleavage and secretion in Caspase-11-deficient 129 wild-type cells. In line with this, some mature IL-1β was released from these cells, suggesting activation of Caspase-1 directly by *E. coli*. *Vice versa*, in Caspase-11-proficient cells, which expressed inactive Caspase-1 minimal IL-1β secretion was detected. This was not found in *Caspase-1*$^{-/-}$ samples from the 129-background indicating cleavage of the cytokine by Caspase-11 or by other proteases activated by Caspase-11. Thus, although my data largely confirmed the dependence of Caspase-11 on Caspase-1 protease activity for processing of proIL-1β (Kayagaki et al., 2011), I also found some deviations from this static model.

The normal induction of the NF-κB-responsive TNFα by the TLR4 and TLR1/2 agonists LPS and Pam3CSK4, respectively, served as a proof for the restriction of the effect of introducing the *melted* mutation in C57Bl/6 mice to the inflammasome pathway.

As a side effect, these experiments also confirmed existing data on the requirement for ASC in Nlrc4-activation. Interestingly, ASC is not needed for the process of cell death following infection with *S. typhimurium*. However, proIL-1β maturation and secretion did not take place. Broz *et al.* have described this phenomenon before (Broz et al., 2010). They claimed that the CARD-containing Nlrc4 protein alone could induce activation of Caspase-1, which caused pyroptosis. In contrast, in the absence of ASC, Caspase-1 was unable to undergo autocleavage and thus incapable of processing proIL-1β. The group has thereby proposed activity of uncleaved Caspase-1.

Taken together, data from *Caspase-1*$^{mlt/mlt}$ mice manifested with the same phenotype to activators of the Nlrp3-, Aim2, and Nlrc4-inflammasome irrespective of the genetic background. Selective stimulation of the non-canonical inflammasome revealed the presence and functionality of Caspase-11 in the C57Bl/6 background. Thus, I demonstrated the full requirement for Caspase-1 protease activity for all downstream effects of canonical

inflammasome activation and for substantial IL-1β maturation and secretion downstream of Caspase-11.

4.4 Protease-dead Caspase-1 in TLR and Ripk2 signaling

To exclude that other pathways crucial in innate immune signaling were affected by mutation of Caspase-1, I tested several TLR and Dectin-1 agonists. In contrast to the statements of Kuida *et al.* and Li *et al.* for *Caspase-1* knockout animals, I did not detect a reduction in TNFα and IL-6 secretion following TLR4 stimulation (LPS) in BMDCs and BMDMs of *Caspase-1*$^{mlt/mlt}$ versus *wild-type* mice (Kuida et al., 1995; Li et al., 1995). This discrepancy can be explained by the use of different cell types and stimulation protocols. However, Li *et al.* noted comparable expression levels of proIL-1β in Caspase-1-deficient and -proficient cells, indicating functional priming. Similarly, I found normal levels of proIL-1β in cell lysates of *Caspase-1*$^{mlt/mlt}$ BMDCs by Western blotting. Like for TLR4, activation of plasma membrane-bound TLR1 and TLR2, endosomal TLR7, TLR8, and TLR9, and Dectin-1 produced equal amounts of the NF-κB-controlled cytokines TNFα and IL-6 in *wild-type* and mutant cells. Taken together, my data revealed that targeting *Caspase-1* did not disturb inflammasome-independent pathways engaged by other PRRs. This is in line with the healthy state and the normal general immunophenotype of *Caspase-1*$^{mlt/mlt}$ mice discussed above. Furthermore, it rules out that the lack of cytokine secretion seen with mutant Caspase-1 was caused by reduced intracellular levels of proIL-1β protein due to compromised priming.

Another signaling pathway I investigated in the context of *Caspase-1*^{melted}, was the interaction with Ripk2. Based on Caspase-1 variants found in humans (Luksch et al., 2013), Heymann *et al.* have performed reconstitution experiments of various Caspase-1 mutants in cell lines (Heymann et al., 2014). The authors described a more efficient co-immunoprecipitation of Ripk2 with Caspase-1 mutants that were impaired in their proteolytic function than with the wild-type protease. Additionally, an increase in NF-κB activity was observed, caused by the Caspase-1 mutants and the authors claim a critical role for Ripk2 in this interplay. I was therefore wondering whether *Caspase-1*$^{mlt/mlt}$ mice would

exhibit an autoinflammatory phenotype due to overshooting NF-κB signaling. Luksch *et al.* found varying extends of reduction of Caspase-1 activity in the patients' mutants (Luksch et al., 2013). Complete elimination of Caspase-1 activity by direct mutation of the active site, as done in *Caspase-1*^{melted} mice, should consequently cause the most pronounced phenotype. However, as homozygous mice developed normally and aged without any signs of illnesses, I did not find any indication for relevance of the proposed pathway *in vivo*.

Nevertheless, I proceeded to investigate the connection between Caspase-1 and Ripk2 *in vitro*. In accordance to Heymann *et al.*, I saw an interaction between the two proteins after overexpression in HEK293T cells, which was more pronounced with Caspase-1-melted than with wild-type Caspase-1. I also noticed the described decrease in Ripk2 protein levels in the presence of active Caspase-1. Studying BMDCs treated with MDP, a well-known stimulus of NF-κB relying on Ripk2, no difference in the extent of NF-κB activity appeared in *wild-type* versus *melted* cells. *Vice versa*, Caspase-1 activation by inflammasome stimuli did not cause enhanced NF-κB responses.

Based on the results from overexpression studies, it will be worth to clarify whether Ripk2 is processed following Nod2 and/or inflammasome activation in a Caspase-1 activity-dependent manner under physiological conditions. However, the consequences of this potential regulation might differ from the proposed overactivation of NF-κB as the phenotype described in patients was not recapitulated in *Caspase-1*$^{mlt/mlt}$ mice.

4.5 (Non-substrate) Interaction partners of Caspase-1

As introduced above, inflammasome activation leads to assembly of a supramolecular platform called ASC "speck". Visualization of this complex by immunofluorescence imaging revealed that this "speck" formation is not impaired in *Caspase-1*$^{mlt/mlt}$ BMDCs. We found a clustering of ASC comparable to the signal in wild-type cells. These results were expected as recruitment of ASC to the respective inflammasome receptor takes place independently and upstream of Caspase-1. However, it was relevant for this study to investigate whether mutant Caspase-1 was still redirected to the ASC complex upon

stimulation. As mentioned above, imaging did not only confirm the presence of *Caspase-1*^{melted} on the “speck” but also, compared to wild-type Caspase-1, detected higher amounts of the protease on the “speck”. This was concluded from a bigger diameter of the punctate staining. Accordingly, in Western blot analysis of purified ASC “specks”, I found considerately more Caspase-1 protein in samples from *Caspase-1*$^{mlt/mlt}$ than from *wild-type* cells. As discussed in 5.2, this phenomenon was most likely caused by the inability of proteolytically inactive Caspase-1 to release itself from the inflammasome platform. It is generally accepted that concentration of proCaspase-1 on the ASC “speck” induces autoproteolytic processing. First, the protease cuts between the p20 and p10 domain and subsequently in the part linking the CARD and p20 domain (Ramage et al., 1995; Yamin et al., 1996). By this last event, the enzyme can break the connection to ASC and is enabled to move freely in the cytosol to find substrates and possibly other non-substrate interaction partners. Thus, a proteolytically incompetent Caspase-1 molecule would be stuck at the “speck”. Accordingly, the total mass of Caspase-1 on the speck would increase because the dynamic process of recruitment and release was shifted towards recruitment. As this was indeed the case as seen in imaging and Western blotting, my data supported the existing model. Taken together, I found protease activity to not be required prior to and during binding of Caspase-1 to ASC but for its later dissociation from the inflammasome complex. Furthermore, these results support my previous hypothesis that the lack of detachment of Caspase-1 from the protein complex could account for the phenotype of *Caspase-1*$^{mlt/mlt}$ myeloid cells.

The treatment of wild-type BMDCs with Ac-YVAD-cmk also led to a stronger immunofluorescent signal for Caspase-1 on the assembled speck as compared to uninhibited *wild-type* cells, albeit not as strong as in *Caspase-1*^{melted} cells. According to the discussion in 5.2, only active and therefore cleaved Caspase-1 binds the inhibitor. The finding that under such conditions more Caspase-1 was agglomerated than in untreated cells seemed contradictory to the explanations given for *Caspase-1*^{melted}. An answer to this conflict was given by Ramage *et al.* and Yamin *et al.* (Ramage et al., 1995; Yamin et al., 1996). They investigated the cleavage process of Caspase-1 and the binding affinities of the different

cleavage products for Ac-YVAD-derivatives. Their study revealed that the first cleavage event takes place in the linker between the p20 and p10 domains, generating a p35 fragment consisting of the CARD and p20. This intermediate is usually further processed into the p20 domain, which, together with the p10 domain, forms the fully active Caspase-1 enzyme. Nevertheless, the p35 fragment already possesses substantial activity. Furthermore, in the presence of inhibitor concentrations as used within the study at hand, Caspase-1 autoprocessing became stuck at the stage of p35 generation. Taken together, it is therefore conceivable that in inhibitor-treated cells, Caspase-1 is recruited to an ASC “speck”, undergoes the first autocleavage event, and with the thereby gained activity binds efficiently to the abundantly present Ac-YVAD-cmk. Like for Caspase-1-melted, this results in the accumulation of the protease on the inflammasome. An antibody raised against the p10 domain of Caspase-1 was used in our imaging studies. This might indicate that the p10 subunit stays attached to the rest of the Caspase-1 molecule even following cleavage in the p20-p10 linker.

The discovered enrichment of Caspase-1-melted on ASC “specks” offered a new possibility to study interaction partners of Caspase-1. The signal specific greater abundance of the bait promised to subsequently attract more binding proteins. While still in a native system, this setting made it more feasible to identify physiologically relevant interactions. Substrate targets will bind only very transiently and are thus difficult to detect. However, as elaborated above, I hypothesized that non-substrate interaction partners of Caspase-1 might be relevant in inflammasome signaling. These connections are more stable and sufficient amounts should be attracted by Caspase-1-melted to be identified by mass spectrometry. In collaboration with the group of Prof. Bernhard Küster at the Technical University Munich, I performed label-free mass spectrometry analysis on purified ASC “specks”. The first approach, using native, nigericin-induced ASC “specks” proved that the label-free measurement of four replicates per genotype resulted in the elimination of any substantial background issues. However, besides the controls ASC and Caspase-1, which served as a prove-of principle of the assay, no new interaction partners were found. I suspected the loss of Caspase-1-bound proteins during sample preparation as the reason for

this outcome. To stabilize weaker and less stable interactions I repeated the assay, including a cell-permeable crosslinker. As before, the setup of the experiment prevented serious background problems. However, covalent crosslinking during inflammasome signaling did not result in the discovery of novel Caspase-1 interaction partners.

All known interaction partners of Caspase-1 that engage in stable domain-domain interactions are the upstream activators ASC, Nlrc4 and Nlrp1b. Approaches to identify downstream partners of Caspase-1 have so far focused on substrates (Agard et al., 2010; Lamkanfi et al., 2008; Shao et al., 2007). Among these is for example the recently highlighted Gasdermin D (Kayagaki et al., 2015; Shi et al., 2015). We did not identify any of the known substrates in our mass spectrometry analyses. While the interaction of ASC and Caspase-1 was clearly stable enough, this indicated that substrate interactions are too weak and transient to be detected by our method. The 2000 most abundant proteins in the insoluble fraction were identified in my approaches. Potential interaction partners with a low abundance would therefore be missed. As an example, despite its indispensability in nigericin-induced inflammasome activation, Nlrp3 was not enriched in *wild-type* versus Nlrp3 knockout cells. Such rare proteins might still be highly relevant in pathways downstream of Caspase-1 activation.

To my knowledge, no comparable attempt has been made before to uncover binding proteins of Caspase-1. I could clearly demonstrate that our label-free approach in combination with repetitive measurements resulted in elimination of background noise while controls stuck out significantly. Based on my results, ASC and Caspase-1 seem to represent the major components persisting in ASC “specks”. These findings in combination with the novel identification of Gasdermin D, a Caspase-11 and/or Caspase-1 substrate, as initiator of pyroptosis, favor the hypothesis that proteolytic targets execute the functions of Caspase-1 rather than non-substrate interaction partners.

4.6 The role of autoprocessing for Caspase-1 catalytic activity

The data from *Caspase-1^{melted}* transgenic mice implied the requirement for Caspase-1 protease activity in the induction of cytokine secretion and cell death. I was thus interested to test what role autoprocessing of Caspase-1 plays during inflammasome activation.

First of all, transfection experiments in HEK293T cells using various different cleavage mutants of murine Caspase-1 were in line with data published by Broz *et al.* (Broz et al., 2010). Eight aspartic acid residues in Caspase-1 could potentially serve as autocleavage sites. Both mutation studies revealed, however, that only six sites were relevant in overexpression-induced processing of Caspase-1. D103 and D122 in the linker region between the CARD and p20 domain and D296, D308, D313, and D314 between the p20 and p10 domains served as cleavage sites. The autocleavage sites identified in Caspase-1 presented with an inhomogeneous pattern of P_4-P_2 residues (P_4-P_1: D103=ATED, D122=NKED, D296=LLKD, D308=FLTD, D313=IFED, D314=FEDD). Early studies on Caspase-1 substrate specificity revealed a broad tolerance for its recognition sequence, which is limited by a strict requirement for aspartic acid in the P_1 position (Rano et al., 1997; Thornberry et al., 1992). Together with the observed absence of Caspase-1 processing in cells transfected with *Caspase-1^{melted}*, this knowledge strengthens the assumption that Caspase-1 was indeed able and responsible for autocleavage at these variable sites.

ProIL-1β is the physiological substrate of Caspase-1 described best to date. Interestingly, Caspase-1 exhibited a higher selectivity for modified peptide sequences (Y-V-A-D, W-E-H-D) than for the natural recognition site in proIL-1β (Y-V-H-D) as demonstrated by the group around N. Thornberry (Rano et al., 1997; Thornberry et al., 1992). This promiscuity of Caspase-1 renders it very difficult to predict recognition sites. Therefore, the number of probable cleavage sites could not be narrowed down by computational methods and autocleavage of Caspase-1 could only be analyzed by sequential mutation of all potential sites.

The cleavage sites at the borders of the linkers to the three subunits of human Caspase-1, the CARD, p20, and p10 domain, have been identified more than

20 years ago (D103, D119 and D297, D316) (Ramage et al., 1995; Thornberry et al., 1992). Broz *et al.*, who extended these studies to murine Caspase-1, determined residues D103, D122 and D296, D314 analogous to the human sites. Furthermore, the group found three non-conserved aspartate residues in the linker-II of mouse Caspase-1, namely D300, D304, and D308. Of these, only D308 was used by Caspase-1. Additionally, D313, corresponding to D315 in human Caspase-1, was cut in their and my studies.

Besides this basic analysis, my secondary goal was to investigate the functional role of Caspase-1 processing at certain positions. I tested whether the blockage of cleavage in one of the Caspase-1 linkers had an impact on processing of the other linker. Inhibition of cleavage between the CARD and p20 domain and between the p10 and p20 domain, respectively, still allowed for separation of the respective other subunit when overexpressed. To my knowledge, this has not been investigated in detail before and demonstrated that oligomerized proCaspase-1 is able to cleave both of its linkers independently. Processing of linker-II was shown to proceed cleavage in linker-I (Elliott et al., 2009; Ramage et al., 1995; Yamin et al., 1996). Thus, I was not surprised to observe cleavage of linker-II in the D103N+D122N mutant. Notably however, as the linker-II mutant was also still cleaved in linker-I, this order of events was not necessary for reactivity of Caspase-1 on this site.

Of the two cutting sites in the CARD-p20 linker, position D103 appeared to possess special functions in Caspase-1 processing. Mutation of this residue abolished not only the generation of a p20 fragment but also changed the overall cleavage pattern, indicating a regulatory role. In wild-type Caspase-1, D103 and D122 can be cleaved as indicated by the presence of two bands for the p20 domain. Yamin *et al.*, demonstrated that both fragments possess protease activity (Yamin et al., 1996). Nevertheless, it is still possible that use of one or the other site has differential effects on, for example, stability of the active enzyme.

Substitution of aspartic acid by asparagine at position D103 or at positions D103 and D122 induced the formation of new Caspase-1 fragments, which were detected by the anti-p20 antibody. I anticipated to find one band for the CARD-p20 product in Western blot analysis but was surprised by the

appearance of several additional bands. These cleavage fragments most likely correspond to sections of CARD-p20 cleaved at unidentified sites within the CARD. Several aspartate residues are found in the peptide sequence of this Caspase-1 subunit. The physiological relevance of these sites in Caspase-1 processing and function remain to be studied.

Another focus of investigation was to elucidate how the different autocleavage events influence the effector functions of Caspase-1. First, I aimed at testing the proteolytic activity of the cleavage mutants in co-expression experiments. When wild-type Caspase-1 was co-expressed with Caspase-1-melted at levels, which independently did not lead to autoprocessing, formation of a p20 fragment was observed. This finding was noticeable as it indicated cleavage of Caspase-1-melted proteins by other, active Caspase-1 molecules. In contrast, uncleavable Caspase-1 exhibited clearly reduced protease activity and was unable to process co-transfected Caspase-1-melted protein. In the non-cleavable construct, several negatively charged amino acids were replaced with neutral, hydrophobic residues. This might interfere with protein folding, which could explain the lack of activity. However, the fully uncleavable construct can still induce cell death (Broz et al., 2010), indicating at least partial activity. The single linker-mutants were incapable of rescuing the phenotype observed with non-cleavable Caspase-1. While quiescence of the p20-p10 fragment that formed in the linker-II mutant has been described, the same study claimed proteolytic activity of the CARD-p20 fragment (linker-I mutant), albeit with reduced kinetics compared to p20 alone (Yamin et al., 1996). This discrepancy was unexpected but detailed analysis showed that despite the absence of a p20 fragment with any of the linker-mutants, two higher molecular weight bands appeared when Caspase-1 melted and Caspase-1 D103N+D122N were simultaneously expressed. These bands were also visible in the sample of wild-type Caspase-1 plus Caspase-1-melted and could represent either CARD-p20 or p20-p10 fragments. Answering which of the two fragments arises, could reveal whether Caspase-1 activation is based on inter- or intramolecular cleavage. Presence of p20-p10 fragments in this setting would demonstrate cleavage of Caspase-1-melted by the linker-I mutant, indicating the existence of intermolecular processing. Thus, the results of co-expression of Caspase-1-

melted with both, wild-type and uncleavable Caspase-1, suggest the possibility that Caspase-1 functions as its own initiator Caspase-1. This hypothesis is supported by the findings for Caspase-1 cleavage in the presence of Ac-YVAD-cmk, as discussed above. Independently of this central question, the results given herein are indicative of protease activity in the D103N+D122N mutant, although complete degradation to the p20 fragment was impaired.

To confirm the relevance of the overexpression results in a more physiological model, I reconstituted non-cleavable Caspase-1 in BMDMs from *wild-type* or homozygous *melted* animals using retroviral transduction. This method led to expression levels of the cleavage mutant comparable to endogenous Caspase-1-melted. In agreement with the previous results, no p20 product was restored by reconstitution of non-cleavable Caspase-1 in BMDMs from *Caspase-1*$^{mlt/mlt}$ mice. Accordingly, proIL-1β was neither matured nor secreted following Nlrp3-inflammasome stimulation in these cells. These data are preliminary but the finding that expression rates of transduced protein were similar to native levels indicates the suitability of this method for further investigations. The assay can be extended to other partial Caspase-1 cleavage mutants to identify the minimal number and combination of cleavage sites required for Caspase-1 activity under physiological conditions.

Different groups have documented that processing of Caspase-1 was dispensable for its ability to induce pyroptosis or pyroptosis and cytokine secretion by Nlrc4 and Nlrp1b stimuli, respectively (Broz et al., 2010; Guey et al., 2014). The established retroviral transduction system can be applied to elucidate the mechanisms underlying this differential behavior of non-cleavable and inactive Caspase-1. In combination, the *Caspase-1*^{melted} transgenic mouse lines will hereby serve as a valuable tool. These systems will allow for straightforward co-expression analyses, which will facilitate investigation of the molecular activation mechanism of Caspase-1.

4.7 Conclusions and outlook

Within this study, I provided evidence for the requirement of Caspase-1 protease activity not only for proteolytic maturation of proIL-1β, but also for unconventional secretion of IL-1 family cytokines and for induction of pyroptosis under native conditions. There was inconsistency in the field on whether Caspase-1 protease activity was essential for IL-1 family cytokine secretion and cell death. This discrepancy in the results arose from methodical differences in the approaches using variable cell types and stimulation settings. My results were obtained from primary cells, which resemble the situation in an organism best. Furthermore, they expressed completely inactive Caspase-1 at native levels. Therefore, using this new model, I was able to eliminate the existing uncertainty and provided new physiological insights into Caspase-1 function in myeloid cells.

One might speculate that the functional incompetence of protease-dead Caspase-1 is caused by an abnormal conformation due to a lack of autoprocessing following activation. However, data on cell death and cytokine secretion caused by uncleavable Caspase-1 stand in contrast to this hypothesis. Thus, Caspase-1-specific functions must take place independently of structural rearrangements after autoprocessing and absence of this refolding is therefore unlikely to account for the phenotype of *Caspase-1*^{melted} mice. Notably, the mentioned observations for non-cleavable Caspase-1 have been made exclusively with stimulation of the Nlrc4 and Nlrp1b inflammasomes. Although the exact mechanism has to date not been uncovered in detail, these receptors represent special cases because they contain a CARD. This feature enables them to control Caspase-1 activation autonomously of ASC.

Comparison of inactive and non-cleavable Caspase-1 becomes especially interesting in light of the novel data on Gasdermin D. Shi *et al.* observed intracellular cleavage of proIL-1β in the absence of Gasdermin D, whereas cell death was abolished (Shi et al., 2015). On the other hand, an uncleavable Caspase-1 mutant was shown to be able to induce cell death in response to Nlrc4-activation but lacked proIL-1β maturation capacity (Broz et al., 2010). In combination with the novel data that Gasdermin D is obviously essential for execution of pyrotosis, I reason differential enzymatic properties of Caspase-1

depending on its conformation. I propose catalytic activity in full-length Caspase-1 (p45) to be responsible for cell death induction, whereas degradation into a heterotetramer (2x p20/p10) is required for proIL-1β maturation. Based on this hypothesis, evaluation of Gasdermin D as a substrate of unprocessed Caspase-1 will be an exciting subject to further investigation. In this context, my established retroviral transduction system in combination with the existing cleavage site mutants offers a suitable model to efficiently address this question.

The uncovering of incomplete inhibition of Caspase-1 by available peptide-based inhibitors was only made possible by genetically targeting *Caspase-1*. This finding has important implications for the future design of novel Caspase-1 inhibitors. Such compounds are under investigation for the treatment of inflammasome-associated (auto-)inflammatory diseases. Targeting Caspase-1 as the executioner enzyme in inflammasome-related pathologies will bring a greater benefit to the patients than the currently used IL-1 receptor antagonists. Besides the prevention of IL-1 family cytokine secretion, inhibition of Caspase-1 will also suppress the highly inflammatory event of pyroptosis. However, my data revealed that an incomplete inhibitory effect still allows for release of proinflammatory cytokines and cell death. Thus, in combination with the toxicity of the degradation products of many compounds (Poreba et al., 2013), the available peptide inhibitors appear unsuitable for use in medical applications. Based on my results, I suggest the development of inhibitors for Caspase-1, which target the protease prior to activation and autoprocessing. Due to their competitive mode-of-action, pseudosubstrate-based inhibitors will only result in leaky inhibition. Therefore, I propose the investigation of novel small molecule inhibitors with allosteric characteristics to abolish all proinflammatory functions of Caspase-1. Potential prospective insights into the exact mechanisms downstream of Caspase-1 activation by further studies involving *Caspase-1*^{melted} mice might open new possibilities for attacking deregulated inflammasome signaling.

5 References

Agard, N.J., Maltby, D., and Wells, J.A. (2010). Inflammatory Stimuli Regulate Caspase Substrate Profiles. Mol. Cell Proteomics *9*, 880–893.

Agostini, L., Martinon, F., Burns, K., McDermott, M.F., Hawkins, P.N., and Tschopp, J. (2004). NALP3 Forms an IL-1β-Processing Inflammasome with Increased Activity in Muckle-Wells Autoinflammatory Disorder. Immunity *20*, 319–325.

Akhter, A., Gavrilin, M.A., Frantz, L., Washington, S., Ditty, C., Limoli, D., Day, C., Sarkar, A., Newland, C., Butchar, J., et al. (2009). Caspase-7 activation by the Nlrc4/Ipaf inflammasome restricts Legionella pneumophila infection. PLoS Pathog. *5*, e1000361.

Akira, S., Hemmi, H., Takeuchi, O., Kawai, T., Kaisho, T., Sato, S., Sanjo, H., Matsumoto, M., Hoshino, K., Wagner, H., et al. (2000). A Toll-like receptor recognizes bacterial DNA : Article : Nature. Nature *408*, 740–745.

Akira, S., Uematsu, S., and Takeuchi, O. (2006). Pathogen recognition and innate immunity. Cell *124*, 783–801.

Alexopoulou, L., Holt, A.C., Medzhitov, R., and Flavell, R.A. (2001). Recognition of double-stranded RNA and activation of NF-kappaB by Toll-like receptor 3. Nature *413*, 732–738.

Allen, I.C., Scull, M.A., Moore, C.B., Holl, E.K., McElvania-TeKippe, E., Taxman, D.J., Guthrie, E.H., Pickles, R.J., and Ting, J.P.-Y. (2009). The NLRP3 Inflammasome Mediates In Vivo Innate Immunity to Influenza A Virus through Recognition of Viral RNA. Immunity *30*, 556–565.

Alnemri, E.S., Livingston, D.J., Nicholson, D.W., Salvesen, G., Thornberry, N.A., Wong, W.W., and Yuan, J. (1996). Human ICE/CED-3 protease nomenclature. Cell *87*, 171.

Andrei, C., Dazzi, C., Lotti, L., Torrisi, M.R., Chimini, G., and Rubartelli, A. (1999). The Secretory Route of the Leaderless Protein Interleukin 1beta Involves Exocytosis of Endolysosome-related Vesicles. Molecular Biology of the Cell *10*, 1463–1475.

Arbour, N.C., Lorenz, E., Schutte, B.C., Zabner, J., Kline, J.N., Jones, M., Frees, K., Watt, J.L., and Schwartz, D.A. (2000). TLR4 mutations are associated with endotoxin hyporesponsiveness in humans. Nat Genet *25*, 187–191.

Arthur, J.C., Lich, J.D., Ye, Z., Allen, I.C., Gris, D., Wilson, J.E., Schneider, M., Roney, K.E., O'Connor, B.P., Moore, C.B., et al. (2010). Cutting edge: NLRP12 controls dendritic and myeloid cell migration to affect contact hypersensitivity. The Journal of Immunology *185*, 4515–4519.

Baker, P.J., Boucher, D., Bierschenk, D., Tebartz, C., Whitney, P.G., D'Silva, D.B., Tanzer, M.C., Monteleone, M., Robertson, A.A.B., Cooper, M.A., et al. (2015). NLRP3 inflammasome activation downstream of cytoplasmic LPS recognition by both caspase-4 and caspase-5. Eur. J. Immunol.

Bauernfeind, F.G., Horvath, G., Stutz, A., Alnemri, E.S., MacDonald, K., Speert, D., Fernandes-Alnemri, T., Wu, J., Monks, B.G., Fitzgerald, K.A., et al. (2009). Cutting Edge: NF- B Activating Pattern Recognition and Cytokine Receptors License NLRP3 Inflammasome Activation by Regulating NLRP3 Expression. The Journal of Immunology *183*, 787–791.

Bevan, M.J. (1976). Cross-priming for a secondary cytotoxic response to minor H antigens with H-2 congenic cells which do not cross-react in the cytotoxic assay. 1976.

Black, R.A., Kronheim, S.R., and Sleath, P.R. (1989). Activation of interleukin-1 beta by a co-induced protease. FEBS Lett. *247*, 386–390.

Borregaard, N. (2010). Neutrophils, from marrow to microbes. Immunity *33*, 657–670.

Boxer, M.B., Shen, M., Auld, D.S., Wells, J.A., and Thomas, C.J. (2011). A small molecule inhibitor of Caspase 1.

Boyden, E.D., and Dietrich, W.F. (2006). Nalp1b controls mouse macrophage susceptibility to anthrax lethal toxin. Nat Genet *38*, 240–244.

Brennan, M.A., and Cookson, B.T. (2000). Salmonella induces macrophage death by caspase-1-dependent necrosis. Molecular Microbiology *38*, 31–40.

Brinkmann, V., Reichard, U., Goosmann, C., Fauler, B., Uhlemann, Y., Weiss, D.S., Weinrauch, Y., and Zychlinsky, A. (2004). Neutrophil extracellular traps kill bacteria. Science *303*, 1532–1535.

Brown, G.D., and Gordon, S. (2001). Immune recognition. A new receptor for beta-glucans. Nature *413*, 36–37.

Brown, G.D., Herre, J., Williams, D.L., Willment, J.A., Marshall, A.S.J., and Gordon, S. (2003). Dectin-1 mediates the biological effects of beta-glucans. J. Exp. Med. *197*, 1119–1124.

Broz, P., Moltke, von, J., Jones, J.W., Vance, R.E., and Monack, D.M. (2010). Differential Requirement for Caspase-1 Autoproteolysis in Pathogen-Induced Cell Death and Cytokine Processing. Cell Host & Microbe *8*, 471–483.

Broz, P., Ruby, T., Belhocine, K., Bouley, D.M., Kayagaki, N., Dixit, V.M., and Monack, D.M. (2012). Caspase-11 increases susceptibility to Salmonella infection in the absence of caspase-1. Nature *490*, 288–291.

Bryan, N.B., Dorfleutner, A., Rojanasakul, Y., and Stehlik, C. (2009). Activation

of inflammasomes requires intracellular redistribution of the apoptotic speck-like protein containing a caspase recruitment domain. The Journal of Immunology *182*, 3173–3182.

Bürckstümmer, T., Baumann, C., Blüml, S., Dixit, E., Dürnberger, G., Jahn, H., Planyavsky, M., Bilban, M., Colinge, J., Bennett, K.L., et al. (2009). An orthogonal proteomic-genomic screen identifies AIM2 as a cytoplasmic DNA sensor for the inflammasome. Nat Immunol *10*, 266–272.

Cao, W., Zhang, L., Rosen, D.B., Bover, L., Watanabe, G., Bao, M., Lanier, L.L., and Liu, Y.-J. (2007). BDCA2/Fc epsilon RI gamma complex signals through a novel BCR-like pathway in human plasmacytoid dendritic cells. PLoS Biol. *5*, e248.

Cella, M., Engering, A., Pinet, V., Pieters, J., and Lanzavecchia, A. (1997). Inflammatory stimuli induce accumulation of MHC class II complexes on dendritic cells. Nature *388*, 782–787.

Cerretti, D.P., Kozlosky, C.J., Mosley, B., Nelson, N., Van Ness, K., Greenstreet, T.A., March, C.J., Kronheim, S.R., Druck, T., and Cannizzaro, L.A. (1992). Molecular cloning of the interleukin-1 beta converting enzyme. Science *256*, 97–100.

Chen, C.-H., Floyd, H., Olson, N.E., Magaletti, D., Li, C., Draves, K., and Clark, E.A. (2006). Dendritic-cell-associated C-type lectin 2 (DCAL-2) alters dendritic-cell maturation and cytokine production. Blood *107*, 1459–1467.

Chen, K.W., Groß, C.J., Sotomayor, F.V., Stacey, K.J., Tschopp, J., Sweet, M.J., and Schroder, K. (2014). The neutrophil NLRC4 inflammasome selectively promotes IL-1β maturation without pyroptosis during acute Salmonella challenge. Cell Rep *8*, 570–582.

Cridland, J.A., Curley, E.Z., Wykes, M.N., Schroder, K., Sweet, M.J., Roberts, T.L., Ragan, M.A., Kassahn, K.S., and Stacey, K.J. (2012). The mammalian PYHIN gene family: Phylogeny, evolution and expression. BMC Evol Biol *12*, 140.

Cruz, C.M., Rinna, A., Forman, H.J., Ventura, A.L.M., Persechini, P.M., and Ojcius, D.M. (2007). ATP Activates a Reactive Oxygen Species-dependent Oxidative Stress Response and Secretion of Proinflammatory Cytokines in Macrophages. Journal of Biological Chemistry *282*, 2871–2879.

Davies, L.C., Jenkins, S.J., Allen, J.E., and Taylor, P.R. (2013). Tissue-resident macrophages. Nat Immunol *14*, 986–995.

Davies, L.C., Rosas, M., Smith, P.J., Fraser, D.J., Jones, S.A., and Taylor, P.R. (2011). A quantifiable proliferative burst of tissue macrophages restores homeostatic macrophage populations after acute inflammation. Eur. J. Immunol. *41*, 2155–2164.

Diebold, S.S., Kaisho, T., Hemmi, H., Akira, S., and Reis e Sousa, C. (2004).

Innate antiviral responses by means of TLR7-mediated recognition of single-stranded RNA. Science *303*, 1529–1531.

Dinarello, C.A. (2009). Immunological and inflammatory functions of the interleukin-1 family. Annu. Rev. Immunol. *27*, 519–550.

Dostert, C., Pétrilli, V., Van Bruggen, R., Steele, C., Mossman, B.T., and Tschopp, J. (2008). Innate immune activation through Nalp3 inflammasome sensing of asbestos and silica. Science *320*, 674–677.

Drickamer, K. (1989). Demonstration of carbohydrate-recognition activity in diverse proteins which share a common primary structure motif. Biochem. Soc. Trans. *17*, 13–15.

Dudziak, D., Kamphorst, A.O., Heidkamp, G.F., Buchholz, V.R., Trumpfheller, C., Yamazaki, S., Cheong, C., Liu, K., Lee, H.-W., Park, C.G., et al. (2007). Differential antigen processing by dendritic cell subsets in vivo. Science *315*, 107–111.

Duewell, P., Kono, H., Rayner, K.J., Sirois, C.M., Vladimer, G., Bauernfeind, F.G., Abela, G.S., Franchi, L., Nuñez, G., Schnurr, M., et al. (2010). NLRP3 inflammasomes are required for atherogenesis and activated by cholesterol crystals. Nature *464*, 1357–1361.

Dzionek, A., Sohma, Y., Nagafune, J., Cella, M., Colonna, M., Facchetti, F., Günther, G., Johnston, I., Lanzavecchia, A., Nagasaka, T., et al. (2001). BDCA-2, a novel plasmacytoid dendritic cell-specific type II C-type lectin, mediates antigen capture and is a potent inhibitor of interferon alpha/beta induction. J. Exp. Med. *194*, 1823–1834.

Elinav, E., Strowig, T., Kau, A.L., Henao-Mejia, J., Thaiss, C.A., Booth, C.J., Peaper, D.R., Bertin, J., Eisenbarth, S.C., Gordon, J.I., et al. (2011). NLRP6 inflammasome regulates colonic microbial ecology and risk for colitis. Cell *145*, 745–757.

Elliott, J.M., Rouge, L., Wiesmann, C., and Scheer, J.M. (2009). Crystal structure of procaspase-1 zymogen domain reveals insight into inflammatory caspase autoactivation. J. Biol. Chem. *284*, 6546–6553.

Faustin, B., Lartigue, L., Bruey, J.-M., Luciano, F., Sergienko, E., Bailly-Maitre, B., Volkmann, N., Hanein, D., Rouiller, I., and Reed, J.C. (2007). Reconstituted NALP1 Inflammasome Reveals Two-Step Mechanism of Caspase-1 Activation. Molecular Cell *25*, 713–724.

Feldmann, J., Prieur, A.-M., Quartier, P., Berquin, P., Certain, S., Cortis, E., Teillac-Hamel, D., Fischer, A., and de Saint Basile, G. (2002). Chronic infantile neurological cutaneous and articular syndrome is caused by mutations in CIAS1, a gene highly expressed in polymorphonuclear cells and chondrocytes. Am. J. Hum. Genet. *71*, 198–203.

Fernandes-Alnemri, T., Wu, J., Yu, J.-W., Datta, P., Miller, B., Jankowski, W.,

Rosenberg, S., Zhang, J., and Alnemri, E.S. (2007). The pyroptosome: a supramolecular assembly of ASC dimers mediating inflammatory cell death via caspase-1 activation. Cell Death Differ. *14*, 1590–1604.

Fernandes-Alnemri, T., Yu, J.-W., Datta, P., Wu, J., and Alnemri, E.S. (2009). AIM2 activates the inflammasome and cell death in response to cytoplasmic DNA. Nature *458*, 509–513.

Fink, S.L., Bergsbaken, T., and Cookson, B.T. (2008). Anthrax lethal toxin and Salmonella elicit the common cell death pathway of caspase-1-dependent pyroptosis via distinct mechanisms. Proceedings of the National Academy of Sciences *105*, 4312–4317.

Fink, S.L., and Cookson, B.T. (2006). Caspase-1-dependent pore formation during pyroptosis leads to osmotic lysis of infected host macrophages. Cell Microbiol *8*, 1812–1825.

Franchi, L., Amer, A., Body-Malapel, M., Kanneganti, T.-D., Ozören, N., Jagirdar, R., Inohara, N., Vandenabeele, P., Bertin, J., Coyle, A., et al. (2006). Cytosolic flagellin requires Ipaf for activation of caspase-1 and interleukin 1beta in salmonella-infected macrophages. Nat Immunol *7*, 576–582.

Garcia-Calvo, M., Peterson, E.P., Leiting, B., Ruel, R., Nicholson, D.W., and Thornberry, N.A. (1998). Inhibition of human caspases by peptide-based and macromolecular inhibitors. J. Biol. Chem. *273*, 32608–32613.

Geijtenbeek, T.B.H., van Vliet, S.J., Koppel, E.A., Sanchez-Hernandez, M., Vandenbroucke-Grauls, C.M.J.E., Appelmelk, B., and van Kooyk, Y. (2002). Mycobacteria Target DC-SIGN to Suppress Dendritic Cell Function. Journal of Experimental Medicine *197*, 7–17.

Geissmann, F., Manz, M.G., Jung, S., Sieweke, M.H., Merad, M., and Ley, K. (2010). Development of monocytes, macrophages, and dendritic cells. Science *327*, 656–661.

Gewies, A., Gorka, O., Bergmann, H., Pechloff, K., Petermann, F., Jeltsch, K.M., Rudelius, M., Kriegsmann, M., Weichert, W., Horsch, M., et al. (2014). Uncoupling Malt1 threshold function from paracaspase activity results in destructive autoimmune inflammation. Cell Rep *9*, 1292–1305.

Ginhoux, F., and Jung, S. (2014). Monocytes and macrophages: developmental pathways and tissue homeostasis. Nat Rev Immunol *14*, 392–404.

Goldbach-Mansky, R., Shroff, S.D., Wilson, M., Snyder, C., Plehn, S., Barham, B., Pham, T.-H., Pucino, F., Wesley, R.A., Papadopoulos, J.H., et al. (2008). A pilot study to evaluate the safety and efficacy of the long-acting interleukin-1 inhibitor rilonacept (interleukin-1 Trap) in patients with familial cold autoinflammatory syndrome. Arthritis Rheum. *58*, 2432–2442.

Gringhuis, S.I., Dunnen, den, J., Litjens, M., van Het Hof, B., van Kooyk, Y., and Geijtenbeek, T.B.H. (2007). C-type lectin DC-SIGN modulates Toll-like receptor signaling via Raf-1 kinase-dependent acetylation of transcription factor NF-kappaB. Immunity *26*, 605–616.

Groß, O. (2011). Measuring the Inflammasome. In Methods in Molecular Biology, (Totowa, NJ: Humana Press), pp. 199–222.

Groß, O., Gewies, A., Finger, K., Schäfer, M., Sparwasser, T., Peschel, C., Förster, I., and Ruland, J. (2006). Card9 controls a non-TLR signalling pathway for innate anti-fungal immunity. Nature *442*, 651–656.

Groß, O., Poeck, H., Bscheider, M., Dostert, C., Hannesschläger, N., Endres, S., Hartmann, G., Tardivel, A., Schweighoffer, E., Tybulewicz, V., et al. (2009). Syk kinase signalling couples to the Nlrp3 inflammasome for anti-fungal host defence. Nature *459*, 433–436.

Groß, O., Yazdi, A.S., Thomas, C.J., Masin, M., Heinz, L.X., Guarda, G., Quadroni, M., Drexler, S.K., and Tschopp, J. (2012). Inflammasome Activators Induce Interleukin-1α Secretion via Distinct Pathways with Differential Requirement for the Protease Function of Caspase-1. Immunity *36*, 388–400.

Gu, Y., Kuida, K., Tsutsui, H., Ku, G., Hsiao, K., Fleming, M.A., Hayashi, N., Higashino, K., Okamura, H., Nakanishi, K., et al. (1997). Activation of Interferon-gamma Inducing Factor Mediated by Interleukin-1beta Converting Enzyme. Science *275*, 206–209.

Guey, B., Bodnar, M., Manié, S.N., Tardivel, A., and Pétrilli, V. (2014). Caspase-1 autoproteolysis is differentially required for NLRP1b and NLRP3 inflammasome function. Proceedings of the National Academy of Sciences *111*, 17254–17259.

Hagar, J.A., Powell, D.A., Aachoui, Y., Ernst, R.K., and Miao, E.A. (2013). Cytoplasmic LPS Activates Caspase-11: Implications in TLR4-Independent Endotoxic Shock. Science *341*, 1250–1253.

Halle, A., Hornung, V., Petzold, G.C., Stewart, C.R., Monks, B.G., Reinheckel, T., Fitzgerald, K.A., Latz, E., Moore, K.J., and Golenbock, D.T. (2008). The NALP3 inflammasome is involved in the innate immune response to amyloid-beta. Nat Immunol *9*, 857–865.

Hannum, C.H., Wilcox, C.J., Arend, W.P., Joslin, F.G., Dripps, D.J., Heimdal, P.L., Armes, L.G., Sommer, A., Eisenberg, S.P., and Thompson, R.C. (1990). Interleukin-1 receptor antagonist activity of a human interleukin-1 inhibitor. Nature *343*, 336–340.

Harris, J., Hartman, M., Roche, C., Zeng, S.G., O'Shea, A., Sharp, F.A., Lambe, E.M., Creagh, E.M., Golenbock, D.T., Tschopp, J., et al. (2011). Autophagy Controls IL-1 Secretion by Targeting Pro-IL-1 for Degradation. Journal of Biological Chemistry *286*, 9587–9597.

Hasegawa, M., Imamura, R., Kinoshita, T., Matsumoto, N., Masumoto, J., Inohara, N., and Suda, T. (2005). ASC-mediated NF-kappaB activation leading to interleukin-8 production requires caspase-8 and is inhibited by CLARP. J. Biol. Chem. *280*, 15122–15130.

Hashimoto, D., Chow, A., Noizat, C., Teo, P., Beasley, M.B., Leboeuf, M., Becker, C.D., See, P., Price, J., Lucas, D., et al. (2013). Tissue-resident macrophages self-maintain locally throughout adult life with minimal contribution from circulating monocytes. Immunity *38*, 792–804.

Hayashi, F., Smith, K.D., Ozinsky, A., Hawn, T.R., Yi, E.C., Goodlett, D.R., Eng, J.K., Akira, S., Underhill, D.M., and Aderem, A. (2001). The innate immune response to bacterial flagellin is mediated by Toll-like receptor 5 : Article : Nature. Nature *410*, 1099–1103.

Heil, F., Hemmi, H., Hochrein, H., Ampenberger, F., Kirschning, C., Akira, S., Lipford, G., Wagner, H., and Bauer, S. (2004). Species-specific recognition of single-stranded RNA via toll-like receptor 7 and 8. Science *303*, 1526–1529.

Hemmi, H., Kaisho, T., Takeuchi, O., Sato, S., Sanjo, H., Hoshino, K., Horiuchi, T., Tomizawa, H., Takeda, K., and Akira, S. (2002). Small anti-viral compounds activate immune cells via the TLR7 MyD88–dependent signaling pathway. Nat Immunol *3*, 196–200.

Henry, T., and Monack, D.M. (2007). Activation of the inflammasome upon Francisella tularensis infection: interplay of innate immune pathways and virulence factors. Cell Microbiol *9*, 2543–2551.

Heymann, M.C., Winkler, S., Luksch, H., Flecks, S., Franke, M., Ruß, S., Ozen, S., Yilmaz, E., Klein, C., Kallinich, T., et al. (2014). Human procaspase-1 variants with decreased enzymatic activity are associated with febrile episodes and may contribute to inflammation via RIP2 and NF-κB signaling. The Journal of Immunology *192*, 4379–4385.

Hiscott, J., Marois, J., Garoufalis, J., D'Addario, M., Roulston, A., Kwan, I., Pepin, N., Lacoste, J., Nguyen, H., and Bensi, G. (1993). Characterization of a functional NF-kappa B site in the human interleukin 1 beta promoter: evidence for a positive autoregulatory loop. Mol. Cell. Biol. *13*, 6231–6240.

Hoebe, K., Du, X., Georgel, P., Janssen, E., Tabeta, K., Kim, S.O., Goode, J., Lin, P., Mann, N., Mudd, S., et al. (2003). Identification of Lps2 as a key transducer of MyD88-independent TIR signalling. Nature *424*, 743–748.

Hoffman, H.M., Mueller, J.L., Broide, D.H., Wanderer, A.A., and Kolodner, R.D. (2001). Mutation of a new gene encoding a putative pyrin-like protein causes familial cold autoinflammatory syndrome and Muckle-Wells syndrome. Nat Genet *29*, 301–305.

Hoffman, H.M., Rosengren, S., Boyle, D.L., Cho, J.Y., Nayar, J., Mueller, J.L., Anderson, J.P., Wanderer, A.A., and Firestein, G.S. (2004). Prevention of cold-associated acute inflammation in familial cold autoinflammatory syndrome by interleukin-1 receptor antagonist. Lancet *364*, 1779–1785.

Hoglen, N.C., Chen, L.-S., Fisher, C.D., Hirakawa, B.P., Groessl, T., and Contreras, P.C. (2004). Characterization of IDN-6556 (3-[2-(2-tert-butyl-phenylaminooxalyl)-amino]-propionylamino]-4-oxo-5-(2,3,5,6-tetrafluoro-phenoxy)-pentanoic acid): a liver-targeted caspase inhibitor. J. Pharmacol. Exp. Ther. *309*, 634–640.

Hornung, V., Ablasser, A., Charrel-Dennis, M., Bauernfeind, F., Horvath, G., Caffrey, D.R., Latz, E., and Fitzgerald, K.A. (2009). AIM2 recognizes cytosolic dsDNA and forms a caspase-1-activating inflammasome with ASC. Nature *458*, 514–518.

Hornung, V., Bauernfeind, F., Halle, A., Samstad, E.O., Kono, H., Rock, K.L., Fitzgerald, K.A., and Latz, E. (2008). Silica crystals and aluminum salts activate the NALP3 inflammasome through phagosomal destabilization. Nat Immunol *9*, 847–856.

Hornung, V., Ellegast, J., Kim, S., Brzózka, K., Jung, A., Kato, H., Poeck, H., Akira, S., Conzelmann, K.-K., Schlee, M., et al. (2006). 5'-Triphosphate RNA is the ligand for RIG-I. Science *314*, 994–997.

Hoshino, K., Takeuchi, O., Kawai, T., Sanjo, H., Ogawa, T., Takeda, Y., Takeda, K., and Akira, S. (1999). Cutting edge: Toll-like receptor 4 (TLR4)-deficient mice are hyporesponsive to lipopolysaccharide: evidence for TLR4 as the Lps gene product. J. Immunol. *162*, 3749–3752.

Howard, A.D., Kostura, M.J., Thornberry, N., Ding, G.J., Limjuco, G., Weidner, J., Salley, J.P., Hogquist, K.A., Chaplin, D.D., and Mumford, R.A. (1991). IL-1-converting enzyme requires aspartic acid residues for processing of the IL-1 beta precursor at two distinct sites and does not cleave 31-kDa IL-1 alpha. J. Immunol. *147*, 2964–2969.

Inohara, Chamaillard, McDonald, C., and Nuñez, G. (2005). NOD-LRR proteins: role in host-microbial interactions and inflammatory disease. Annu. Rev. Biochem. *74*, 355–383.

Jain, K., Verma, P.J., and Liu, J. (2014). Isolation and handling of mouse embryonic fibroblasts. Methods Mol. Biol. *1194*, 247–252.

Kaisho, T., Takeuchi, O., Kawai, T., Hoshino, K., and Akira, S. (2001). Endotoxin-induced maturation of MyD88-deficient dendritic cells. J. Immunol. *166*, 5688–5694.

Kawai, T., and Akira, S. (2007). TLR signaling. Semin. Immunol. *19*, 24–32.

Kayagaki, N., Stowe, I.B., Lee, B.L., O'Rourke, K., Anderson, K., Warming, S., Cuellar, T., Haley, B., Roose-Girma, M., Phung, Q.T., et al. (2015). Caspase-11 cleaves gasdermin D for non-canonical inflammasome signaling. Nature.

Kayagaki, N., Warming, S., Lamkanfi, M., Walle, L.V., Louie, S., Dong, J., Newton, K., Qu, Y., Liu, J., Heldens, S., et al. (2011). Non-canonical inflammasome activation targets caspase-11. Nature *479*, 117–121.

Keller, M., Rüegg, A., Werner, S., and Beer, H.-D. (2008). Active Caspase-1 Is a Regulator of Unconventional Protein Secretion. Cell *132*, 818–831.

Kerur, N., Veettil, M.V., Sharma-Walia, N., Bottero, V., Sadagopan, S., Otageri, P., and Chandran, B. (2011). IFI16 acts as a nuclear pathogen sensor to induce the inflammasome in response to Kaposi Sarcoma-associated herpesvirus infection. Cell Host & Microbe *9*, 363–375.

Khare, S., Dorfleutner, A., Bryan, N.B., Yun, C., Radian, A.D., de Almeida, L., Rojanasakul, Y., and Stehlik, C. (2012). An NLRP7-Containing Inflammasome Mediates Recognition of Microbial Lipopeptides in Human Macrophages. Immunity *36*, 464–476.

Kirshenbaum, A.S., Kessler, S.W., Goff, J.P., and Metcalfe, D.D. Demonstration of the origin of human mast cells from CD34+ bone marrow progenitor cells. Jimmunol.org *146*, 1410–1415.

Kolaczkowska, E., and Kubes, P. (2013). Neutrophil recruitment and function in health and inflammation. Nat Rev Immunol *13*, 159–175.

Kostura, M.J., Tocci, M.J., Limjuco, G., Chin, J., Cameron, P., Hillman, A.G., Chartrain, N.A., and Schmidt, J.A. (1989). Identification of a monocyte specific pre-interleukin 1 beta convertase activity. Proc. Natl. Acad. Sci. U.S.a. *86*, 5227–5231.

Kufer, T.A., Banks, D.J., and Philpott, D.J. (2006). Innate immune sensing of microbes by Nod proteins. Annals NY Acad Sci *1072*, 19–27.

Kuida, K., Lippke, J.A., Ku, G., Harding, M.W., Livingston, D.J., Su, M.S., and Flavell, R.A. (1995). Altered cytokine export and apoptosis in mice deficient in interleukin-1 beta converting enzyme. Science *267*, 2000–2003.

Lamkanfi, M., Kanneganti, T.-D., Van Damme, P., Vanden Berghe, T., Vanoverberghe, I., Vandekerckhove, J., Vandenabeele, P., Gevaert, K., and Nuñez, G. (2008). Targeted peptidecentric proteomics reveals caspase-7 as a substrate of the caspase-1 inflammasomes. Mol. Cell Proteomics *7*, 2350–2363.

Ley, K., Laudanna, C., Cybulsky, M.I., and Nourshargh, S. (2007). Getting to the site of inflammation: the leukocyte adhesion cascade updated. Nat Rev Immunol *7*, 678–689.

Li, P., Allen, H., Banerjee, S., Franklin, S., Herzog, L., Johnston, C., McDowell, J., Paskind, M., Rodman, L., and Salfeld, J. (1995). Mice deficient in IL-1 beta-converting enzyme are defective in production of mature IL-1 beta and resistant to endotoxic shock. Cell *80*, 401–411.

Liu, T., Yamaguchi, Y., Shirasaki, Y., Shikada, K., Yamagishi, M., Hoshino, K., Kaisho, T., Takemoto, K., Suzuki, T., Kuranaga, E., et al. (2014). Single-cell imaging of caspase-1 dynamics reveals an all-or-none inflammasome signaling response. Cell Rep *8*, 974–982.

Lu, A., Magupalli, V.G., Ruan, J., Yin, Q., Atianand, M.K., Vos, M.R., Schröder, G.F., Fitzgerald, K.A., Wu, H., and Egelman, E.H. (2014). Unified polymerization mechanism for the assembly of ASC-dependent inflammasomes. Cell *156*, 1193–1206.

Luksch, H., Romanowski, M.J., Chara, O., Tüngler, V., Caffarena, E.R., Heymann, M.C., Lohse, P., Aksentijevich, I., Remmers, E.F., Flecks, S., et al. (2013). Naturally occurring genetic variants of human caspase-1 differ considerably in structure and the ability to activate interleukin-1β. Hum. Mutat. *34*, 122–131.

Lutz, M.B., Kukutsch, N., Ogilvie, A.L., Rössner, S., Koch, F., Romani, N., and Schuler, G. (1999). An advanced culture method for generating large quantities of highly pure dendritic cells from mouse bone marrow. J. Immunol. Methods *223*, 77–92.

MacKenzie, A., Wilson, H.L., Kiss-Toth, E., Dower, S.K., North, R.A., and Surprenant, A. (2001). Rapid secretion of interleukin-1beta by microvesicle shedding. Immunity *15*, 825–835.

Manzanero, S. (2012). Generation of Mouse Bone Marrow-Derived Macrophages. In Methods in Molecular Biology, R.B. Ashman, ed. (Humana Press), pp. 177–181–181.

Mariathasan, S., Newton, K., Monack, D.M., Vucic, D., French, D.M., Lee, W.P., Roose-Girma, M., Erickson, S., and Dixit, V.M. (2004). Differential activation of the inflammasome by caspase-1 adaptors ASC and Ipaf. Nature *430*, 213–218.

Mariathasan, S., Weiss, D.S., Newton, K., McBride, J., O'Rourke, K., Roose-Girma, M., Lee, W.P., Weinrauch, Y., Monack, D.M., and Dixit, V.M. (2006). Cryopyrin activates the inflammasome in response to toxins and ATP. Nature *440*, 228–232.

Martinon, F., and Tschopp, J. (2007). Inflammatory caspases and inflammasomes: master switches of inflammation. Cell Death Differ. *14*, 10–22.

Martinon, F., Burns, K., and Tschopp, J. (2002). The inflammasome: a molecular platform triggering activation of inflammatory caspases and processing of proIL-beta. Molecular Cell *10*, 417–426.

Martinon, F., Pétrilli, V., Mayor, A., Tardivel, A., and Tschopp, J. (2006). Gout-associated uric acid crystals activate the NALP3 inflammasome. Nature *440*, 237–241.

Masters, S.L., Dunne, A., Subramanian, S.L., Hull, R.L., Tannahill, G.M., Sharp, F.A., Becker, C., Franchi, L., Yoshihara, E., Chen, Z., et al. (2010). Activation of the NLRP3 inflammasome by islet amyloid polypeptide provides a mechanism for enhanced IL-1β in type 2 diabetes. Nat Immunol *11*, 897–904.

Masumoto, J., Taniguchi, S., Ayukawa, K., Sarvotham, H., Kishino, T., Niikawa, N., Hidaka, E., Katsuyama, T., Higuchi, T., and Sagara, J. (1999). ASC, a novel 22-kDa protein, aggregates during apoptosis of human promyelocytic leukemia HL-60 cells. J. Biol. Chem. *274*, 33835–33838.

McGreal, E.P., Rosas, M., Brown, G.D., Zamze, S., Wong, S.Y.C., Gordon, S., Martinez-Pomares, L., and Taylor, P.R. (2006). The carbohydrate-recognition domain of Dectin-2 is a C-type lectin with specificity for high mannose. Glycobiology *16*, 422–430.

Medzhitov, R., Preston-Hurlburt, P., Kopp, E., Stadlen, A., Chen, C., Ghosh, S., and Janeway, C.A., Jr. (1998). MyD88 Is an Adaptor Protein in the hToll/IL-1 Receptor Family Signaling Pathways. Molecular Cell *2*, 253–258.

Metchnikoff, E. (1892). Leçons sur la pathologie comparée de l“inflammation : faites à l” Institut Pasteur en avril et mai 1891.

Meyer-Wentrup, F., Benitez-Ribas, D., Tacken, P.J., Punt, C.J.A., Figdor, C.G., de Vries, I.J.M., and Adema, G.J. (2008). Targeting DCIR on human plasmacytoid dendritic cells results in antigen presentation and inhibits IFN-production. Blood *111*, 4245–4253.

Meyer-Wentrup, F., Cambi, A., Joosten, B., Looman, M.W., de Vries, I.J.M., Figdor, C.G., and Adema, G.J. (2009). DCIR is endocytosed into human dendritic cells and inhibits TLR8-mediated cytokine production. J. Leukoc. Biol. *85*, 518–525.

Miao, E.A., Mao, D.P., Yudkovsky, N., Bonneau, R., Lorang, C.G., Warren, S.E., Leaf, I.A., and Aderem, A. (2010). Innate immune detection of the type III secretion apparatus through the NLRC4 inflammasome. Proceedings of the National Academy of Sciences *107*, 3076–3080.

Miao, E.A., Alpuche-Aranda, C.M., Dors, M., Clark, A.E., Bader, M.W., Miller, S.I., and Aderem, A. (2006). Cytoplasmic flagellin activates caspase-1 and secretion of interleukin 1β via Ipaf. Nat Immunol *7*, 569–575.

Molofsky, A.B., Byrne, B.G., Whitfield, N.N., Madigan, C.A., Fuse, E.T., Tateda, K., and Swanson, M.S. (2006). Cytosolic recognition of flagellin by mouse macrophages restricts Legionella pneumophila infection. J. Exp. Med. *203*, 1093–1104.

Monack, D.M., Detweiler, C.S., and Falkow, S. (2001). Salmonella pathogenicity island 2-dependent macrophage death is mediated in part by the host cysteine protease caspase-1. Cell Microbiol *3*, 825–837.

Mosley, B., Urdal, D.L., Prickett, K.S., Larsen, A., Cosman, D., Conlon, P.J., Gillis, S., and Dower, S.K. (1987). The interleukin-1 receptor binds the human interleukin-1 alpha precursor but not the interleukin-1 beta precursor. J. Biol. Chem. *262*, 2941–2944.

Muñoz-Planillo, R., Kuffa, P., Martínez-Colón, G., Smith, B.L., Rajendiran, T.M., and Nuñez, G. (2013). K+ Efflux Is the Common Trigger of NLRP3 Inflammasome Activation by Bacterial Toxins and Particulate Matter. Immunity *38*, 1142–1153.

Murray, P.J., and Wynn, T.A. (2011). Protective and pathogenic functions of macrophage subsets. Nat Rev Immunol *11*, 723–737.

Nakanishi, K., Yoshimoto, T., Tsutsui, H., and Okamura, H. (2001). Interleukin-18 regulates both Th1 and Th2 responses. Annu. Rev. Immunol. *19*, 423–474.

Negishi, H., Fujita, Y., Yanai, H., Sakaguchi, S., Ouyang, X., Shinohara, M., Takayanagi, H., Ohba, Y., Taniguchi, T., and Honda, K. (2006). Evidence for licensing of IFN-gamma-induced IFN regulatory factor 1 transcription factor by MyD88 in Toll-like receptor-dependent gene induction program. Proc. Natl. Acad. Sci. U.S.a. *103*, 15136–15141.

Nickel, W., and Rabouille, C. (2009). Mechanisms of regulated unconventional protein secretion. Nat. Rev. Mol. Cell Biol. *10*, 148–155.

Okamura, H., Tsutsui, H., Komatsu, T., Yutsudo, M., Hakura, A., Tanimoto, T., Torigoe, K., Okura, T., Nukada, Y., Hattori, K., et al. (1995). Cloning of a new cytokine that induces IFN-γ production by T cells. Nature *378*, 88–91.

Ozinsky, A., Underhill, D.M., Fontenot, J.D., Hajjar, A.M., Smith, K.D., Wilson, C.B., Schroeder, L., and Aderem, A. (2000). The repertoire for pattern recognition of pathogens by the innate immune system is defined by cooperation between Toll-like receptors. Proceedings of the National Academy of Sciences *97*, 13766–13771.

Palma, A.S., Feizi, T., Zhang, Y., Stoll, M.S., Lawson, A.M., Díaz-Rodríguez, E., Campanero-Rhodes, M.A., Costa, J., Gordon, S., Brown, G.D., et al. (2006). Ligands for the beta-glucan receptor, Dectin-1, assigned using “designer” microarrays of oligosaccharide probes (neoglycolipids) generated from glucan polysaccharides. J. Biol. Chem. *281*, 5771–5779.

Paz, S., Sun, Q., Nakhaei, P., Romieu-Mourez, R., Goubau, D., Julkunen, I., Lin, R., and Hiscott, J. (2006). Induction of IRF-3 and IRF-7 phosphorylation following activation of the RIG-I pathway. Cell. Mol. Biol. (Noisy-Le-Grand) *52*, 17–28.

Perregaux, D., and Gabel, C.A. (1994). Interleukin-1 beta maturation and release in response to ATP and nigericin. Evidence that potassium depletion mediated by these agents is a necessary and common feature of their activity. J. Biol. Chem. *269*, 15195–15203.

Poeck, H., Bscheider, M., Groß, O., Finger, K., Roth, S., Rebsamen, M., Hannesschläger, N., Schlee, M., Rothenfusser, S., Barchet, W., et al. (2009). Recognition of RNA virus by RIG-I results in activation of CARD9 and inflammasome signaling for interleukin 1β production. Nat Immunol *11*, 63–69.

Pooley, J.L., Heath, W.R., and Shortman, K. (2001). Cutting edge: intravenous soluble antigen is presented to CD4 T cells by CD8- dendritic cells, but cross-presented to CD8 T cells by CD8+ dendritic cells. J. Immunol. *166*, 5327–5330.

Poreba, M., Strózyk, A., Salvesen, G.S., and Drag, M. (2013). Caspase substrates and inhibitors. Cold Spring Harb Perspect Biol *5*, a008680.

Powlesland, A.S., Ward, E.M., Sadhu, S.K., Guo, Y., Taylor, M.E., and DRICKAMER, K. (2006). Widely divergent biochemical properties of the complete set of mouse DC-SIGN-related proteins. J. Biol. Chem. *281*, 20440–20449.

Qu, Y., Franchi, L., Nunez, G., and Dubyak, G.R. (2007). Nonclassical IL-1 Secretion Stimulated by P2X7 Receptors Is Dependent on Inflammasome Activation and Correlated with Exosome Release in Murine Macrophages. The Journal of Immunology *179*, 1913–1925.

Rajan, J.V., Rodriguez, D., Miao, E.A., and Aderem, A. (2011). The NLRP3 Inflammasome Detects Encephalomyocarditis Virus and Vesicular Stomatitis Virus Infection. Journal of Virology *85*, 4167–4172.

Ramage, P., Cheneval, D., Chvei, M., Graff, P., Hemmig, R., Heng, R., Kocher, H.P., MacKenzie, A., Memmert, K., and Revesz, L. (1995). Expression, refolding, and autocatalytic proteolytic processing of the interleukin-1 beta-converting enzyme precursor. J. Biol. Chem. *270*, 9378–9383.

Rano, T.A., Timkey, T., Peterson, E.P., Rotonda, J., Nicholson, D.W., Becker, J.W., Chapman, K.T., and Thornberry, N.A. (1997). A combinatorial approach for determining protease specificities: application to interleukin-1β converting enzyme (ICE). Chemistry & Biology *4*, 149–155.

Rathinam, V.A.K., Jiang, Z., Waggoner, S.N., Sharma, S., Cole, L.E., Waggoner, L., Vanaja, S.K., Monks, B.G., Ganesan, S., Latz, E., et al. (2010). The AIM2 inflammasome is essential for host defense against cytosolic bacteria and DNA viruses. Nat Immunol *11*, 395–402.

Rathinam, V.A.K., Vanaja, S.K., Waggoner, L., Sokolovska, A., Becker, C., Stuart, L.M., Leong, J.M., and Fitzgerald, K.A. (2012). TRIF licenses caspase-11-dependent NLRP3 inflammasome activation by gram-negative bacteria. Cell *150*, 606–619.

Reizis, B., Bunin, A., Ghosh, H.S., Lewis, K.L., and Sisirak, V. (2011). Plasmacytoid dendritic cells: recent progress and open questions. Annu. Rev. Immunol. *29*, 163–183.

Ritter, M., Groß, O., Kays, S., Ruland, J., Nimmerjahn, F., Saijo, S., Tschopp, J., Layland, L.E., and da Costa, C.P. (2010). Schistosoma mansoni triggers Dectin-2, which activates the Nlrp3 inflammasome and alters adaptive immune responses. Proceedings of the National Academy of Sciences *107*, 20459–20464.

Roberts, T.L., Idris, A., Dunn, J.A., Kelly, G.M., Burnton, C.M., Hodgson, S., Hardy, L.L., Garceau, V., Sweet, M.J., Ross, I.L., et al. (2009). HIN-200 proteins regulate caspase activation in response to foreign cytoplasmic DNA. Science *323*, 1057–1060.

Robinson, M.J., Osorio, F., Rosas, M., Freitas, R.P., Schweighoffer, E., Gross, O., Verbeek, J.S., Ruland, J., Tybulewicz, V., Brown, G.D., et al. (2009). Dectin-2 is a Syk-coupled pattern recognition receptor crucial for Th17 responses to fungal infection. Journal of Experimental Medicine *206*, 2037–2051.

Rosenberg, H.F., Dyer, K.D., and Foster, P.S. (2012). Eosinophils: changing perspectives in health and disease. Nat Rev Immunol *13*, 9–22.

Röck, J., Schneider, E., Grün, J.R., Grützkau, A., Küppers, R., Schmitz, J., and Winkels, G. (2007). CD303 (BDCA-2) signals in plasmacytoid dendritic cellsvia a BCR-like signalosome involving Syk, Slp65 and PLCγ2. Eur. J. Immunol. *37*, 3564–3575.

Rubartelli, A., Cozzolino, F., Talio, M., and Sitia, R. (1990). A novel secretory pathway for interleukin-1 beta, a protein lacking a signal sequence. Embo J. *9*, 1503–1510.

Rudolphi, K., Gerwin, N., Verzijl, N., van der Kraan, P., and van den Berg, W. (2003). Pralnacasan, an inhibitor of interleukin-1β converting enzyme, reduces joint damage in two murine models of osteoarthritis. Osteoarthritis and Cartilage *11*, 738–746.

Rühl, S., and Broz, P. (2015). Caspase-11 activates a canonical NLRP3 inflammasome by promoting K +efflux. Eur. J. Immunol. n/a–n/a.

Saïd-Sadier, N., Padilla, E., Langsley, G., and Ojcius, D.M. (2010). Aspergillus fumigatus Stimulates the NLRP3 Inflammasome through a Pathway Requiring ROS Production and the Syk Tyrosine Kinase. PLoS ONE *5*, e10008.

Salvesen, G.S., and Dixit, V.M. (1999). Caspase activation: the induced-proximity model. Proc. Natl. Acad. Sci. U.S.a. *96*, 10964–10967.

Satpathy, A.T., Wu, X., Albring, J.C., and Murphy, K.M. (2012). Re(de)fining the dendritic cell lineage. Nat Immunol *13*, 1145–1154.

Schlee, M., Roth, A., Hornung, V., Hagmann, C.A., Wimmenauer, V., Barchet, W., Coch, C., Janke, M., Mihailovic, A., Wardle, G., et al. (2009). Recognition of 5' triphosphate by RIG-I helicase requires short blunt double-stranded RNA as contained in panhandle of negative-strand virus. Immunity *31*, 25–34.

Schmid-Burgk, J.L., Gaidt, M.M., Schmidt, T., Ebert, T.S., Bartok, E., and Hornung, V. (2015). Caspase-4 mediates non-canonical activation of the NLRP3 inflammasome in human myeloid cells. Eur. J. Immunol.

Schmitz, F., Heit, A., Guggemoos, S., Krug, A., Mages, J., Schiemann, M., Adler, H., Drexler, I., Haas, T., Lang, R., et al. (2007). Interferon-regulatory-factor 1 controls Toll-like receptor 9-mediated IFN-β production in myeloid dendritic cells. Eur. J. Immunol. *37*, 315–327.

Schneider, K.S., Thomas, C.J., and Groß, O. (2013). Inflammasome activation and inhibition in primary murine bone marrow-derived cells, and assays for IL-1α, IL-1β, and caspase-1. Methods Mol. Biol. *1040*, 117–135.

Schroder, K., and Tschopp, J. (2010). The inflammasomes. Cell *140*, 821–832.

Schwenk, F., Baron, U., and Rajewsky, K. (1995). A cre-transgenic mouse strain for the ubiquitous deletion of loxP-flanked gene segments including deletion in germ cells. Nucleic Acids Res. *23*, 5080–5081.

Shao, W., Yeretssian, G., Doiron, K., Hussain, S.N., and Saleh, M. (2007). The Caspase-1 Digestome Identifies the Glycolysis Pathway as a Target during Infection and Septic Shock. Journal of Biological Chemistry *282*, 36321–36329.

Shi, J., Zhao, Y., Wang, K., Shi, X., Wang, Y., Huang, H., Zhuang, Y., Cai, T., Wang, F., and Shao, F. (2015). Cleavage of GSDMD by inflammatory caspases determines pyroptotic cell death. Nature.

Shi, J., Zhao, Y., Wang, Y., Gao, W., Ding, J., Li, P., Hu, L., and Shao, F. (2014). Inflammatory caspases are innate immune receptors for intracellular LPS. Nature *514*, 187–192.

Shirasaki, Y., Yamagishi, M., Suzuki, N., Izawa, K., Nakahara, A., Mizuno, J., Shoji, S., Heike, T., Harada, Y., Nishikomori, R., et al. (2014). Real-time single-cell imaging of protein secretion. Sci Rep *4*, 4736.

Srinivasula, S.M., Poyet, J.-L., Razmara, M., Datta, P., Zhang, Z., and Alnemri, E.S. (2002). The PYRIN-CARD protein ASC is an activating adaptor for caspase-1. J. Biol. Chem. *277*, 21119–21122.

Stack, J.H., Beaumont, K., Larsen, P.D., Straley, K.S., Henkel, G.W., Randle, J.C.R., and Hoffman, H.M. (2005). IL-converting enzyme/caspase-1 inhibitor VX-765 blocks the hypersensitive response to an inflammatory stimulus in monocytes from familial cold autoinflammatory syndrome patients. J. Immunol. *175*, 2630–2634.

Steinman, R.M., and Cohn, Z.A. (1973). Identification of a novel cell type in peripheral lymphoid organs of mice. I. Morphology, quantitation, tissue distribution. J. Exp. Med. *137*, 1142–1162.

Surh, C.D., and Sprent, J. (1994). T-cell apoptosis detected in situ during positive and negative selection in the thymus. Nature *372*, 100–103.

Takeuchi, O., Kawai, T., Mühlradt, P.F., Morr, M., Radolf, J.D., Zychlinsky, A., Takeda, K., and Akira, S. (2001). Discrimination of bacterial lipoproteins by Toll-like receptor 6. Int. Immunol. *13*, 933–940.

Takeuchi, O., and Akira, S. (2010). Pattern recognition receptors and inflammation. Cell *140*, 805–820.

Tanne, A., Ma, B., Boudou, F., Tailleux, L., Botella, H., Badell, E., Levillain, F., Taylor, M.E., DRICKAMER, K., Nigou, J., et al. (2009). A murine DC-SIGN homologue contributes to early host defense against Mycobacterium tuberculosis. Journal of Experimental Medicine *206*, 2205–2220.

Thornberry, N.A., Bull, H.G., Calaycay, J.R., Chapman, K.T., Howard, A.D., Kostura, M.J., Miller, D.K., Molineaux, S.M., Weidner, J.R., and Aunins, J. (1992). A novel heterodimeric cysteine protease is required for interleukin-1 beta processing in monocytes. Nature *356*, 768–774.

Underhill, D.M., Rossnagle, E., Lowell, C.A., and Simmons, R.M. (2005). Dectin-1 activates Syk tyrosine kinase in a dynamic subset of macrophages for reactive oxygen production. Blood *106*, 2543–2550.

Unterholzner, L., Keating, S.E., Baran, M., Horan, K.A., Jensen, S.B., Sharma, S., Sirois, C.M., Jin, T., Latz, E., Xiao, T.S., et al. (2010). IFI16 is an innate immune sensor for intracellular DNA. Nat Immunol *11*, 997–1004.

Urb, M., and Sheppard, D.C. (2012). The role of mast cells in the defence against pathogens. PLoS Pathog. *8*, e1002619.

Van Opdenbosch, N., Gurung, P., Vande Walle, L., Fossoul, A., Kanneganti, T.-D., and Lamkanfi, M. (2014). Activation of the NLRP1b inflammasome independently of ASC-mediated caspase-1 autoproteolysis and speck formation. Nat Commun *5*.

Villani, A.-C., Lemire, M., Fortin, G., Louis, E., Silverberg, M.S., Collette, C., Baba, N., Libioulle, C., Belaiche, J., Bitton, A., et al. (2008). Common variants in the NLRP3 region contribute to Crohn's disease susceptibility. Nat Genet *41*, 71–76.

Vivier, E., Raulet, D.H., Moretta, A., Caligiuri, M.A., Zitvogel, L., Lanier, L.L., Yokoyama, W.M., and Ugolini, S. (2010). Innate or Adaptive Immunity?The Example of Natural Killer Cells. Science 1–6.

Voehringer, D. (2013). Protective and pathological roles of mast cells and basophils. Nat Rev Immunol *13*, 362–375.

Walev, I., Reske, K., Palmer, M., Valeva, A., and Bhakdi, S. (1995). Potassium-inhibited processing of IL-1 beta in human monocytes. Embo J. *14*, 1607–1614.

Walker, N.P., Talanian, R.V., Brady, K.D., Dang, L.C., Bump, N.J., Ferenz, C.R., Franklin, S., Ghayur, T., Hackett, M.C., and Hammill, L.D. (1994). Crystal structure of the cysteine protease interleukin-1 beta-converting enzyme: a (p20/p10)2 homodimer. Cell *78*, 343–352.

Walsh, J.G., Logue, S.E., Lüthi, A.U., and Martin, S.J. (2011). Caspase-1 promiscuity is counterbalanced by rapid inactivation of processed enzyme. Journal of Biological Chemistry *286*, 32513–32524.

Wannamaker, W., Davies, R., Namchuk, M., Pollard, J., Ford, P., Ku, G., Decker, C., Charifson, P., Weber, P., Germann, U.A., et al. (2007). (S)-1-((S)-2-{[1-(4-amino-3-chloro-phenyl)-methanoyl]-amino}-3,3-dimethyl-butanoyl)-pyrrolidine-2-carboxylic acid ((2R,3S)-2-ethoxy-5-oxo-tetrahydro-furan-3-yl)-amide (VX-765), an orally available selective interleukin (IL)-converting enzyme/caspase-1 inhibitor, exhibits potent anti-inflammatory activities by inhibiting the release of IL-1beta and IL-18. J. Pharmacol. Exp. Ther. *321*, 509–516.

Wells, C.A., Salvage-Jones, J.A., Li, X., Hitchens, K., Butcher, S., Murray, R.Z., Beckhouse, A.G., Lo, Y.L.S., Manzanero, S., Cobbold, C., et al. (2008). The Macrophage-Inducible C-Type Lectin, Mincle, Is an Essential Component of the Innate Immune Response to Candida albicans. The Journal of Immunology *180*, 7404–7413.

Wilson, K.P., Black, J.A., Thomson, J.A., Kim, E.E., Griffith, J.P., Navia, M.A., Murcko, M.A., Chambers, S.P., Aldape, R.A., and Raybuck, S.A. (1994). Structure and mechanism of interleukin-1 beta converting enzyme. Nature *370*, 270–275.

Yamamoto, M., Sato, S., Hemmi, H., Hoshino, K., Kaisho, T., Sanjo, H., Takeuchi, O., Sugiyama, M., Okabe, M., Takeda, K., et al. (2003). Role of adaptor TRIF in the MyD88-independent toll-like receptor signaling pathway. Science *301*, 640–643.

Yamamoto, M., Sato, S., Mori, K., Hoshino, K., Takeuchi, O., Takeda, K., and Akira, S. (2002). Cutting edge: a novel Toll/IL-1 receptor domain-containing adapter that preferentially activates the IFN-beta promoter in the Toll-like receptor signaling. J. Immunol. *169*, 6668–6672.

Yamasaki, S., Matsumoto, M., Takeuchi, O., Matsuzawa, T., Ishikawa, E., Sakuma, M., Tateno, H., Uno, J., Hirabayashi, J., Mikami, Y., et al. (2009). C-type lectin Mincle is an activating receptor for pathogenic fungus, Malassezia. Proceedings of the National Academy of Sciences *106*, 1897–1902.

Yamin, T.T., Ayala, J.M., and Miller, D.K. (1996). Activation of the native 45-kDa precursor form of interleukin-1-converting enzyme. J. Biol. Chem. *271*, 13273–13282.

Yona, S., Kim, K.-W., Wolf, Y., Mildner, A., Varol, D., Breker, M., Strauss-Ayali, D., Viukov, S., Guilliams, M., Misharin, A., et al. (2013). Fate mapping reveals origins and dynamics of monocytes and tissue macrophages under homeostasis. Immunity *38*, 79–91.

Yoneyama, M., Kikuchi, M., Matsumoto, K., Imaizumi, T., Miyagishi, M., Taira, K., Foy, E., Loo, Y.M., Gale, M., Akira, S., et al. (2005). Shared and Unique Functions of the DExD/H-Box Helicases RIG-I, MDA5, and LGP2 in Antiviral Innate Immunity. The Journal of Immunology *175*, 2851–2858.

Yoneyama, M., Kikuchi, M., Natsukawa, T., Shinobu, N., Imaizumi, T., Miyagishi, M., Taira, K., Akira, S., and Fujita, T. (2004). The RNA helicase RIG-I has an essential function in double-stranded RNA-induced innate antiviral responses. Nat Immunol *5*, 730–737.

Zelensky, A.N., and Gready, J.E. (2005). The C-type lectin-like domain superfamily. Febs J. *272*, 6179–6217.

Zhao, Y., Yang, J., Shi, J., Gong, Y.-N., Lu, Q., Xu, H., Liu, L., and Shao, F. (2011). The NLRC4 inflammasome receptors for bacterial flagellin and type III secretion apparatus. Nature *477*, 596–600.

Zhou, R., Yazdi, A.S., Menu, P., and Tschopp, J. (2010). A role for mitochondria in NLRP3 inflammasome activation. Nature *469*, 221–225.Agard, N.J., Maltby, D., and Wells, J.A. (2010). Inflammatory Stimuli Regulate Caspase Substrate Profiles. Mol. Cell Proteomics *9*, 880–893.

6 Publications

Submitted manuscript:

Groß C.J., Mishra R., Dittlein D.C., Gorka O., Schneider K.S., Wettmarshausen J., Robertson A.A.B, Cooper M.A., Schroder K., Ruland J., Traidl-Hoffmann C., Perocchi F., Groß O. (2015) Imiquimod Inhibits Mitochondrial Complex I Activity and Induces K+ efflux-independent Activation of the NLRP3 Inflammasome.

Published manuscript:

Schneider, K.S., Thomas, C.J., and Groß, O. (2013). Inflammasome activation and inhibition in primary murine bone marrow-derived cells, and assays for IL-1α, IL-1β, and caspase-1. Methods Mol. Biol. *1040*, 117–135.

7 Appendix

7.1 Sequence References

7.1.1 *Caspase-1* (murine)

NCBI Reference Sequence (genomic sequence, strain C57Bl/6J):

NC_000075 REGION: 5298517...5307281

NCBI Consensus CDS (coding sequence) ID: CCDS22798.1

7.1.2 *Pycard* (murine)

NCBI Consensus CDS ID: CCDS21888.1

7.1.3 *Ripk2* (murine)

NCBI Consensus CDS ID: CCDS17988.1

7.2 Remarks

The originality of the dissertation at hand was analyzed on the 5th of January 2015 using the ”Docol©c” software.